Triplet Energy Transfer and Migration in Polymer Matrices

Kenji Hisada

1997

Contents

Part I   Triplet Energy Migration and Triplet Energy Transfer among Chromophores with a Restricted Spatial Distribution

Chapter 1.   Triplet Excimer Formation and Triplet Energy Migration in Polymer Langmuir–Blodgett Films of Poly[2-(9-carbazolyl) ethyl methacrylate-*co*-isobutyl methacrylate]

Part II Triplet Energy Migration among Energetically Disordered Chromophores in Polymer Matrices

Chapter 5. Monte Carlo Simulation for the Hopping of Triplet Excitons in Poly[(9-phenanthrylmethyl methacrylate)-*co*-(methyl

Chapter 6. Thermally Induced Super Trap Formation in Poly[(9-phenanthrylmethyl methacrylate)-*co*-(methyl methacrylate)] Films

General Introduction

G.1. Historical Background of This Thesis

G.1.1. Triplet State in Polymer System

Materials made up of high polymers have a wide range of functions based on the characteristic chemical and physical properties.   As an example of photofunctional polymers, photoresist is now widely utilized in the industry.   One of the most common photoinduced reactions in photoresist is photocrosslinking.   Historically the first of these photoreactions, and perhaps the most important in practical application, is the photodimerization of cinnamic acid derivatives which leads to crosslinking of polymer chain in thin solid films.   In 1959, Minsk *et al.* reported that photocrosslinking of poly(vinyl cinnamate) could be applied for a negative-type photoresist.[1]   Since then, various kinds of photofunctional polymers have been developed, and simultaneously, the practical values of photopolymers also stimulated basic research in the field of "photochemistry and photophysics in polymer systems".

Photofunctional polymers are composed of the photosensitive groups (chromophore) introduced into the main chain and/or to the side chains, and the polymers are utilized as the feature of solids or thin films.   Therefore, understanding of the excited state behavior of aromatic chromophores in polymer systems is important for the design of photofunctional polymer systems.[2]   However, most of the workers in this field have investigated the singlet state, since fluorescence is usually intense and easily detectable.   The triplet state has not been studied so much as the singlet state, owing to the weak phosphorescence emission.   However, its behavior is important in view of the fundamental research as well as application, because most photoreactions take place *via* triplet state of the reactant.   The chemical process can be initiated by so-called "triplet-sensitizer", which transfers the excitation energy to the reactant with a high efficiency.[3]   Furthermore, a large portion of the excitation energy, often exceeding 50 %, dissipates to the ground state *via* the triplet state.   Thus, the triplet state plays an

important role in the photofunctional polymers. The results obtained on many chromophoric polymer systems show that there are two critical factors governing the behavior of excited state in polymers at an extremely high concentration: one is the formation of a trap site, *e.g.*, excimer site, and the other is the migration and transfer of triplet energy.[4,5,]

G.1.2. Excimer-site Formation

Excimer formation in polymer systems has been widely reported for the singlet state.[6-20] Extensive studies on singlet excimer of aromatic hydrocarbons have been performed by Birks *et al.*[4] As for the geometrical structure of singlet excimer, the "$n = 3$ rule" was firstly reported by Hirayama,[21] followed by the investigation of the intramolecular excimer formation for small molecular weight model compounds in liquid solutions by many workers.[22-30] Two types of singlet excimers have been reported previously, *i.e.*, the full-overlap-type and the partial-overlap-type. On the other hand, triplet excimers appear less common than singlet excimers. The first evidence for triplet excimers was presented by Castro and Hochstrasser in halobenzene crystals,[31] and reported for pyrene crystals.[32] Köppfer *et al.* first reported on the triplet excimer phosphorescence in polymer systems.[33] Subsequently, triplet excimer formation has been reported by many workers for several chromophoric polymers.[34-40] However the geometrical structure of triplet excimers has not been clarified yet, because it is very difficult to observe phosphorescence in liquid solutions. Lim *et al.* reported the phosphorescence from the triplet excimer of bichromophoric compounds in liquid solutions and discussed the structure.[41] However, their work raise an argument by Nickel *et al.*[42] Hence, the structure of the triplet excimer is still an issue to be solved in the future. Beside the excimer-site, there is another kind of trap-site formed by interaction of neighboring chromophores. In a glassy solvent, the chromophoric polymers show slightly red-shifted phosphorescence spectra maintaining the vibrational band structure.[36,43-46] This type of excited species is called a "*shallow trap*" to distinguish it from the triplet excimer. The interaction energy at the *shallow trap-site* is weaker than that at the excimer-site. For chromophoric polymer films, the triplet state interactions are also classified into two types: excimer-type[47] and trap-type.[48]

G.1.3. Energy Transfer and Energy Migration

The electronic energy transfer within a single molecule and from one molecule to another is one of the most important problems in polymer chemistry. In principle, electronic excitation is originally located within the localized region of space described by the molecular orbitals involved in the ground and excited states. Normally this localized excitation is restricted to a small number of atoms involved in the chromophore itself. However, it is well known that the excitation energy can be transferred to other parts of the same molecule, or indeed from one molecule to another.

At least two types of energy transfer can be distinguished. One is the transfer of the excitation energy from the locus of the absorbing group (chromophore) to the bonds adjacent to the chromophore within the same molecule. An example is aliphatic ketones where the light is absorbed by the carbonyl group of the ketone, but the reaction occurs by breaking of bonds adjacent to the carbonyl group, such as the α-β or β-γ carbon-carbon bond.[49] Another type is energy transfer, where the electronic excitation localized on one group is transferred to another group on the same or different molecules as a result of the overlap of electronic charge clouds. The term "energy migration" is used for the energy transfer between the same kind of chromophores, and "energy transfer" usually used for the transfer between different kinds of chromophores. The mechanism of the energy transfer (or migration) is classified into three types.[5] The first one is the radiative mechanism, *i.e.*, energy transfer by re-absorption of a photon emitted from another chromophore. The second mechanism is Coulombic interaction between chromophores. This mechanism is called "Förster type".[50] The rate of energy transfer is proportional to the inverse sixth power of the distance between chromophores. The last one is electron exchange mechanism. The first two mechanisms are spin forbidden for the triplet state. Therefore, the only electron exchange mechanism is effective in the triplet state, which is theoretically worked out by Dexter, and this mechanism is called "Dexter type".[51] In this theory, the rate of energy transfer is expressed as:

$$k_{TT} = \left(\frac{2\pi}{h}\right) Z^2 J_{ex} \qquad (G-1)$$

$$Z^2 = K^2 \exp\left(-\frac{2R}{L}\right) \qquad (G-2)$$

Where R is the distance between chromophores, K is a constant with the dimension of energy, L is an average van der Waals radius for initial and final molecular orbitals of the donor–acceptor

system which is called the effective average Bohr radius, J_{ex} is the exchange interaction integral of spectral overlap between donor emission and acceptor absorption spectra:

$$J_{ex} = \int_0^\infty f_D(\bar{v}) \varepsilon_A(\bar{v}) d\bar{v} \qquad \text{(G-3)},$$

where $f_D(\bar{v})$ and $\varepsilon_A(\bar{v})$ are the normalized donor emission and acceptor absorption spectra, respectively:

$$\int_0^\infty f_D(\bar{v}) d\bar{v} = 1 \qquad \int_0^\infty \varepsilon_A(\bar{v}) d\bar{v} = 1 \qquad \text{(G-4)}.$$

The rate of energy transfer by the exchange mechanism varies with R exponentially, hence it is sensitive to the distance between chromophores. Therefore, the critical radius of triplet energy transfer, R_0, is relatively short compared with that of the singlet energy transfer. The ordinary value of critical radius for the triplet energy transfer is 1.0–1.5 nm,[5,52] whereas that for the singlet energy transfer is 1–10 nm.[53]

When the interchromophore distance is small, electron exchange is considered to be the dominant interaction promoting energy transfer. This was expressed by Dexter in terms of exchange integral Z and a spectral overlap integral J_{ex}. The J_{ex} value was defined in terms of normalized donor emission spectrum and normalized acceptor absorption spectrum (eq G-4). This form of an overlap integral was supported by experimental observations made by Ermoraev[52] and questioned by others.[54] Even if there is no ambiguity in the value of J_{ex}, the difficulties associated with the actual calculation of Z and the lack of direct connection between K and spectroscopic data make eq G-1 useless for calculating the exchange contribution to the energy transfer.

G.1.4. Intramolecular Triplet Energy Transfer

Since the discovery of the triplet–triplet excitation transfer by Terenin and Ermolaev for the benzophenone–naphthalene system,[52] many investigations have been performed to elucidate its mechanism. Although in some experiments the aspects of the decay kinetics due to short-range exchange interaction were studied,[55-57] the most effective way to confirm the validity of Dexter theory is by examining intramolecular energy transfer in bichromophoric compounds,[58-73] where the detailed dependence of the energy transfer rate on interchromophore distances and on the geometrical factors can be studied. The bichromophoric compound may be defined as a molecule built of two chromophoric units connected by a chemical bridge. However, there are few works to determine the rate of triplet energy transfer. Lamola *et al.*[58,74] studied triplet–triplet (T–T) energy transfer of bichromophoric compounds; benzophenone as a donor and naphthalene as an acceptor, connected by a methylene chain where the chain length was one to three. The quantum yields of T–T energy transfer were unity for all compounds in the EPA glass matrix at 77 K since the distance between chromophores, R, was shorter than 1.0 nm. Keller *et al.*[60] also studied T–T energy transfer of systems similar to those used by Lamola *et al.*, where the phthalimide group was used as the triplet energy donor, and the quantum yield was also unity in a rigid glass at 77 K. Since the distances R of these compounds were too short, the transfer process was finished completely within a picosecond time order,[67] and no structural effect was observed on the transfer efficiency. Keller *et al.*[61] estimated the rate constant of T–T energy transfer for the first time, by using bichromophoric compounds connected with a large steroid spacer. Rentzepis and co-workers measured the rate constant of the intramolecular T–T energy transfer process from anthron to naphthalene, for a rigid spiran system, to be 3×10^{10} s^{-1}.[67] The results were discussed in terms of Dexter theory. In another study, highly efficient triplet–triplet intramolecular energy transfer was found for a series of dyes attached to a 9-methylanthryl donor, but, no mechanistic conclusion was presented.[75]

The dependence of the transfer rate on the relative orientation of donor and acceptor was effectively studied using bichromophoric compounds, particularly at small R values. In earlier experiments, an orientational effect was elusive in the case of triplet–triplet energy transfer,[76] but recent studies on the singlet–singlet short-range intramolecular energy transfer showed that the orientational dependence of exchange interaction can be of importance.[77,78] The effect of relative orientation was studied also by Engel *et al.* in the series of benzophenone donor attached through an ester spacer group to cyclic azoalkane acceptor.[79] The exchange integral can be calculated using more realistic orbitals than the hydrogen atomic orbitals used by Dexter.[78,80] The orientation dependence of Z was calculated for the xylene–biacetyl pair, showing that while for $R > 3$ Å Z falls exponentially with increasing R; for smaller R values Z depends on the relative orientation of the two molecules.[78]

Recently, Closs *et al.*,[69,81] Speiser *et al.*,[72,82] and Paddon-Row[83] also investigated bichromophoric systems connected by a rigid spacer and estimated the rate constant of T–T energy transfer and electron transfer at room temperature by picosecond laser photolysis.

They found that those processes occur through σ-bonds of the spacer for compounds with rigid spacer units. These results indicate that there are two mechanisms for triplet energy transfer; *through-space* mechanism and *through-bond* mechanism. Close *et al.* compared the rates of both T–T energy transfer and electron transfer in the series of compounds, consisting of a 4-biphenyl or 4-benzophenoyl donor chromophore, a 2-naphthyl acceptor, and cyclohexane or decalin spacer as the interchromophore bridge. They investigated the dependence of the transfer rate on the orientation of donor and acceptor as well as on the separation distance.[69]

Wagner reported that triplet energy transfer proceeds predominantly *"through-space"* rather than *"through-bond"* for compounds with flexible spacer units exceeding five atoms.[84,85] Katayama *et al.* studied the intramolecular triplet energy transfer from carbazole (Cz) to naphthalene (Np) chromophore for the bichromophoric compounds with a flexible alkyl spacer, Cz-$(CH_2)_n$-Np, in 2-methyltetrahydrofuran glass at 77 K.[71,86,87] Their studies have shown that the transfer rate can be modeled by the *"through-space"* mechanism when the chromophores are connected by a simple alkyl chain.[86,87] These studies were based on computational determination of the distribution of interchromophore distances between Cz and Np. By incorporating this distribution into Dexter's equation, they have been able to simulate the decay of the phosphorescence[86] and the transient absorption of Cz.[87] For longer spacer compounds ($n = 8$–12), R_i, the interchromophore distance, was defined as the distance between the centers of Cz and Np.[86] In the case of shorter spacer compounds ($n = 4$–8), however, two sets of distances and probabilities were calculated and the results were combined by giving equal weight to each of the calculated sets.[87] The first set was calculated using a center-to-center distance, while the second set was calculated as the distance between the closest atoms of Cz and Np, to be referred to as the edge-to-edge separation. In these cases, the parameters in Dexter's equation were different and this discrepancy remained unsettled.

G.1.5. Energy Migration and Transfer in a Condensed System

In a concentrated chromophore system, efficient migration of triplet energy causes efficient energy flow from donor molecules to a small amount of acceptor molecules or trap sites. T–T annihilation, *i.e.*, collision of triplet exciton, provides an excited singlet state which emits fluorescence with a long lifetime, *i.e.*, delayed fluorescence. In the 1960's, many works have been reported for the triplet energy migration in molecular crystals.[80,88-99] Then, Cozzen
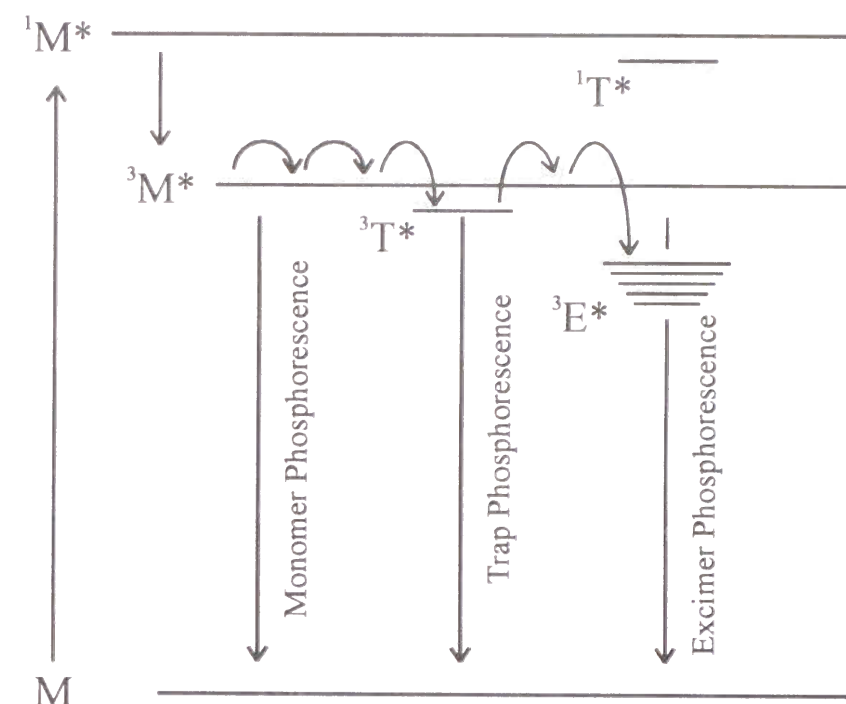
Figure G–1. Energy level in amorphous matrices.

and Fox first reported the triplet energy migration in polymer systems using a solid solution of poly(1-vinylnaphthalene).[100] Since then, many workers have studied the triplet energy migration in various polymer systems by phosphorescence measurements[101-107] and by ESR spectroscopy.[108] In concentrated chromophoric polymer films, the triplet *trap sites* act as shallow traps for energy migration. The trapped exciton can be thermally released from the *trap site*, and it migrates through the polymer film with iterative trapping and detrapping processes.[48] The decay profiles of phosphorescence from trap sites are characterized by multi-exponential functions or stretched exponential functions. Such decay profiles are observed when the excitons diffuse in the spatially or energetically inhomogeneous matrices.[109,110] Many models have been proposed to describe the complicated relaxation process of excited states.[38,111-118]

Similar phenomena have been observed on electron transport in disordered solids, which called "dispersive transport".[119] The transport properties in inhomogeneous systems are described by a distribution of microscopic (site-to-site) transfer rates (temporal disorder) and by dispersive magnitudes of interactions with the surroundings (energetic disorder). Simultaneous treatment of both disorders is an arduous task, which calls for extensive numerical simulations. Spatial randomness may be modeled by fractals,[120,121] and temporal
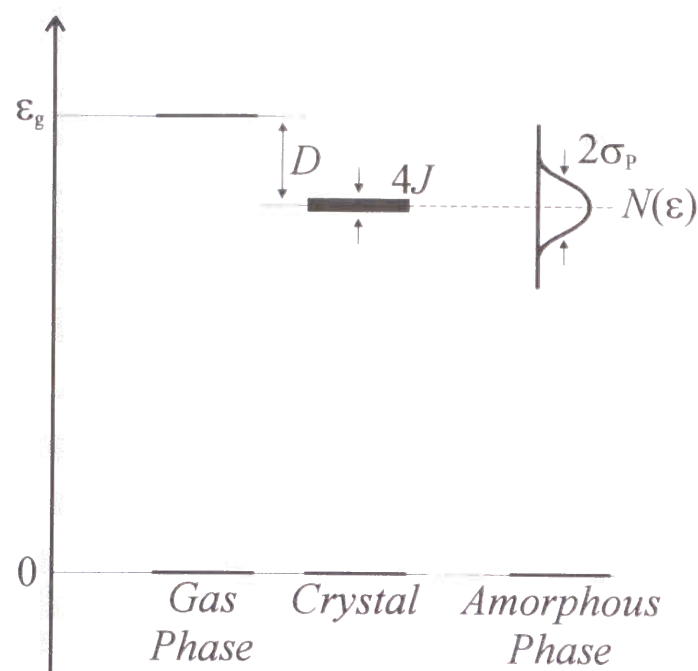
Figure G–2. Energy level spectrum in molecular solids. ε_g is the gas phase value of electronic excitation energy. D is the solvent shift. J is the matrix element for charge exchange between neighboring molecules. σ denotes the energetic width of the distribution of states in the amorphous solid.[126]

disorder can be accounted for by using a waiting-time distribution, as familiar in continuous-time random walk (CTRW),[122,123] and multiple trapping (MT)[123,124] approaches. A drastic temperature effect on excitation energy migration and trapping could not be explained by both CTRW and MT models. Bässler *et al.* analyzed the migration process of triplet excitons in organic matrices by Monte Carlo simulation.[125,126,127] They assumed that the distribution of site energies (DOS) is expressed by a Gaussian function and an exciton hops among these sites. They also reported that this DOS model is adequate for expressing the electron transport, photophysical hole burning, singlet energy migration and thermally induced transformation of spiropyran in polymer solids.[126,127] Kopelman *et al.* also treated the migration of incoherent excitation in energetically disordered systems using a self-consistent diagrammatic approximation.[128] Katayama *et al.* applied Bässler's model to chromophoric polymer systems and successfully represented the phosphorescence decay profiles of poly[(2-naphthylalkyl methacrylate)-*co*-methyl methacrylate]s and poly[(9-phenanthrylmethyl methacrylate)-*co*-methyl methacrylate] solid films in a temperature range of 115–165 K.[110] Recently, the hopping mobility of the electron was also studied concerning the energetical disorder of sites.[129,130]

G.2.   Outline of This Thesis

The purpose of this work is to clarify the triplet state behavior in polymer matrices, especially energy migration and transfer process between chromophores embedded in polymer matrices. This thesis consists of two parts: in Part I, the effect of spatial distribution of the chromophores was studied. In Chapter 1–3, chromophores were distributed on a *pseudo-two-dimensional* plane by using polymer Langmuir–Blodgett (LB) films, and in Chapter 4, the distance between chromophores was restricted by using bichromophoric compounds. In Part II, the triplet energy migration among the energetically disordered sites was studied at low temperatures (Chapter 5 and 6).

In Chapter 1, the excited triplet state of carbazole chromophores and triplet energy migration in Langmuir–Blodgett films was investigated for carbazole containing polymers, *i.e.*, poly[(2-(9-carbazolyl)ethyl methacrylate)-*co*-(isobutyl methacrylate)] (P(C-iB)) and poly[(2-(9-carbazolyl)ethyl methacrylate)-*co*-(octadecyl methacrylate)] (P(C-OD)). In the case of poly[(2-(9-carbazolyl)ethyl methacrylate)-*co*-(isobutyl methacrylate)], an interlayer interaction played a considerable role when more than four layers of chromophoric layers were deposited. It was confirmed that triplet energy migration between chromophores mainly depends on the interchromophore distance, whether the system consists of two-dimensional LB film or three-dimensional amorphous polymer film.

P(C-iB)   P(C-OD)
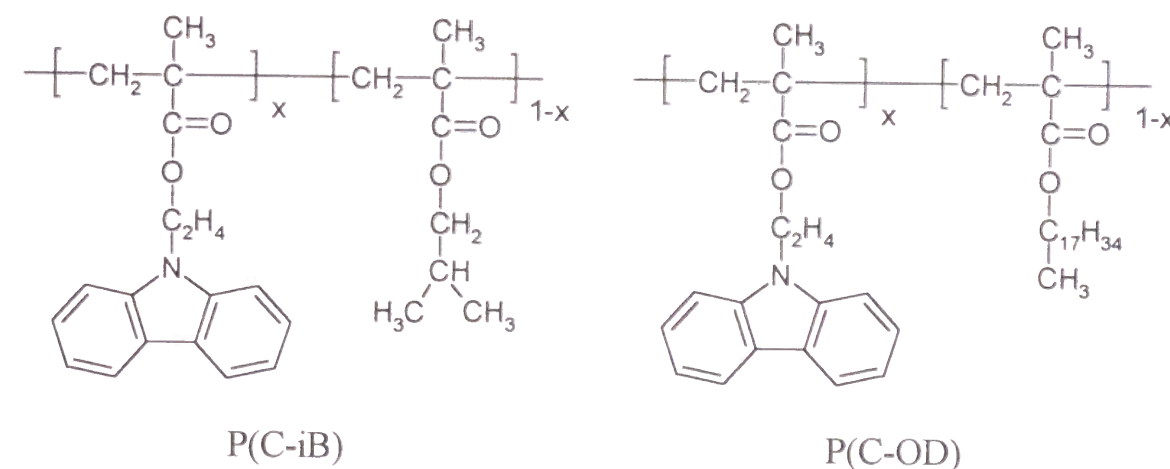
In Chapter 2, the triplet energy migration and transfer in LB films prepared by the copolymers of octadecyl methacrylate with 2-(9-carbazolyl)ethyl methacrylate (donor unit) and (4-bromo-1-naphthyl)methyl methacrylate (acceptor unit), P(CN-OD), were investigated. The dependence of the quenching efficiency of carbazole phosphorescence upon the acceptor

density in the film plane was investigated. The quenching efficiencies at a low donor density were reproduced by the active sphere model with a planar distribution of chromophores in a monolayer. When the donor density was high, the apparent radius of the active sphere was larger than the value at a low donor density. This suggests that the energy transfer occurs by a dynamic process, *i.e.*, a few steps of energy migration among donors, followed by energy transfer to the acceptor.

P(CN-OD)
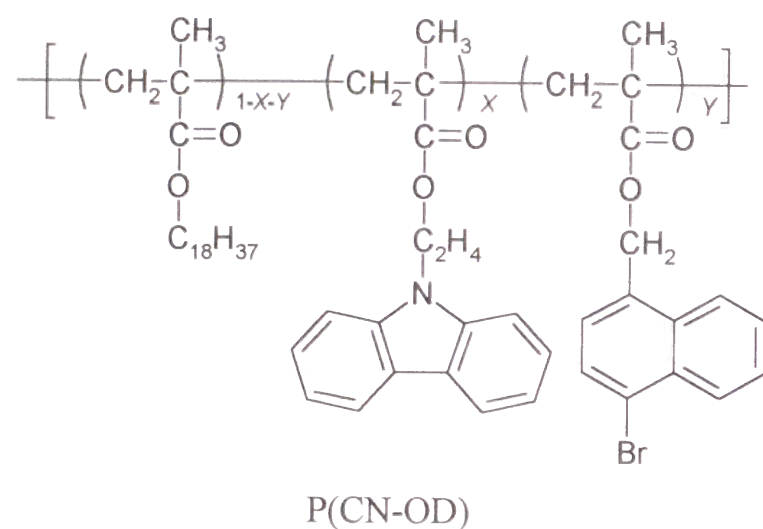
In Chapter 3, the triplet energy migration and transfer were simulated by the Monte Carlo method for the LB films prepared by the copolymers of octadecyl methacrylate with 2-(9-carbazolyl)ethyl methacrylate and (4-bromo-1-naphthyl)methyl methacrylate. By solving the differential equations relevant to the energy migration and energy transfer on a two-dimensional square lattice, the time evolution of the triplet energy quenching was successfully simulated. The calculated quenching efficiencies were in agreement with the experimental values observed in the LB film of poly(octadecyl methacrylate) containing both the donor and acceptor moieties.

In Chapter 4, the rates of intramolecular triplet energy transfer from carbazole (Cz) to naphthalene (Np) chromophore were measured by phosphorescence spectroscopy and laser flash photolysis. Bichromophoric compounds with a flexible alkyl spacer, Cz-*n*-Np, *n* = 4–12, were doped in poly(methyl methacrylate) matrices. The results were interpreted by using Dexter's equation in terms of a model that allows a distribution of donor–acceptor distances for a given spacer length. This model allowed one to predict the transfer rate for all the compounds investigated, and the comparative study with experimental results indicated that the *"through-space"* mechanism mainly governs the intramolecular triplet–triplet energy transfer in

flexible spacer compounds. The temperature dependence of the rates of triplet energy transfer was also investigated.

Cz-*n*-Np
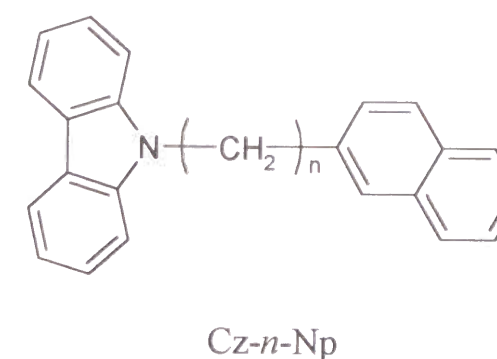
In Chapter 5, triplet energy migration in poly[(9-phenanthrylmethyl methacrylate)-*co*-(methyl methacrylate)] films was investigated by time-resolved phosphorescence spectroscopy in the temperature range of 15–100 K. Phosphorescence spectra from *triplet trap sites* were slightly shifted toward the low energy side with the elapse of time. The spectral shift was simulated by the Monte Carlo method. The simulation allowed estimation of the dispersity of the site energies. Due to homogeneous broadening, the distribution function became broader with the increase of temperature.
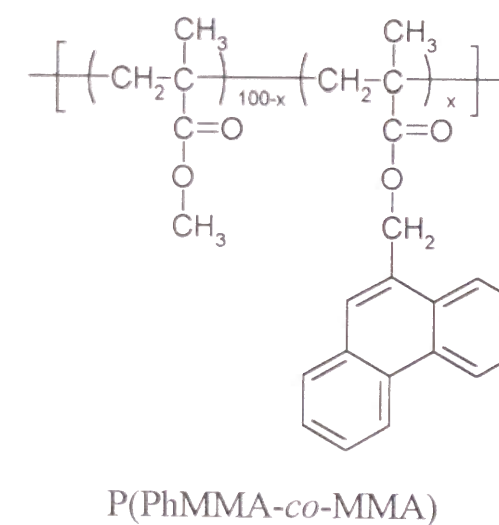
P(PhMMA-*co*-MMA)

In Chapter 6, the triplet energy migration in poly[(9-phenanthrylmethyl methacrylate)-*co*-(methyl methacrylate)] (P(PhMMA-*co*-MMA)) films was investigated by phosphorescence decay profiles. The energy migration rates in these systems are various since the trap sites have various energy levels depending on the amplitude of interaction energies. The kinetic

analysis was made on the basis of Bässler's model in which the site energies have a Gaussian distribution. The fitting procedure well reproduced the phosphorescence decay data in a temperature range of 15–100 K, indicating that the concentration of super–trap increased steeply with the motion of the matrix polymer.

References

1   L. M. Minsk, J. G. Smith, W. P. Van Deusen and J. F. Wright, *J. Appl. Polym. Sci.*, **2**, 302 (1959).

2   J. E. Guillet, *"Polymer Photophysics and Photochemistry"*, Cambridge Univ. Press, Cambridge, 1985; D. Phillips Ed., *"Polymer Photophysics"*, Chapman and Hall, London, 1985; M. A. Winnik Ed., *"Photophysical and Photochemical Tools in Polymer Science"*, NATO ASI Series, Reidel, Dordrecht, 1986; C. E. Hoyle and J. M. Torkelson Eds., *"Photophysics of Polymers"*, ACS Symposium Series 358, American Chemical Society, Washington, DC, 1987.

3   W. Galley and L. Stryer, *Proc. Natl. Acd. Sci. U. S. A.*, **60**, 108 (1968); J. Eisinger and R. G. Shulman, *Science*, **161**, 1311 (1968); Z. Wu and H. Morrison, *Photochem. Photobiol.*, **50**, 525 (1989).

4   J. B. Birks, *"Photophysics of Aromatic Molecules"*, Wiley, London, 1970.

5   N. J. Turro, *"Modern Molecular Photochemistry"*, Benjamin: Menlo Park, CA, 1978.

6   M. T. Vala, J. Haebig, and S. A. Rice, *J. Chem. Phys.*, **43**, 886 (1965).

7   W. Klöpffer, *J. Chem. Phys.*, **50**, 2337 (1969).

8   Y. Nishijima, *J. Polym. Sci. C*, **31**, 353 (1970); S. Ito, M. Yamamoto, and Y. Nishijima, *Polym. J.*, **13**, 791 (1981).

9   R. B. Fox, T. R. Price, R. F. Cozzens, and J. R. McDonald, *J. Chem. Phys.*, **57**, 534 (1972); R. B. Fox, *Pure Appl. Chem.*, **30**, 87 (1972).

10   C. David, M. Piens, and G. Geuskens, *Eur. Polym. J.*, **8**, 1019 (1972).

11   L. A. Harrah, *J. Chem. Phys.*, **56**, 385 (1972); C. W. Frank and L. A. Harrah, *J. Chem. Phys.*, **61**, 1526 (1974).

12   G. E. Johnson, *J. Chem. Phys.*, **62**, 4697 (1975).

13   K. P. Ghiggino, R. D. Wright, and D. Phillips, *J. Polym. Sci., Polym. Phys. Ed.*, **16**, 1499 (1978); *Eur. Polym. J.*, **14**, 567 (1978); D. Phillips and A. J. Roberts. *J. Polym. Sci., Polym. Phys. Ed.*, **18**, 2401 (1980); A. J. Roberts, D. Phillips, F. A. M. Abdul–Rasoul, and A. Ledwith, *J. Chem. Soc., Faraday Trans. 1*, **77**, 2725 (1981); S. W. Bigger, K. P Ghiggino, and S. K. Ng, *Macromolecules*, **22**, 800 (1989).

14　C. E. Hoyle, T. L. Nemzek, A. Mar, and J. E. Guillet, *Macromolecules*, **11**, 429 (1978); C. E. Hoyle and J. E. Guillet, *J. Polym. Sci., Polym. Lett. Ed.*, **16**, 185 (1978); M. Keyanpour–Rad, A. Ledwith, A. Hallam, A. M. North, M, Breton, C. Hoyle, and J. E. Guillet, *Macromolecules*, **11**, 1114 (1978); L. Merle–Aubry, D. A. Holden, Y. Merle, and J. E. Guillet, *Macromolecules*, **13**, 1138 (1980); X. Ren and J. E. Guillet, *Macromolecules*, **18**, 2012 (1985).

15　R. F. Reid and I. Soutar, *J. Polym. Sci., Polym. Phys. Ed.*, **16**, 231 (1978).

16　T. Nakahira, I. Maruyama, S. Iwabuchi, and K. Kojima, *Makromol. Chem.*, **180**, 1853 (1979); *Makromol. Chem. Rapid Commun.*, **1**, 437 (1980); T. Nakahira, S. Ishizuka, S. Iwabuchi, and K. Kojima, *Macromolecules*, **16**, 297 (1983); T. Nakahira, I. Maruyama, S. Iwabuchi, and K. Kojima, *Makromol. Chem. Rapid Commun.*, **6**, 489 (1985).

17　H. F. Kauffmann, W. Weixelbaumer, J. Buerbaumer, A. Schmoltner, and O. F. Olaj, *Mocromolecules*, **18**, 104 (1985).

18　Y. Morishima, H. S. Lim, S. Nozakura, and J. L. Sturtevant, *Macromolecules*, **22**, 1148 (1989).

19　L. Cheng, G. Wang, and M. A. Winnik, *Polymer*, **31**, 1611 (1990).

20　A. Itaya, K. Okamoto, and S. Kusabayashi, *Bull. Chem. Soc. Jpn.*, **49**, 2082 (1976); A. Itaya, H. Sakai, and H. Masuhara, *Chem. Phys. Lett.*, **138**, 231 (1987).

21　F. Hirayama, *J. Chem. Phys.*, **42**, 3163 (1965).

22　E. A. Chandross and C. J. Dempster, *J. Am. Chem. Soc.*, **92**, 704 (1970); *J. Am. Chem. Soc.*, **92**, 3586 (1970).

23　K. Zachariasse and W. Kühnle, *Z. Phys. Chem. (Wiesbaden)*, **101**, 267 (1976); K. Zachariasse and G. Duveneck, *J. Am. Chem. Soc.*, **109**, 3790 (1987).

24　T. Takemura, M. Aikawa, H. Baba, and Y. Shindo, *J. Am. Chem. Soc.*, **98**, 2205 (1976).

25　S. Ito, M. Yamamoto, and Y. Nishijima, *Bull. Chem. Soc. Jpn.*, **54**, 35 (1981); *Bull. Chem. Soc. Jpn.*, **55**, 363 (1982); *Bull. Chem. Soc. Jpn.*, **57**, 3295 (1984).

26　D. Ng and J. E. Guillet, *Macromolecules*, **14**, 405 (1981).

27　F. C. De Schryver, J. Vandendriessche, S. Toppet, K. Demeyer, and N. Boens, *Macromolecules*, **15**, 406 (1982); J. Vandendriessche, P. Palmans, S. Toppet, N. Boens, F. C. De Schryver, and H. Masuhara, *J. Am. Chem. Soc.*, **106**, 8057 (1984).

28　F. Evers, K. Kobs, R. Memming, and D. R. Terrell, *J. Am. Chem. Soc.*, **105**, 5988 (1983).

29　D. A. Holden, J. B. Gray, and I. McEwan, *J. Org. Chem.*, **50**, 866 (1985); D. A. Holden, A. Safarzadeh–Amiri, C. P. Sloan, and P. Martin, *Macromolecules*, **22**, 315 (1989).

30　S. Irie and M. Irie, *Macromolecules*, **19**, 2182 (1986).

31　G. Castro and R. M. Hochstrasser, *J. Chem. Phys.*, **45**, 4352 (1966).

32　O. L. J. Gijzeman, J. Langelaar, and J. D. W. Van Voorst, *Chem. Phys. Lett.*, **5**, 269 (1970).

33　W. Klöpffer and D. Fischer, *J. Polym. Sci. Symp.*, **40**, 43 (1973).

34　R. B. Fox, T. R. Price, R. F. Cozzens, and J. R. McDonald, *J. Chem. Phys.*, **57**, 2284 (1972); R. B. Fox, T. R. Price, R. F. Cozzens, and W. H. Echols, *Macromolecules*, **7**, 937 (1974).

35　R. D. Burkhart, *Macromolecules*, **9**, 234 (1976); *Macromolecules*, **16**, 820 (1983); R. D. Burkhart and R. G. Avilés, *J. Phys. Chem.*, **83**, 1897 (1979); *Macromolecules*, **12**, 1073 (1979); *Macromolecules*, **12**, 1078 (1979); A. A. Abia and R. D. Burkhart, *Macromolecules*, **17**, 2739 (1984); R. D. Burkhart, O. Lee, S. Boileau, and S. Boivin, *Macromolecules*, **18**, 1277 (1985); R. D. Burkhart and I. Dawood, *Macromolecules*, **19**, 447 (1986); R. D. Burkhart, R. G. Avilés, and K. Magrini, *Macromolecules*, **14**, 91 (1981); D. K. Chakraborty and R. D. Burkhart, *J. Phys. Chem.*, **93**, 4797 (1989).

36　M. Aikawa, T. Takemura, and H. Baba, *Bull. Chem. Soc. Jpn.*, **49**, 437 (1976); M. Aikawa, T. Takemura, H. Baba, M. Irie, and K. Hayashi, *Bull. Chem. Soc. Jpn.*, **51**, 3643 (1978).

37　S. E. Webber and P. E. Avots–Avotins, *Macromolecules*, **12**, 708 (1979); N. Kim and S. E. Webber, *Macromolecules*, **13**, 1233 (1980).

38　C. S. Li and R. Kopelman, *Macromolecules*, **23**, 2223 (1990).

39　N. Tamai, H. Masuhara, and N. Mataga, *J. Phys. Chem.*, **87**, 4461 (1983).

40　R. D. Burkhart and D. K. Chakraborty, *J. Phys. Chem.*, **94**, 4143 (1990); R. D. Burkhart, N.–I. Jhon, and S. Boileau, *Macromolecules*, **24**, 6310 (1990); R. D. Burkhart, D. K. Chakraborty, and Y. Shirota, *Macromolecules*, **24**, 1511 (1991); R. D. Burkhart and N.–I. Jhon, *J. Phys. Chem.*, **95**, 7189 (1991).

41　S. Okajima, P. C. Subudhi, and E. C. Lim, *J. Chem. Phys.*, **67**, 4611 (1977); A. K. Chanfra and E. C. Lim, *Chem. Phys. Lett.*, **45**, 79 (1977); P. C. Subudhi and E. C. Lim, *Chem. Phys. Lett.*, **56**, 59 (1978); E. C. Lim, *Acc. Chem. Res.*, **20**, 8 (1987); R. J. Locke

and E. C. Lim, *J. Phys. Chem.*, **93**, 6017 (1989); J. Cai and E. C. Lim, *J. Phys. Chem.*, **94**, 8387 (1990).

42   B. Nickel and M. F. Rodriguez, *Z. Phys. Chem. NF*, **150**, 31 (1986); *Chem. Phys. Lett.*, **146**, 125 (1988).

43   M. Yokoyama, T. Tamamura, and T. Nakano, H. Mikawa, *J. Chem. Phys.*, **65**, 272 (1976).

44   A. Itaya, K. Okamoto, and S. Kusabayashi, *Bull. Chem. Soc. Jpn.*, **50**, 52 (1977).

45   S. Ito, S. Nishino, M. Yamamoto, and Y. Nishijima, *Rep. Prog. Polym. Phys. Jpn.*, **26**, 483 (1983).

46   D. A. Holden and A. Safarzadeh–Amiri, *Macromolecules*, **20**, 1588 (1987).

47   S. Ito, H. Katayama, and M. Yamamoto, *Macromolecules*, **21**, 2456 (1988); *J. Photopolym. Sci. Technol.*, **4**, 217 (1991).

48   S. Ito, N. Numata, H. Katayama, and Yamamoto, M. *Macromolecules*, **22**, 2207 (1989); H. Katayama, T. Tawa, S. Ito, and M. Yamamoto, *J. Chem. Soc., Faraday Trans. 2*, **88**, 2743 (1992).

49   J. E. Guillet and R. G. W. Norrish, *Nature*, **173**, 625 (1954); *La Ricerca Scientifica*, **25**, 1 (1955); *Proc. R. Soc. London, Ser. A*, **233**, 153 (1955).

50   T. Förster, *Ann. Phys.*, **2**, 55 (1948); *Z. Naturforsch*, **4a,** 321 (1949); T. Förster and K. Kasper, *Z. Electrochem.*, **59**, 976 (1955); T. Förster, *"Modern Quantum Chemistry"*, O. Sinanoglu Ed.; Academic Press: New York, 1965; Part III.

51   D. L. Dexter, *J. Chem. Phys.*, **21**, 836 (1953).

52   A. N. Terenin and V. L. Ermolaev, *Doklady Acad. Sci. U. S. S. R.*, **85**, 547 (1952); *Trans. Faraday Soc.*, **52**, 1042 (1956); V. L. Ermolaev, *Doklady Acad. Sci. U. S. S. R.*, **102**, 925 (1955); *Sov. Phys.—Dokl. (Engl. Transl.)*, **6**, 600 (1962); *Sov. Phys. JETP*, **6**, 333 (1963).

53   I. B. Berlman, *"Energy Transfer Parameters of Aromatic Compounds"*, Academic, New York, 1973.

54   M. A. Davidovich and R. S. Knox, *Chem. Phys. Lett.*, **68**, 391 (1979).

55   H. Kobashi, T. Morita, and N. Mataga, *Chem. Phys. Lett.*, **20**, 376 (1973).

56   G. B. Strambini and W. C. Galley, *J. Chem. Phys.*, **63**, 3467 (1975); *Chem. Phys. Lett.*, **39**, 257 (1976).

57   A. Brown and F. Wilkinson, *J. Chem. Soc. Faraday Trans. 2*, **75**, 880 (1979).

58   A. A. Lamola, P. A. Leermakers, G. W. Byers, and G. S. Hammond, *J. Am. Chem. Soc.*, **87**, 2322 (1965).

59   F. W. Wilkinson, *Q. Rev.*, **20**, 403 (1966).

60   R. A. Keller, *J. Am. Chem. Soc.*, **90**, 1940 (1968); D. E. Breen and R. A. Keller, *J. Am. Chem. Soc.*, **90**, 1935 (1968).

61   R. A. Keller and L. J. Dolby, *J. Am. Chem. Soc.*, **91**, 1293 (1969).

62   C. Thiery, *Mol. Photochem.*, **2**, 1 (1970).

63   J. R. Bunting and N. Filipescu, *J. Chem. Soc. (B)*, **1970**, 1750.

64   H. E. Zimmerman and R. D. Mckelvey, *J. Am. Chem. Soc.*, **93**, 3638 (1971).

65   W. Amrein and K. Schaffner, *Helv. Chim. Acta*, **58**, 397 (1975).

66   F. C. De Schryver and N. Boens, *Adv. Photochem.*, **10**, 359 (1977).

67   A. H. Maki, J. G. Weers, E. F. Hilinski, S. V. Milton, and P. M. Rentzepis, *J. Chem. Phys.*, **80**, 2288 (1984).

68   D. Gust, T. A. Moore, R. V. Bensasson, P. Mathis, E. J. Land, C. Chachaty, A. L. Moore, P. A. Liddell, and G. A. Nemeth, *J. Am. Chem. Soc.*, **107**, 3631 (1985).

69   G. L. Closs, P. Piotrowiak, J. M. MacInnis, and G. R. Fleming, *J. Am. Chem. Soc.*, **110**, 2652 (1988); G. L. Closs, M. D. Johnson, J. R. Miller, and P. Piotrowiak, *J. Am. Chem. Soc.*, **111**, 3751 (1989).

70   Y. Ito, Y. Uozu, H. Arai, and T. Matsuura, *J. Org. Chem.*, **54**, 506 (1989).

71   H. Katayama, S. Maruyama, S. Ito, Y. Tsujii, A. Tsuchida, and M. Yamamoto, *J. Phys. Chem.*, **95**, 3480 (1991).

72   S. Speiser, *Chem. Rev.*, **96**, 1953 (1996).

73   M. Asano–Someda, T. Ichino, and Y. Kaizu, *J. Phys. Chem. A*, **101**, 4484 (1997).

74   A. A. Lamola and G. S. Hammond, *J. Chem. Phys.*, **43**, 2129 (1965); A. A. Lamola, *J. Am. Chem. Soc.*, **91**, 4786 (1969).

75   J. Tran and J. Olmsted, *J. Photochem. Photobio. A: Chem.*, **71**, 45 (1993).

76   A. Adamczyk and D. Phillips, *J. Chem. Soc. Faraday Trans. 2*, **70**, 537 (1974).

77   S.–T. Levy, M. B. Rubin, and S. Speiser, *J. Am. Chem. Soc.*, **114**, 10747 (1992); *J. Photochem. Photobio. A: Chem.*, **66**, 159 (1992).

78   S.–T. Levy and S. Speiser, *J. Chem. Phys.*, **96**, 3585 (1992).

79   P. S. Engel, D. W. Horsey, J. N. Scholz, T. Karatsu, and A. Kitamura, *J. Phys. Chem.*, **96**, 7524 (1992).

80   J. Jortner, S.–I. Choi, J. L. Katz, and S. A. Rice, *Phys. Rev. Lett.*, **11**, 323 (1963); J. Jortner, S. A. Rice, J. L. Katz, and S.–I. Choi, *J. Chem. Phys.*, **42**, 309 (1965).

81   M. Sigman and G. L. Closs, *J. Phys. Chem.*, **95**, 5012 (1991).

82   S. Speiser, S. Hassoon, and M. B. Rubin, *J. Phys. Chem.*, **90**, 5085 (1986).

83   M. N. Paddon–Row, *Acc. Chem. Res.*, **27**, 18 (1994).

84   P. J. Wagner and G. M. El–Taliawi, *J. Am. Chem. Soc.*, **114**, 8325 (1992).

85   P. J. Wagner, B. P. Giri, H. W. Freking Jr., and J. DeFrancesco, *J. Am. Chem. Soc.*, **114**, 8326 (1992).

86   H. Katayama, S. Ito, and M. Yamamoto, *J. Phys. Chem.*, **96**, 10115 (1992).

87   G. W. Haggquist, H. Katayama, A. Tsuchida, S. Ito, and M. Yamamoto, *J. Phys. Chem.*, **97**, 9270 (1993).

88   M. A. El–Sayed, M. T. Wauk, and G. W. Robinson, *Mol. Phys.*, **5**, 205 (1962); G. C. Nieman and G. W. Robinson, *J. Chem. Phys.*, **39**, 2550 (1963); S. D. Colson and G. W. Robinson, *J. Chem. Phys.*, **48**, 2550 (1968).

89   R. W. Brandon, R. E. Gerkin, and C. A. Hutchison Jr., *J. Chem. Phys.*, **37**, 447 (1962); N. Hirota and C. A. Hutchison Jr., *J. Chem. Phys.*, **42**, 2869 (1965); N. Hirota, *J. Chem. Phys.*, **43**, 3354 (1965).

90   R. M. Hochstrasser, *J. Chem. Phys.*, **39**, 3153 (1963); *J. Chem. Phys.*, **40**, 1038 (1964); T. F. Hunter, R. D. McAlpine, and R. M. Hochstrasser, *J. Chem. Phys.*, **50**, 1140 (1969).

91   A. Rousset, R. Lochet, and J. P. Cadas, *J. Phys.*, **24**, 141 (1963).

92   T. N. Misra and S. P. McGlynn, *J. Chem. Phys.*, **44**, 3816 (1966); M. Kinoshita, T. N. Misra, and S. P. McGlynn, *J. Chem. Phys.*, **45**, 817 (1966); B. N. Srinivasan, M. Kinoshita, and S. P. McGlynn, *J. Chem. Phys.*, **47**, 5090 (1967).

93   P. Avakian and R. E. Merrifield, *Mol. Cryst.*, **5**, 37 (1968).

94   C. E. Swenberg, *J. Chem. Phys.*, **51**, 1753 (1969).

95   A. Suna, *Phys. Rev. B*, **1**, 1716 (1970).

96   V. Ern, *J. Chem. Phys.*, **56**, 6259 (1972).

97   H. C. Brenner, *J. Chem. Phys.*, **59**, 6362 (1973).

98   P. Evesque and J. Duran, *J. Chem. Phys.*, **80**, 3016 (1984).

99   S. M. Pimblott and A. Mozumder, *Chem. Phys. Lett.*, **180**, 497 (1991).

100 R. F. Cozzens and R. B. Fox, *J. Chem. Phys.*, **50**, 1532 (1969); R. B. Fox and R. F. Cozzens, *Macromolecules*, **2**, 181 (1969).

101 C. David, W. Demarteau, and G. Geuskens, *Eur. Polym. J.*, **6**, 537 (1970); C. David, V. Naegelen, W. Piret, and G. Geuskens, *Eur. Polym. J.*, **11**, 569 (1975); C. David, D. Baeyens–Volant, and G. Geuskens, *Eur. Polym. J.*, **12**, 71 (1976); C. David, D. Baeyens–Volant, P. Macedo de Abreu, and G. Geuskens, *Eur. Polym. J.*, **13**, 841 (1977).

102 A. C. Somersall and J. E. Guillet, *Macromolecules*, **6**, 218 (1973).

103 N. F. Pash, R. D. McKenzie, and S. E. Webber, *Macromolecules*, **11**, 733 (1978); N. F. Pash and S. E. Webber, *Macromolecules*, **11**, 727 (1978); S. E. Webber and P. E. Avots–Avotins, *J. Chem. Phys.*, **72**, 3773 (1980); J. F. Pratte and S. E. Webber, *Macromolecules*, **16**, 1193 (1983); N. Kim and S. E. Webber, *Macromolecules*, **18**, 741 (1985).

104 R. D. Burkhart and E. R. Lonson, *Chem. Phys. Lett.*, **54**, 85 (1978); R. D. Burkhart and A. A. Abia, *J. Phys. Chem.*, **86**, 468 (1982); R. D. Burkhart, *J. Phys. Chem.*, **87**, 1566 (1983); R. D. Burkhart, G. W. Haggquist, and S. E. Webber, *Macromolecules*, **20**, 3012 (1987); T. J. K. S. Siu and R. D. Burkhart, *Macromolecules*, **22**, 336 (1989); D. K. Chakraborty and R. D. Burkhart, *Chem. Phys. Lett.*, **157**, 189 (1989); N. J. Caldwell and R. D. Burkhart, *Macromolecules*, **19**, 1653 (1986); D. K. Chakraborty and R. D. Burkhart, *Macromolecules*, **23**, 121 (1990).

105 T. Nakahira, S. Ishizuka, S. Iwabuchi, and K. Kojima, *Makromol. Chem. Rapid Commun.*, **1**, 759 (1980).

106 E. I. Newhouse and R. Kopelman, *Chem. Phys. Lett.*, **143**, 106 (1988).

107 Y. Itoh and S. E. Webber, *Macromolecules*, **23**, 5065 (1990).

108 J. Higuchi, M. Yagi, J. Saito, and M. Takahashi, *Bull. Chem. Soc. Jpn.*, **54**, 2454 (1981).

111 F. E. El–Sayed, J. R. MacCallum, P. J. Pomery, and T. M. Shepherd, *J. Chem. Soc., Faraday Trans. 2*, **75**, 79 (1979).

112 G. Zumofen, A. Blumen, and J. Klafter, *J. Chem. Phys.*, **82**, 3198 (1985); *J. Chem. Phys.*, **84**, 6679 (1986).

113 Y. Lin, M. C. Nelson, and D. M. Hanson, *J. Chem. Phys.*, **86**, 1586 (1987); Y. Lin, R. C. Dorfman, and M. D. Fayer, *J. Chem. Phys.*, **90**, 159 (1989).

114 J. D. Byers, M. S. Friedrichs, R. A. Friesner, and S. E. Webber, *Macromolecules*, **21**, 3402 (1988); J. D. Byers, W. S. Parsons, R. A. Friesner, and S. E. Webber, *Macromolecules*, **23**, 4835 (1990).

115 E. J. Janse van Rensburg, J. E. Guillet, and S. G. Whittington, *Macromolecules*, **22**, 4212 (1989).

109 I. Yamazaki, N. Tamai, and T. Yamazaki, *J. Phys. Chem.*, **94**, 516 (1990); N. Tamai, T. Yamazaki, and I. Yamazaki, *Can. J. Phys.*, **68**, 1013 (1990).

116 L. A. Harmon and R. Kopelman, *J. Phys. Chem.*, **94**, 3454 (1990).

117 K. Sienicki and G. Durocher, *Macromolecules*, **24**, 1102 (1991).

118 S. H. Kost and H. D. Breuer, *Ber. Bunsenges. Phys. Chem.*, **95**, 480 (1991).

110 H. Katayama, T. Tawa, G. W. Haggquist, S. Ito, and M. Yamamoto, *Macromolecules*, **26**, 1265 (1993).

119 G. Pfister and W. Scher, *Acta Phys. Pol.*, **27**, 747 (1978).

120 B. B. Mondelbrot, *"The Fractal Geometry of Nature"*; Freeman: San Francisco, 1982.

121 A. Blumen, J. Klafter, and G. Zumofen, *Phys. Rev. B*, **27**, 6112 (1983); J. Klafter, A. Blumen, and G. Zumofen, *J. Stat. Phys.*, **36**, 561 (1984).

122 H. Scher and M. Lax, *Phys. Rev. B*, **7**, 4491 (1973); *Phys. Rev. B*, **7**, 4502 (1973).

123 E. W. Montroll and M. F. Shlesinger, in *"Non-Equilibrium Phenomena. II. From Stochastics to Hydrodynamics"*, J. L. Lebowitz and E. W. Montroll Ed.; North-Holland: Amsterdam, 1984, p. 1.

124 M. F. Shlesinger and E. W. Montroll, *Proc. Natl. Acad. Sci. U. S. A.*, **81**,1280 (1984).

125 R. Richert, B. Richert, and H. Bässler, *Philos. Mag. B*, **49**, L25 (1984); R. Richert and H. Bässler, *J. Chem. Phys.*, **84**, 3567 (1986).

126 H. Bässler, *Phys. Status Solidi B*, **107**, 9 (1981).

127 G. Schönherr, H. Bässler, and M. Silver, *Phil. Mag. B*, **44**, 47 (1981); R. Richert, A. Elshner, and H. Bässler, *Z. Phys. Chem. NF.*, **149**, 63 (1986).

128 R. P. Parson and R. Kopelman, *J. Chem. Phys.*, **82**, 3692 (1985).

129 Y. N. Gartstein and E. M. Conwell, *J. Chem. Phys.*, **100**, 9175 (1994).

130 Y. Dakhnovski, V. Lubchenko, and P. Wolynes, *J. Chem. Phys.*, **104**, 1875 (1996).

Part I

Chapter 1

Triplet Excimer Formation and Triplet Energy Migration in Polymeric Langmuir–Blodgett Films of Poly[2-(9-carbazolyl)ethyl methacrylate-*co*-isobutyl methacrylate]

1.1. Introduction

The photophysical properties of Langmuir–Blodgett (LB) films have been widely investigated.[1-3]   Recently, some amphiphilic polymers were found to form a stable monolayer and to be transferable to solid substrates.[4,5]   Polymeric materials have a variety of molecular structures which are easily modified with conventional chemical reactions and are convenient for designing some functional materials.   From the standpoint of photophysicochemical processes, the behavior of the excited triplet state as well as the excited singlet state is very important, because a considerable fraction of the excited energy deactivates to the ground state *via* the excited triplet state.   Therefore, investigation of the triplet state in polymeric LB films is important for designing photofunctional materials by LB methods.   In previous works, Katayama *et al.* have investigated the behavior of the excited triplet states of aromatic chromophores in amorphous polymer films by phosphorescence spectroscopy.[6-10]   Copolymer films of poly[2-(9-carbazolyl)ethyl methacrylate-*co*-methyl methacrylate] exhibit phosphorescence from the triplet excimer, and then vigorous triplet energy migration is observed when the interchromophore distance is shorter than 1.0 nm.

In this chapter, the triplet energy migration and the formation of triplet excimers in polymeric Langmuir–Blodgett (LB) film containing carbazole moieties are studied, and the results are compared with the behavior in the film prepared by a conventional cast method.

1.2. Experimental Section

P(C-iB)   P(C-OD)

PVO
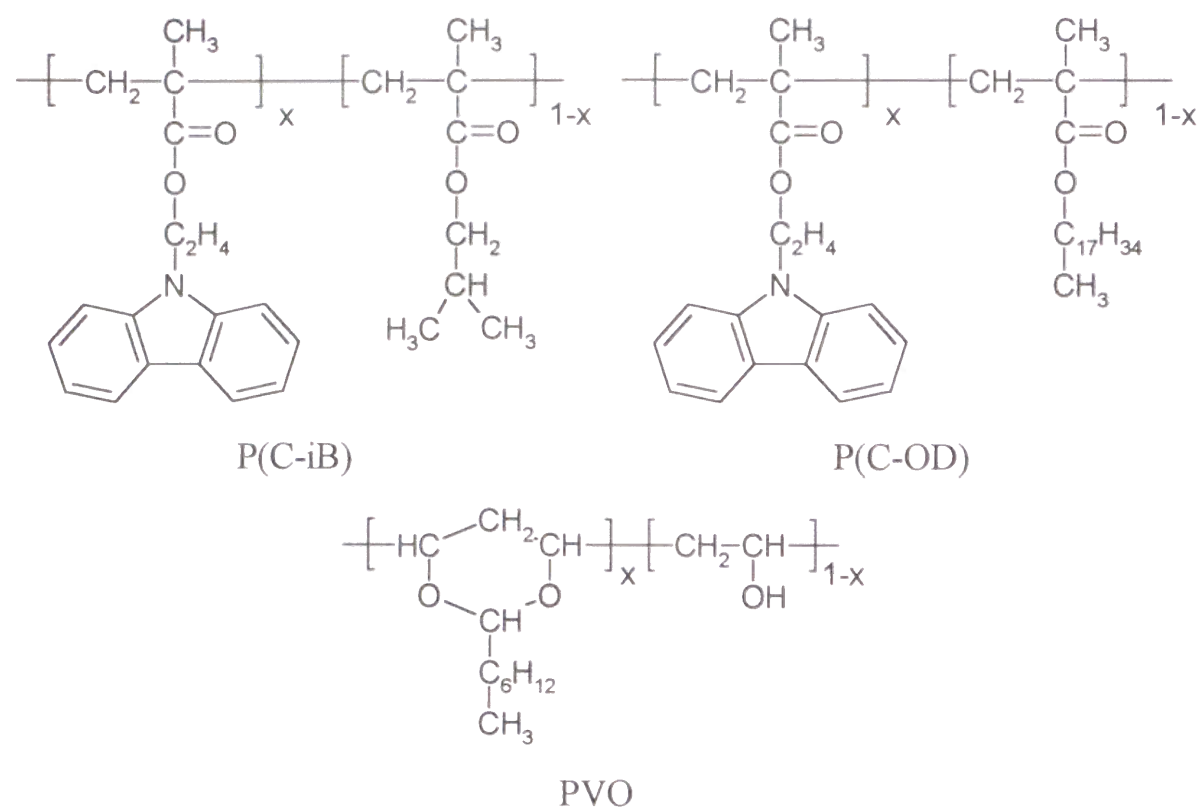
1.2.1. Materials

The chromophoric copolymers were prepared by copolymerization of 2-(9-carbazolyl)ethyl methacrylate (CzEMA) with isobutyl methacrylate or octadecyl methacrylate using azobisisobutyronitrile as an initiator. These copolymers are called P(C-iB) and P(C-OD),

Table 1–1.   Composition of Copolymers, Average Interchromophore Distance, and Surface Pressure at Deposition

Code	CzEMA content [a]	R_{2D} [b]	Π_D
	mol %	nm	mN m^{-1}
P(C-iB)5	5.6	1.98	9
P(C-iB)10	9.8	1.49	8.5
P(C-iB)15	16.3	1.32	6
P(C-OD)	15.7	1.13	20
PODMA	0	–	20
PVO	–	–	20

[a] Determined by UV absorbance.   [b] Obtained from chromophore density in the surface films (mol m^{-2}) at deposition.

respectively.   The obtained copolymers were purified by repeated reprecipitation from benzene to methanol and dried *in vacuo*.   Octadecyl methacrylate (Tokyo Kasei Kogyo Co. Ltd.) was purified by recrystallization from acetone.   Poly(vinyl octanal acetal) (PVO) was synthesized by acetalization of poly(vinyl alcohol) (dp = 2000, Wako Pure Chemical Industries, Ltd.) with octanal.   Further details for preparing P(C-iB) and PVO were described elsewhere.[11-13]   Table 1–1 shows the characteristics of the polymers.   PVO was used as spacer layers between the chromophoric layers.   PVO was also used as precoating layers and surface protection layers to avoid the effect of the interface.

1.2.2.   Sample Preparation

The 0.1 g L^{-1} benzene solution of each copolymer was spread on pure water at 19 °C. The monolayer on the water surface was transferred onto a quartz plate by the lifting up and down method at an appropriate surface pressure (Π_D).   The surface of quartz plate was cleaned in oxidative sulfuric acid, and rinsed repeatedly with water.   To make the surface of substrate hydrophobic, the plate was dipped in a 10% trimethylchlorosilane solution in toluene for 30 min.   The surface film of P(C-iB) was transferred on a hydrophobic substrate and that of P(C-OD) was transferred on a hydrophilic substrate.   For P(C-iB), the deposition rate was 15 mm min^{-1} in both up and down modes and it was maintained at 15 mm min^{-1} in down mode and 2 mm min^{-1} in up mode for P(C-OD).   Under these conditions, the transfer ratio was nearly unity and the transfer mode was in Y-type for P(C-iB) and in Z-type for P(C-OD).   The P(C-iB) LB film without spacer layers has the following layer sequence: (1) 4 layers of PVO (precoating layer); (2) L layers of P(C-iB)x (L = 2–16, x = 5–15); (3) 4 layers of PVO (surface protection layers).   The LB film of P(C-OD) was prepared with the following sequence : (1) 2 layers of poly(octadecyl methacrylate) (PODMA); (2) L layers of P(C-OD) (L = 1–4); (3) 4 layers of PVO.   The P(C-iB) LB film with spacer layers has the following layer sequence : (1) 4 layers of PVO; (2) 2 layers of P(C-iB)15; (3) 2 layers of PVO (spacer layer); (4) 2 layers of P(C-iB)15; (5) 4 layers of PVO.   Hereafter, these films are called iBx(L), OD(L), and iB15(4)S, respectively.   Figure 1–1 illustrates the structures of the LB films.   The average distance (R_{2D}) between the carbazole chromophores in a 2-dimensional plane was calculated from the composition of polymers and the surface area at the deposition.   The data are summarized in Table 1–1.
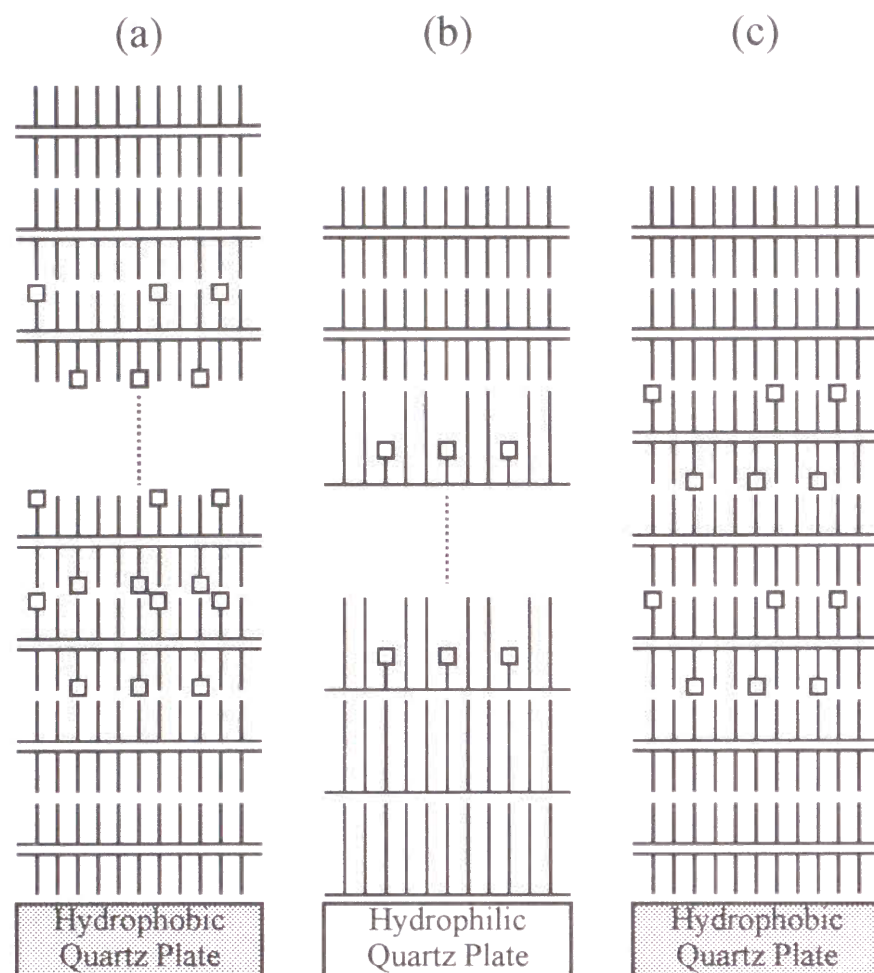
Figure 1–1. Schematic illustration of the multilayer structure of the LB films. Squares represent carbazole chromophores: (a) iB$x(L)$; (b) OD(L); (c) iB15(4)S.

1.2.3. Measurements

Steady state phosphorescence spectra were recorded with a Hitachi 850 spectrofluorophotometer fitted with a phosphorescence attachment. Phosphorescence decay curves were measured by a phosphorimeter assembled in our laboratory using a nitrogen laser as the excitation light source. The details of the system have been described elsewhere.[6] All spectroscopic measurements were performed at 77 K.

1.3. Results and Discussion
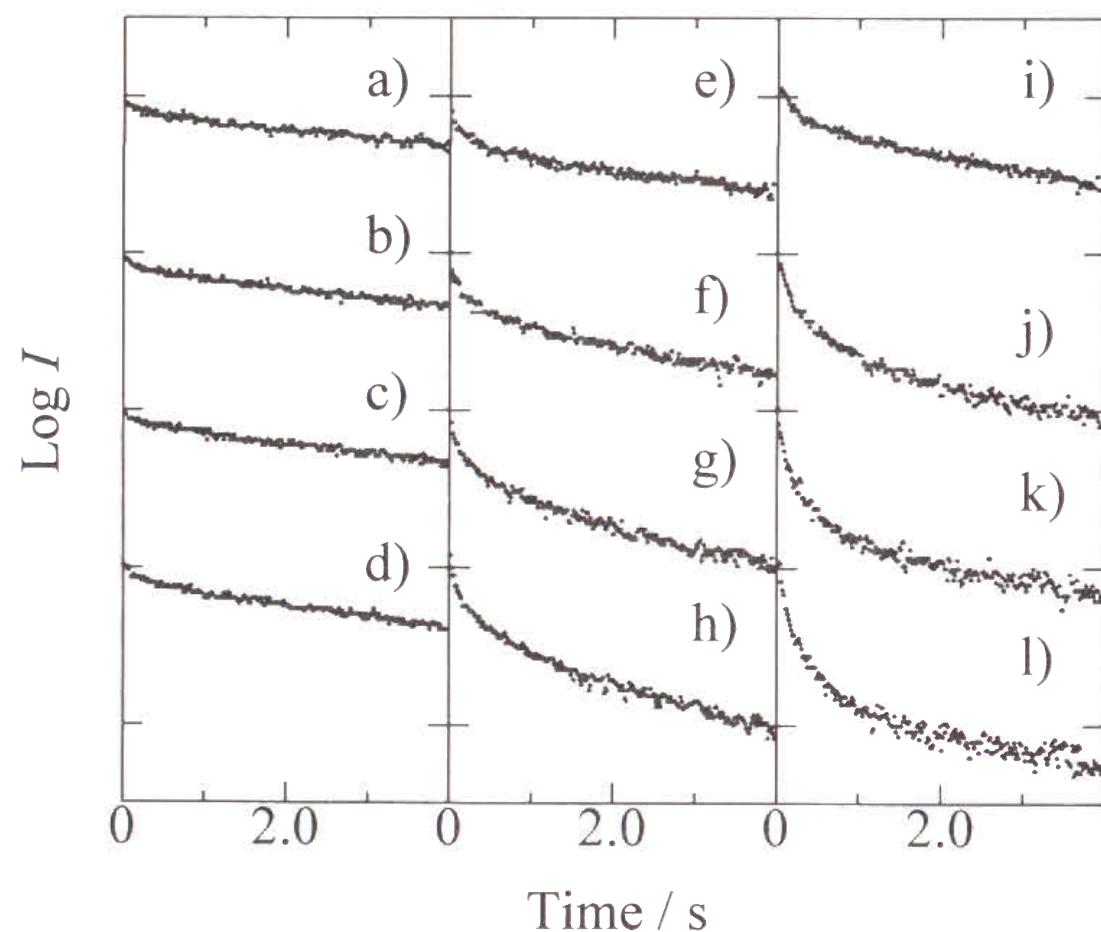
1.3.1. Phosphorescence Characteristics of iB$x(L)$
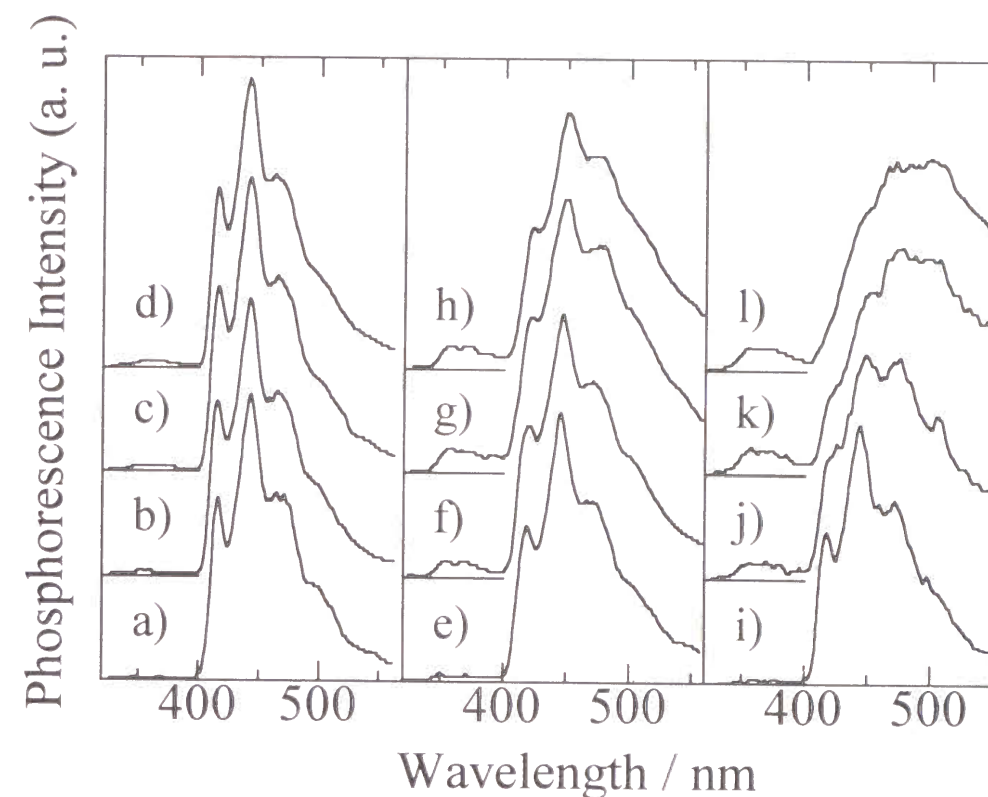
Figure 1–2. Phosphorescence spectra for P(C-iB) LB films: (a) iB5(2); (b) iB5(4); (c) iB5(8); (d) iB5(16); (e) iB10(2); (f) iB10(4); (g) iB10(8); (h) iB10(16); (i) iB15(2); (j) iB15(4); (k) iB15(8); (l) iB15(16). The excitation wavelength is 337 nm. Spectra are recorded with a bandwidth of 10 nm and normalized to the same intensity at the maximum.

Figure 1–2(a) shows the phosphorescence spectra for iB5(L). All the samples exhibit almost the same emission spectra, consisting of the monomer phosphorescence of carbazole chromophore. This indicates that the triplet state chromophores in the P(C-iB)5 LB films have no obvious interaction with neighboring chromophores, and form no stabilized site such as a triplet excimer or a trap site. Figure 1–3(a) shows the phosphorescence decay curves for iB5(L). The phosphorescence decay curves are almost single-exponential function with a lifetime of 8–9 s for all samples. The lifetime is the same as that of an isolated carbazole chromophore in an amorphous film of P(CzEMA-*co*-MMA).[6] The fast decay component seen at the early stage of decay profiles is probably due to the T–T annihilation. In the iB5(L), triplet energy migration hardly occurs, since the R_{2D} is 1.90 nm and is larger than the critical radius (R_0) of the triplet energy transfer: R_0 between carbazole chromophores must be less than 1.5 nm.[14-16] Therefore the T–T annihilation in iB5(L) probably occurs between two neighboring chromophores, both of which are simultaneously excited. The faint delayed

fluorescence for iB5(*L*) supports this inference. Another reason for the occurrence of T–T annihilation is due to the short repetition cycle of laser pulse (1 rps). This repetition cycle is short compared with the triplet lifetime of carbazole. Hence this short repetition cycle may cause store up of the triplet states and may enhance the T–T annihilation.

Figures 1–2 (b) and 1–2 (c) show the phosphorescence spectra for iB10(*L*) and iB15(*L*). The spectrum for *L* = 2 and that for *L* = 4 are quite different. The former is identical to the monomer phosphorescence, but the latter is the phosphorescence of *trap site* or *excimer site*. The spectra for more layers than four are composed of trap phosphorescence for iB10(*L*) and excimer phosphorescence for iB15(*L*). Figures 1–3(b) and 1–3(c) show the phosphorescence decay curves for iB10(*L*) and iB15(*L*). All decay curves show a multiexponential profile. As shown in Figure 1–2, delayed fluorescence emission observed around 350 nm is faint for iB10(2) and iB15(2), while it is clearly observed for *L* = 4, 8 and 16. Therefore, the steep
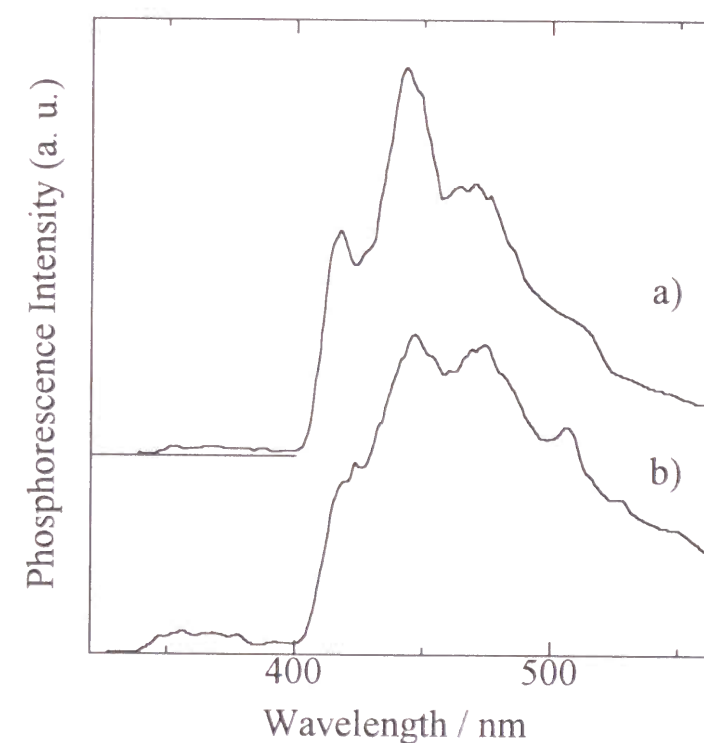
decays in the early stages for *L* = 4, 8 and 16 are ascribed to the T–T annihilation. This indicates that the triplet energy migration in *L* = 4, 8 and 16 occurs more vigorously than in *L* = 2. These findings suggest that the average interchromophore distances for *L* = 4, 8 and 16 are shorter than that for *L* = 2.

1.3.2. Phosphorescence Characteristics of iB15(4) and OD(*L*)

Figure 1–4 shows a comparison of the phosphorescence spectra for P(C-iB)15 with different layer sequences. The upper spectrum is the emission from the sample having spacer layers (iB15(4)S), and the lower is the emission from the LB film without spacer layers (iB15(4)). Both samples have 4 layers of P(C-iB)15. However, the spectrum of iB15(4)S shows the monomeric emission, whereas the one for iB15(4) shows the excimeric emission band. The sample separated with PVO layers is photophysically equivalent to iB15(2). These findings indicate the existence of interlayer interaction in iB15(4), but not in iB15(2) and iB15(4)S. Since the P(C-iB) LB films were deposited as a Y-type film, we must consider a couple of layers transferred with the downward and upward dips, as a structure unit. The

Figure 1–3. Phosphorescence decay curves for P(C-iB) LB films: (a) iB5(2); (b) iB5(4); (c) iB5(8); (d) iB5(16); (e) iB10(2); (f) iB10(4); (g) iB10(8); (h) iB10(16); (i) iB15(2); (j) iB15(4); (k) iB15(8); (l) iB15(16).

Figure 1–4. Phosphorescence spectra for P(C-iB)15 LB films with and without PVO spacer layers: (a) iB15(4)S; (b) iB15(4). Spectra are normalized to the same intensity at the maximum.

inside of a couple of layers is hydrophilic and the outside is hydrophobic and the skin is rather hydrophobic. The hydrophobic carbazole chromophore being attached to the polymer side chain should be localized at the hydrophobic surface of a pair of layers. If many layers are deposited subsequently, the chromophores easily come into contact with the next layer, even if each chromophore exists on a plane of LB films as shown in Figure 1–1(a). Therefore, the plane density of chromophores at the hydrophobic interface between two adjacent layers would be twice of that for a monolayer. Under this assumption, the average interchromophore distance at the hydrophobic interface is calculated to be 1.05 nm for P(C-iB)10 and 0.93 nm for P(C-iB)15. These values are short enough to form a "*shallow trap*" and a "*triplet excimer*", respectively.

Ahuja *et al.* investigated the pyrene fluorescence properties of monolayer at the gas/water interface with various phospholipids.[17] They found that the phospholipids having long alkyl
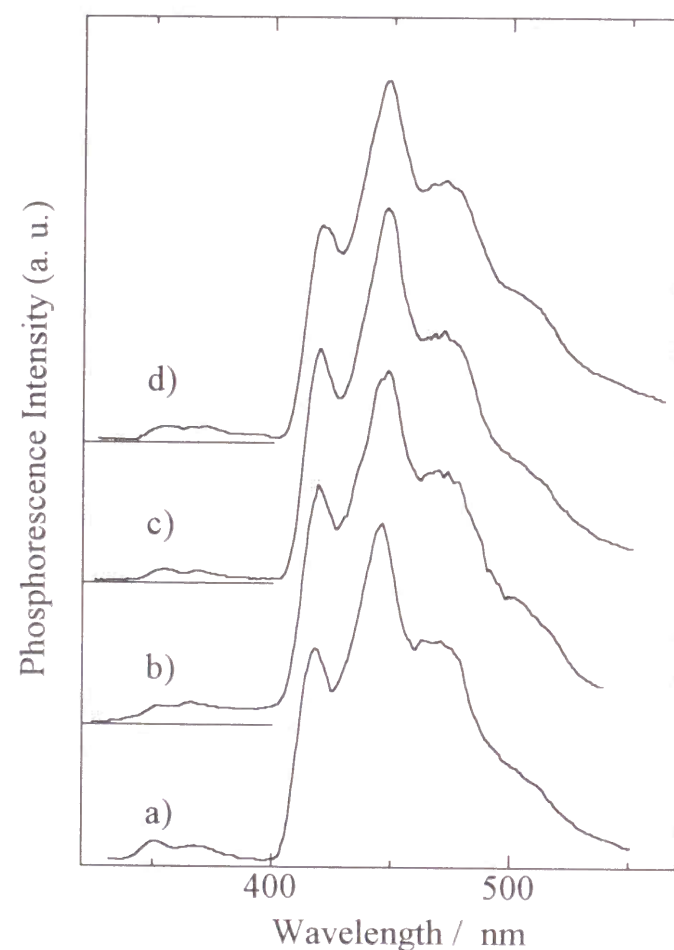
chains inhibit the quenching by oxygen, since the long alkyl chain works as a shelter for the pyrene. Figure 1–5 shows the phosphorescence spectra of OD(L) which has a very long side chain. These spectra are almost the same, and independent on the number of chromophoric layers, although the R_{2D} is nearly equal to that of P(C-iB)15. This result supports the discussion for P(C-iB) LB films that the chromophores come into contact with the next layer at the hydrophobic surface.

1.3.3. Comparison of Phosphorescence for LB Films and Cast Films.

Cast films of P(CzEMA-*co*-MMA) showed excimer phosphorescence and multiexponential phosphorescence decays, when the average interchromophore distance was shorter than 1.0 nm.[6] The decay profiles and the peak position of excimer phosphorescence are similar to those of iB15(4), iB15(8), and iB15(16). The average interchromophore distances for these samples are around 1.0 nm as mentioned previously. The red-shifted spectra are also observed in a cast film with an average interchromophore distance of 1.2 nm. We called this species "*shallow trap*", which is formed by stabilization with a weak interaction between chromophores. The slightly red shifted spectra and multiexponential decay profiles for iB10(4), iB10(8), iB10(16), iB15(2) and OD(L) are ascribed to the emission from "*shallow trap*". It should be noted that the R_{2D} of LB film to form a "*shallow trap*" is 1.05–1.32 nm and the value is in good agreement with the distance for the cast film: 1.2 nm. A similar relation in average distance was seen in the formation of triplet excimer. These findings suggest that the interchromophore distance is a good measure of triplet energy migration between triplet chromophores, whether the system is two dimensional LB film or three dimensional amorphous polymer film.

The drastic change in phosphorescence spectrum at a particular distance must be due to the effect of energy migration, because the carbazole chromophore in LB film and in cast film could hardly change its conformation during the lifetime at 77 K. Therefore the distance, 1.0–1.2 nm, is the critical distance at which the triplet begins to migrate vigorously in amorphous polymer matrices.

1.4. Conclusion

Figure 1–5. Phosphorescence spectra for P(C-OD) LB films: (a) OD(1); (b) OD(2); (c) OD(3); (d) OD(4). Spectra are normalized to the same intensity at the maximum.

Triplet state interactions between carbazole chromophores in polymeric LB films were determined by the interchromophore distance and were analogous to those in amorphous polymer films. The carbazole moieties are in the hydrophobic area of the LB monolayer and exhibit inter-layer interaction at the interface of the hydrophobic layers. This finding is useful for designing photofunctional LB films utilizing photophysical or photochemical processes *via* the excited triplet state.

References

1   H. Kuhn, D. Möbius, and H. Bücher, *"Physical Method of Chemistry"*, A. Weissberger and B. W. Rossiter Ed., Wiley, New York, 1972, Vol. 1, Part 3B, p 557.

2   A. Ulman, *"An Introduction to Ultrathin Organic Films —From Langmuir–Blodgett to Self-Assembly—"*, Academic Press, Boston, 1991, p 210.

3   N. Tamai, T. Yamazaki, and I. Yamazaki, *J. Phys. Chem.*, **91**, 841 (1987); I. Yamazaki, N. Tamai, and T. Yamazaki, *J. Phys. Chem.*, **91**, 3572 (1987); I. Yamazaki, N. Tamai, and T. Yamazaki, *J. Phys. Chem.*, **92**, 5035 (1988).

4   R. H. Tredgold, *Thin Solid Films*, **152**, 223 (1987).

5   K. Naito, *J. Colloid Interface Sci.*, **131**, 218 (1989).

6   S. Ito, H. Katayama, and M. Yamamoto, *Macromolecules*, **21**, 2456 (1988).

7   S. Ito, N. Numata, H. Katayama, and Yamamoto, M. *Macromolecules*, **22**, 2207 (1989).

8   H. Katayama, S. Ito, and M. Yamamoto, *J. Photopolym. Sci. Technol.*, **4**, 217 (1991).

9   H. Katayama, T. Tawa, S. Ito, and M. Yamamoto, *J. Chem. Soc. Faraday Trans.*, **88**, 2743 (1992).

10   H. Katayama, K. Hisada, M. Yanagida, S. Ohmori, S. Ito, and M. Yamamoto, *Thin Solid Films*, **224**, 253 (1993).

11   S. Ito, S. Ohmori, and M. Yamamoto, *Macromolecules*, **25**, 185 (1992).

12   S. Ohmori, S. Ito, and M. Yamamoto, *Macromolecules*, **24**, 2377 (1991).

13   S. Ohmori, S. Ito, and M. Yamamoto, *Macromolecules*, **23**, 4047 (1990).

14   V. L. Ermolaev, *Sov. Phys. Dokl.*, **6**, 600 (1962).

15   H. Katayama, S. Maruyama, S. Ito, Y. Tsujii, A. Tsuchida, and M. Yamamoto, *J. Phys. Chem.*, **95**, 3480 (1991).

16   H. Katayama, S. Ito, and M. Yamamoto, *J. Phys. Chem.*, **96**, 10115 (1992).

17   R. C. Ahuja and D. Möbius, *Langmuir*, **8**, 1136 (1992).

Chapter 2

Triplet Energy Transfer from Carbazole to Bromonaphthalene in a Two-Dimensional Chromophore Plane Prepared by Poly(octadecyl methacrylate) Langmuir–Blodgett Films

2.1. Introduction

The Langmuir–Blodgett technique is an effective method to fabricate artificial molecular assemblies. It enables one to control the thickness of the layers by modifying the chain length of amphiphilic molecules. It is also possible to form a highly ordered film having a preferential orientation to the film plane. Since one can expect to open new aspects of chemical, physical, and biological processes in this uniquely ordered environment, extensive studies have been made on LB films for the past several decades.[1-3]

In the field of photophysics and photochemistry, Kuhn *et al.* studied fundamental photophysical processes.[4] They realized that basic photoprocesses such as singlet energy transfer and electron transfer can be controlled by the "nanostructure" assembled in LB multilayers. They found that the Förster theory[5] for the singlet energy transfer successfully expresses the real systems. Yamazaki *et al.* performed fluorescence spectroscopy using the picosecond single-photon-counting technique.[6] Although the system showed stepwise energy transfer from a donor to acceptors, the chromophores in the LB films of fatty acids became aggregated and formed a fractal distribution in the two-dimensional plane. They concluded that control of the chromophore distribution is one of the key points in constructing photofunctional LB films. The highly ordered structure of these fatty acids is suitable for studying photophysical processes in molecular assemblies, but the multilayers usually do not have much stability; they undergo irreversible degradation readily when exposed to moisture or at an elevated temperature.[7-10]

Recently, some preformed polymers were found to form a stable monolayer at the air–

water interface and to be transferable to solid substrates.[11-20] Ohmori *et al.* have used poly(vinyl octanal acetal) (PVO) as a base polymer for realizing a uniform chromophore distribution in a two-dimensional plane, in which the chromophores were attached to the polymer main chain with covalent bonds.[21,22] The singlet energy transfer in the polymeric LB films was well characterized and controlled by the layered structure, while the quantitative analysis of the transfer efficiency revealed a slight disordering of the LB films after the deposition on the substrate. The regularity of LB films prepared by PVO is not sufficient to control triplet energy transfer because triplet energy transfer takes place at a short interchromophore distance (0.6–1.5 nm), *i.e.*, more precise regulation of chromophore distribution is required for this purpose.

Rabolt *et al.* studied the LB films made from poly(octadecyl methacrylate) (PODMA) using polarized infrared spectroscopy.[23-25] They found that the hydrophobic side chain linked to a hydrophilic main chain shows a high degree of orientation, and surprisingly the orientation is maintained after thermal treatment.

This chapter demonstrates the control of triplet energy transfer in a two-dimensional plane prepared by such polymeric LB films. PODMA is employed as a base polymer bearing chromophoric units, since it is expected to have a well-ordered layer structure. Because of the high quality of this polymeric LB film, the chromophores are expected to situate exactly in a two-dimensional plane in the thickness of PODMA monolayer. The triplet energy transfer is equivalent to electron transfer in essence. Therefore, the LB film can be regarded as a model system for observing, characterizing and controlling electron transfer phenomena in ultrathin
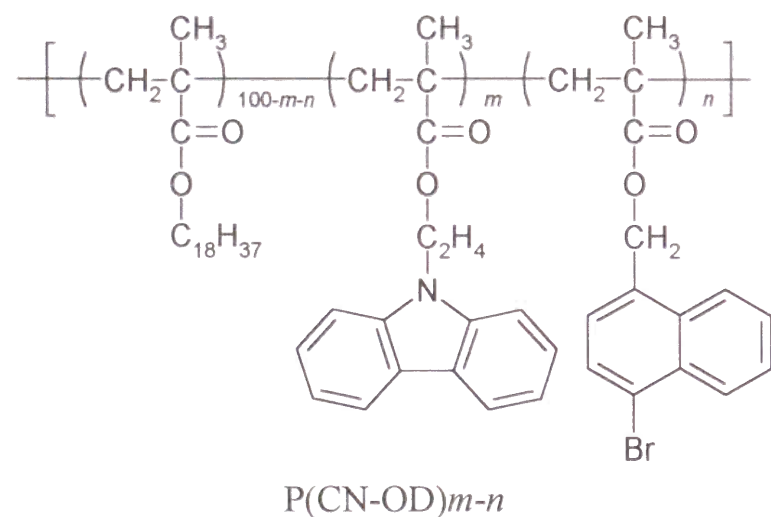
polymer films.

2.2. Experimental Section

2.2.1. Materials

The synthetic method for 2-(9-carbazolyl)ethyl methacrylate (CzEMA) was described previously by Ito *et al.*[26] 4-Bromo-1-naphthaldehyde was synthesized according to the procedure of Shiotani *et al.*[27] 4-Bromo-1-naphthylmethanol was obtained by reduction of 4-bromo-1-naphthaldehyde with sodium borohydride in ethanol. Repeated recrystallization from hexane solution gave white crystals: mp 97–99 °C; ^{1}H NMR(CDCl₃) δ 5.25 (s, 2H, methylene), 7.2–8.4 (m, 6H, aromatic). (4-Bromo-1-naphthyl)methyl methacrylate (BNMMA) was synthesized by esterification of 4-bromo-1-naphthylmethanol with methacryloyl chloride (Tokyo Chemical Industry). Recrystallization from a mixed solvent of methanol and water gave white crystalline BNMMA: mp 82–84 °C; ^{1}H NMR(CDCl₃) δ 1.95 (s, 3H, methyl), 5.60 (m, 1H, vinyl), 6.12 (s, 1H, vinyl), 7.2–8.4 (m, 6H, aromatic). Octadecyl methacrylate (ODMA) (Tokyo Chemical Industry) was purified by recrystallization several

P(CN-OD)*m-n*

Table 2–1. Compositions of Poly(octadecyl methacrylate) Copolymers and Average Distances between Cz Residues

Sample	CzEMA content [a] / mol %	BNMMA content [a] / mol %	R_{D-D} [b] / nm
P(CN-OD)5-0	5.3	0	2.07
P(CN-OD)5-0.5	5.2	0.47	2.04
P(CN-OD)5-1	5.1	1.0	2.04
P(CN-OD)5-2	5.0	2.1	1.96
P(CN-OD)5-4	5.2	4.1	1.98
P(CN-OD)15-0	15.7	0	1.13
P(CN-OD)15-0.1	15.4	0.14	1.13
P(CN-OD)15-0.8	15.3	0.75	1.12
P(CN-OD)15-1	15.2	1.3	1.19
P(CN-OD)15-3	14.7	3.4	1.06
P(N-OD)	0	11.0	-

[a] Determined by UV absorbance. [b] Calculated by $R_{D-D} = n^{-(1/2)}$, where n is the average number of carbazole groups per unit area.
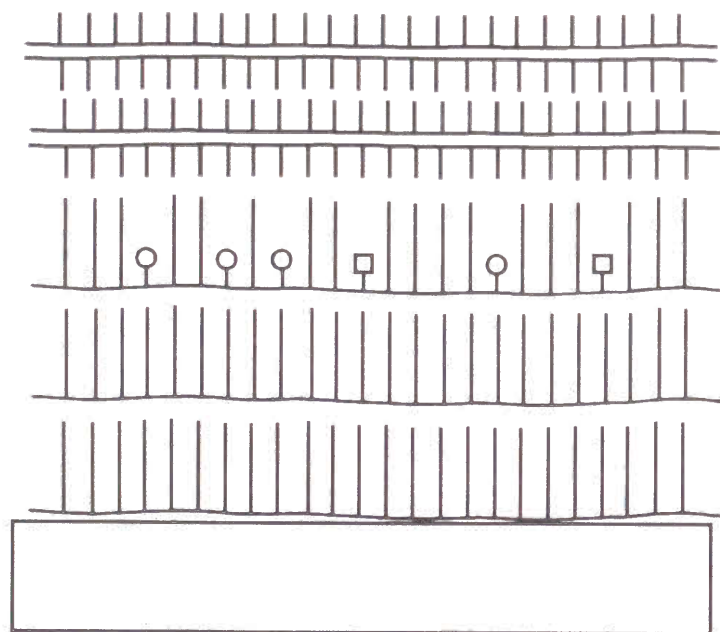
times from methanol or acetone before use.

These monomers, CzEMA, BNMMA, and ODMA, were dissolved in benzene with a small amount of 2,2'-azobis(isobutylonitrile) and polymerized at 60 °C for 20 h. The obtained three-component copolymers, P(CN-OD), were purified by repeated reprecipitation from benzene to methanol and lyophilized from a benzene solution. Table 2–1 shows the characteristics of the polymers. The composition of copolymers is expressed by the addition of numbers such as P(CN-OD)*m-n*, where *m* is the mole percent content of CzEMA units and *n* is that of BNMMA units.

PVO was synthesized by acetalization of poly(vinyl alcohol) with octanal,[22] that was used as a protecting layer of P(CN-OD) LB films.
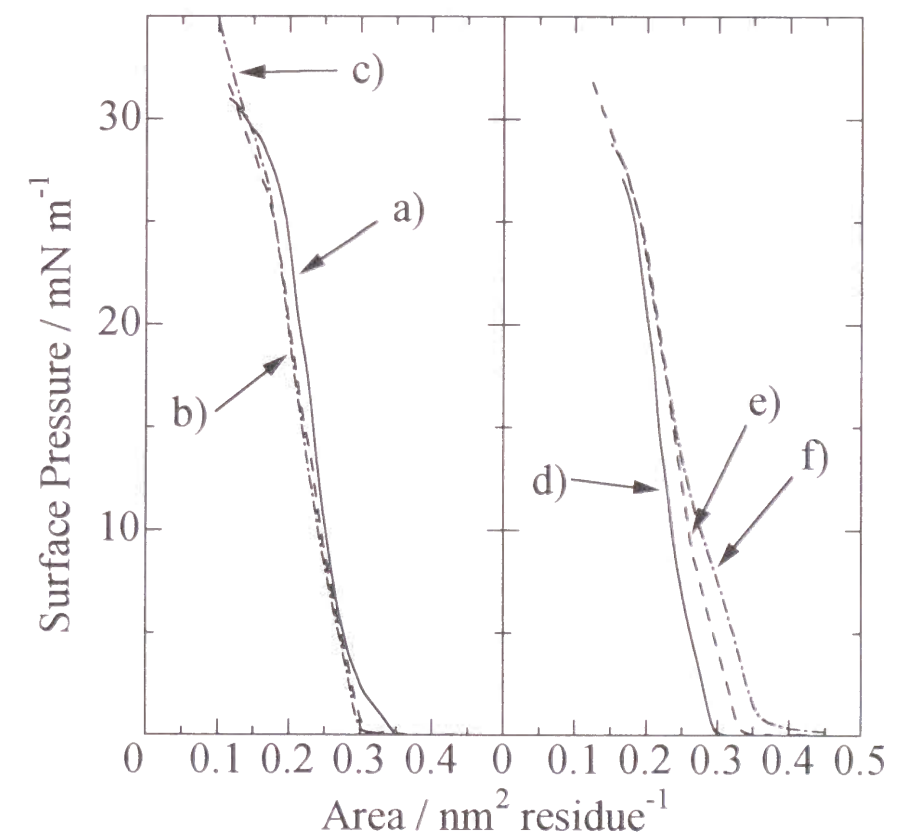
2.2.2. Sample Preparation

Water in the subphase was deionized, distilled, and passed through a water purification system (Barnstead Nanopure II). The sample was spread on the surface of pure water from a dilute benzene solution (*ca.* 0.1 g L^{-1}) at 20 °C, and then the solvent was allowed to evaporate. The compression rate of surface film was maintained at 15 cm^2 min^{-1}. The surface pressure–area (Π–A) isotherm was recorded by using a Wilhelmy type film balance (Shimadzu ST-1). The employed substrate for the emission measurements was the nonfluorescent quartz plate (20

$\times$ 40 mm). The quartz plates were cleaned in oxidative sulfuric acid, dipped in 10% hydrogen peroxide solution, and then rinsed with water. Silicon wafers (10 $\times$ 40 mm), used for ellipsometry, were cleaned with ethanol. The surface film was transferred vertically onto the substrate at a surface pressure of 20 mN m^{-1} for PODMA and PVO, and 17.5 mN m^{-1} for P(CN-OD). For PODMA and P(CN-OD), the deposition rate was 15 mm min^{-1} in down mode and 2 mm min^{-1} in up mode. For PVO, the rate was 15 mm min^{-1} in both up and down modes. The transfer ratio was nearly unity and the transfer mode was the Z-type for PODMA and P(CN-OD), and the Y-type for PVO. In the case of PODMA and P(CN-OD), a drying period of 30 min between subsequent dips was necessary to prevent retransfer of the previously deposited monolayer during the following dips.

Figure 2–1 illustrates the structure of the LB films for the emission measurements. On a quartz plate, polymers were deposited in the following order: (1) two layers of PODMA; (2) a layer of P(CN-OD); (3) four layers of PVO. Since PODMA takes a Z-type deposition, we can observe only intralayer interaction of chromophores and obtain the information on one

Figure 2–1. Schematic illustration of the multilayer structure of the polymeric LB films. Circles represent carbazole chromophores, and squares are bromonaphthalene chromophore.

Figure 2–2. Surface pressure–area isotherms of PODMA copolymers: (a) PODMA; (b) P(CN-OD)15-0; (c) P(CN-OD)15-0.1; (d) P(CN-OD)15-0.8; (e) P(CN-OD)15-1; (f)P(CN-OD)15-3.

chromophoric layer. PODMA and PVO were deposited to remove the effects of interface. For ellipsometry, *l* layers of PODMA (*l* = 1–4) were deposited onto a silicon substrate to measure the thickness of the transferred film.

2.2.3. Measurements

The phosphorescence spectra were recorded with a Hitachi 850 spectrophotometer equipped with a phosphorescence attachment involving a rotating light chopper between the excitation light source and the sample holder. The use of the chopper and a gated electric circuit allowed us to collect selectively the delayed emission later than 1 ms after the excitation. The total emission including both the phosphorescence and fluorescence could be recorded when the chopper was turned off. Sample LB films were immersed into liquid nitrogen in a quartz Dewar vessel. All the emission spectra were recorded with excitation wavelength at 340 nm; this light is not absorbed by the triplet quencher. The lowest singlet state of bromonaphthalene is at a higher energy level than that of carbazole, so that bromonaphthalene does not quench the lowest singlet state of carbazole.

The thickness of the build-up films was measured by an ellipsometer (Mizojiri Kogaku).
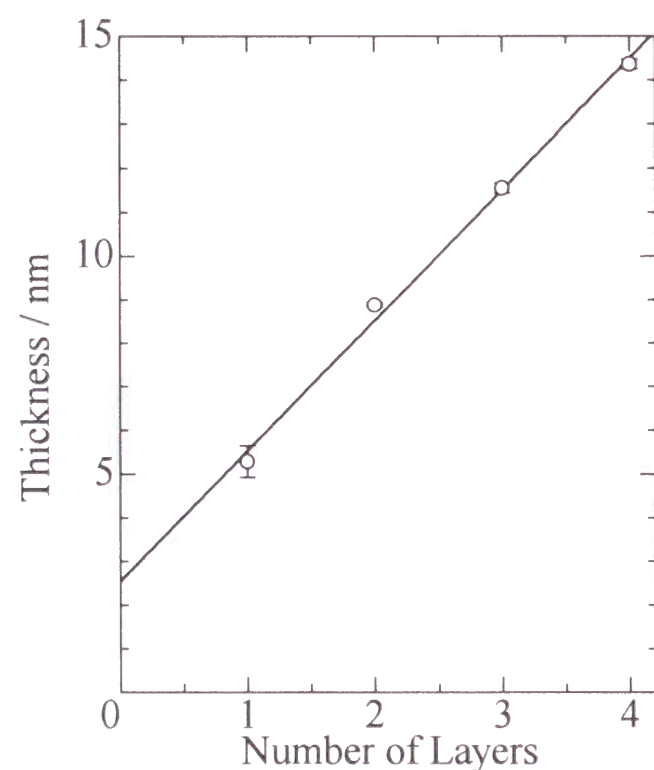
Figure 2–3.   Film thickness vs number of layers for the build-up film of PODMA measured by ellipsometry.

2.3. Results and Discussion

2.3.1.   Surface Pressure–Area Isotherms

Figure 2–2 shows the *Π–A* isotherms of PODMA and P(CN-OD) on pure water at 20 °C. The *Π–A* isotherm of PODMA indicates the formation of a stable condensed monolayer, characterized by a steep rise of the surface pressure and by the high collapse pressure. The *Π–A* isotherms of P(CN-OD) with high chromophore contents, such as P(CN-OD)15-1 and P(CN-OD)15-3, gave somewhat expanded profiles, but the surface area at the deposition was nearly the same for all copolymers. In Figure 2–2, the most packed area per repeat unit in a monolayer, which is attained just before the collapse, is *ca.* 0.20 nm^2. This value is reasonable with the optimum packing area of alkyl side chain.

### 2.3.2.   Deposition of Surface Films onto Solid Substrates

To verify the deposition of the surface film of PODMA onto the substrate, the thickness
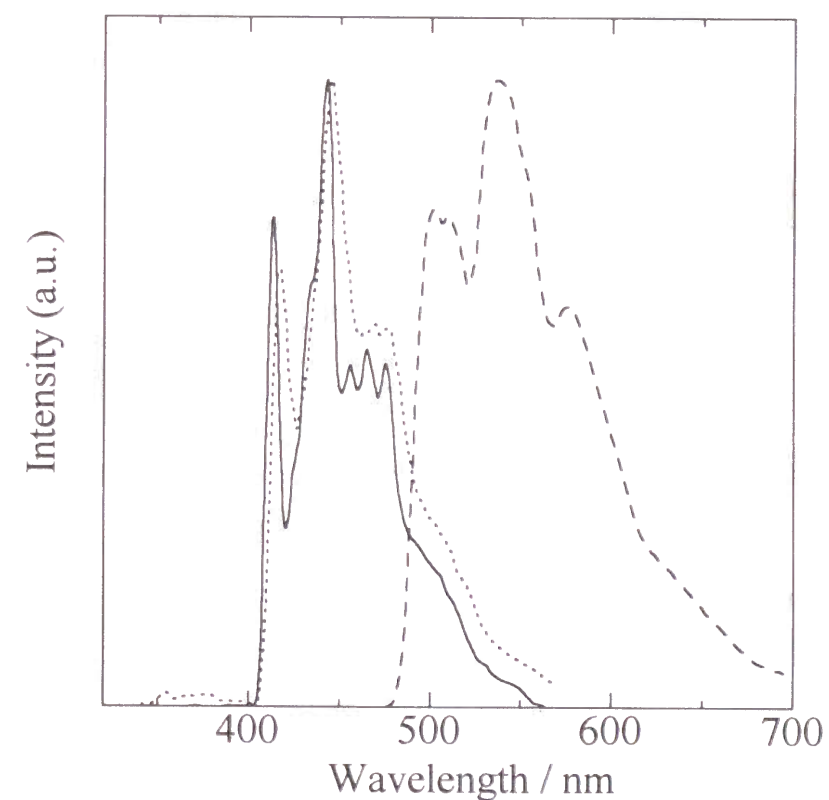
Figure 2–4.   Phosphorescence spectra for the cast films of PODMA copolymers: P(CN-OD)5-0 (——); P(CN-OD)15-0 (- - - -); P(N-OD) (– – –). Spectra are normalized to the same intensity at the maximum.

of the transferred films was determined by ellipsometry. Figure 2–3 shows the thickness of PODMA LB films for various numbers of layers. The linearity of the thickness vs the number of layers was confirmed at least up to four layers. The thickness at zero layer shows the value of the oxidized silicon layer at the surface of the wafer. Assuming that the PODMA layers have a refractive index similar to that of poly(hexadecyl methacrylate): $n^{30} = 1.475$,[28] the layer thickness was estimated to be 3.01 nm from the slope in Figure 2–3. This value is in fair agreement with Mumby's data for PODMA Z-film.[25] This result shows that the surface film of PODMA can be satisfactorily transferred onto the substrate.

2.3.3. Phosphorescence Spectra
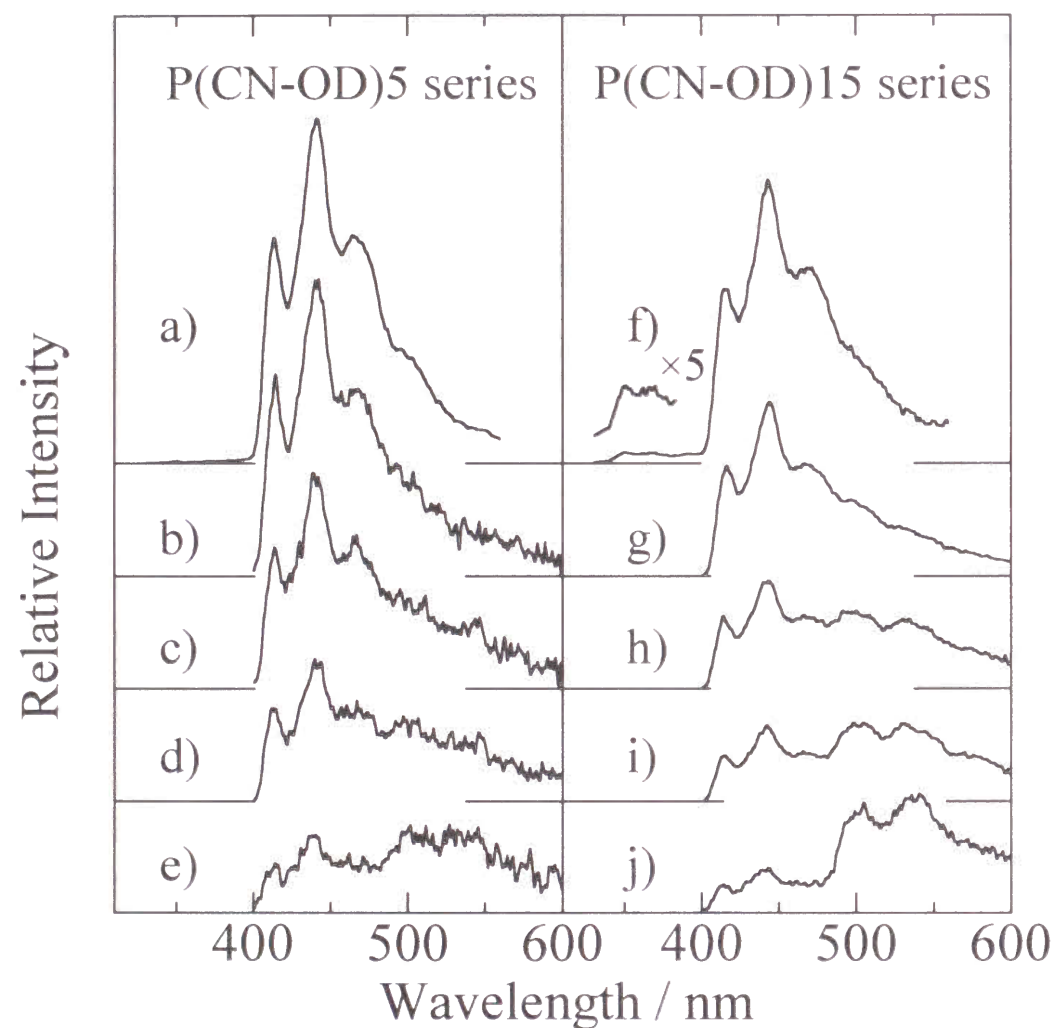
Figure 2–5. Phosphorescence spectra for the LB films of PODMA copolymers: (a) P(CN-OD)5-0; (b) P(CN-OD)5-0.5; (c) P(CN-OD)5-1; (d) P(CN-OD)5-2; (e) P(CN-OD)5-4; (f) P(CN-OD)15-0; (g) P(CN-OD)15-0.1; (h) P(CN-OD)15-0.8; (i) P(CN-OD)15-1; (j)P(CN-OD)15-3.

Figure 2–4 shows the phosphorescence spectra of carbazole and bromonaphthalene moieties in the thick polymer films prepared by the solution cast method. The emission spectrum of P(CN-OD)15-0 is slightly broadened and red-shifted compared to the spectrum of P(CN-OD)5-0. This result indicates that carbazole groups in P(CN-OD)15-0 make shallow traps.[29] However, no excimeric emission, i.e., structureless broadened and red-shifted emission, was seen at all. The phosphorescence emission of P(N-OD), which contains only bromonaphthalene units, appears at ca. 500 nm. The emission is observed at a much longer wavelength than that of carbazole moiety. This means that bromonaphthalene can act as an effective energy acceptor to the carbazole triplet.

Figure 2–5 shows the delayed emission spectra of the LB films. The intensities are normalized by the fluorescence intensities at 367 nm measured without rotating the light chopper. This procedure effectively reduces the error in the measurement of phosphorescence intensities less than a few percent. The delayed emission of P(CN-OD)5-0 LB film showed the phosphorescence only from the carbazole unit at 412, 440 and 460 nm, but P(CN-OD)15-0 LB film gave both phosphorescence and delayed fluorescence around 360 nm. The critical distance for energy migration between carbazole chromophores is known to be 1.0–1.2 nm obtained by the previous works for the cast films and LB films.[29,30] The average distances between the carbazole residues in the present LB films are estimated to be 1.9–2.1 nm for the P(CN-OD)5-n series and 1.0–1.2 nm for the P(CN-OD)15-n series provided that

Table 2–2. Quenching Efficiencies of Carbazole Phosphorescence in P(CN-OD) LB Films

Sample	$[BN]_{2D} \times 10^8$ [a] / mol m^{-2}	Qe
P(CN-OD)5-0.5	3.62	0.18
P(CN-OD)5-1	8.17	0.36
P(CN-OD)5-2	18.2	0.58
P(CN-OD)5-4	33.5	0.79
P(CN-OD)15-0.1	1.18	0.27
P(CN-OD)15-0.8	6.09	0.56
P(CN-OD)15-1	10.1	0.72
P(CN-OD)15-3	26.4	0.86
P(CN-OD)15-5	45.2	0.96

[a] Calculated from the surface area at the deposition.

chromophores uniformly distribute in a two-dimensional plane. This means that energy migration is possible in the P(CN-OD)15-*n* LB films. The quenching efficiency of carbazole phosphorescence (Qe) was determined from the normalized phosphorescence intensity at 412 nm. Table 2–2 shows the values of Qe and acceptor density in one plane. The acceptor density in the LB film was taken to be equal to the acceptor density in the surface film at the deposition. The values of Qe for P(CN-OD)15-*n* films are obviously higher than those for P(CN-OD)5-*n* at the same acceptor density in a plane.

2.3.4. Evaluation of the Distribution of Chromophores

In this section, we consider two types of distribution of chromophores in the monolayer of PODMA as shown in Figure 2–6: one (A) is that they distribute exactly in one plane and the

other (B) is that the chromophores distribute randomly within the interior of PODMA monolayer, 3.0 nm. In the case of B, the active spheres are not completely situated within the interior of the monolayer. To take into account this effect, the volume fraction of the active sphere involved in a PODMA monolayer (V_f) was estimated assuming the random distribution of the centers of the active spheres in a thickness of 3.0 nm. When R_A is greater than $d/2$, V_f is calculated as follows.

Figure 2–6. Schematic illustration of chromophore distributions for the active sphere model: (A) distribution exactly in a two-dimensional plane; (B) distribution randomly within the interior of a monolayer. White squares and black squares represent donors and acceptors, respectively.
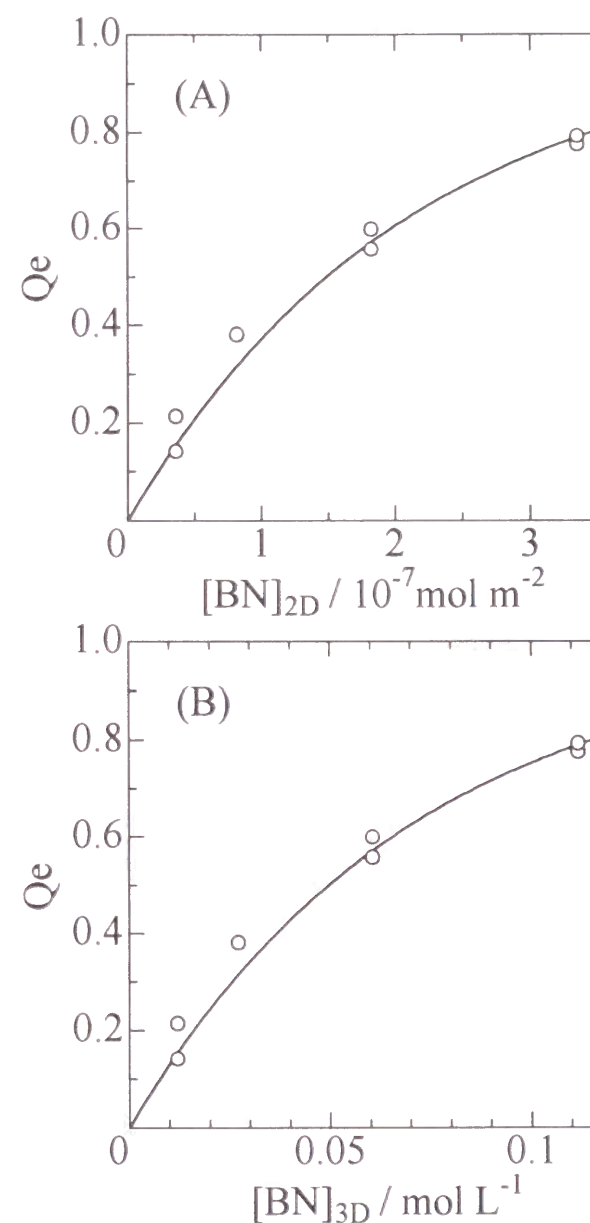
Figure 2–7. Acceptor concentration dependence of quenching efficiency of carbazole phosphorescence of P(CN-OD)5-*n* films: (A) the chromophores distribute exactly in one plane; (B) the chromophores distribute randomly within the interior of PODMA monolayer. Solid lines were calculated with (A) R_A = 1.57 nm and (B) R_A = 1.94 nm.

$$V_f = \frac{\int_0^{d-R_A} \mathrm{d}x \int_{-x}^{R_A} \pi\left(R_A^2 - X^2\right)\mathrm{d}X + \int_{d-R_A}^{d/2} \mathrm{d}x \int_{-x}^{d-x} \pi\left(R_A^2 - X^2\right)\mathrm{d}X}{\int_0^{d/2} \frac{4}{3}\pi R_A^3 \, \mathrm{d}x} \qquad (2\text{-}1)$$

where R_A is the quenching radius of the active sphere, d the thickness of a monolayer, and x the distance between the center of active sphere and the boundary of the chromophoric monolayer. The quenching efficiencies for both cases A and B were calculated from the following equations.

In the case of A

$$Qe = 1 - \exp\left\{-\left(\pi R_A^2\right)N_A[A]_{2D}\right\} \qquad (2\text{-}2)$$

In the case of B

$$Qe = 1 - \exp\left\{-\left(\frac{4}{3}\pi R_A^3\right)V_f N_A[A]_{3D}\right\} \qquad (2\text{-}3)$$

where $[A]_{2D}$ is the two-dimensional acceptor density in a plane, $[A]_{3D}$ the three-dimensional acceptor concentration within the volume of monolayer, and N_A the Avogadro's number. As shown in Figure 2–7, both models can reproduce the values of Qe very well, when an appropriate value of R_A is chosen. For P(CN-OD)5-*n* series, the active radius is 1.57 nm for case A and 1.94 nm for case B. Ermolaev reported the active radius for carbazole–naphthalene pair in a rigid solution is 1.5 nm,[31] and Katayama *et al.* obtained a similar value R_A = 1.5 nm for the carbazole–naphthalene intramolecular system.[32] By a comparison of these results, it is concluded that case A is appropriate and the chromophores distribute in a plane within the interior of the P(CN-OD) monolayer.

The reason why the chromophores can be fixed at a certain position by using LB films of PODMA is explained as follows. Rabolt *et al.* and Wegner *et al.* studied the orientation of alkyl side chain of PODMA monolayer and multilayer on solid substrate using polarized infrared spectroscopy.[11,24,25] Both authors concluded the orientation of alkyl side chains to be approximately perpendicular to the substrate. Wegner *et al.* estimated that four to eight methylene units are needed as spacer units, which fix the amorphous polymer backbone to the crystallized portion of alkyl side chains. That estimation is in agreement with the results from the bulk states.[33,34] The crystalline region of the side chains maintains the structure of multilayer in a highly ordered state. The chromophores are closely attached to the main chain and they will be located at the amorphous region. The crystallized methylene units make the
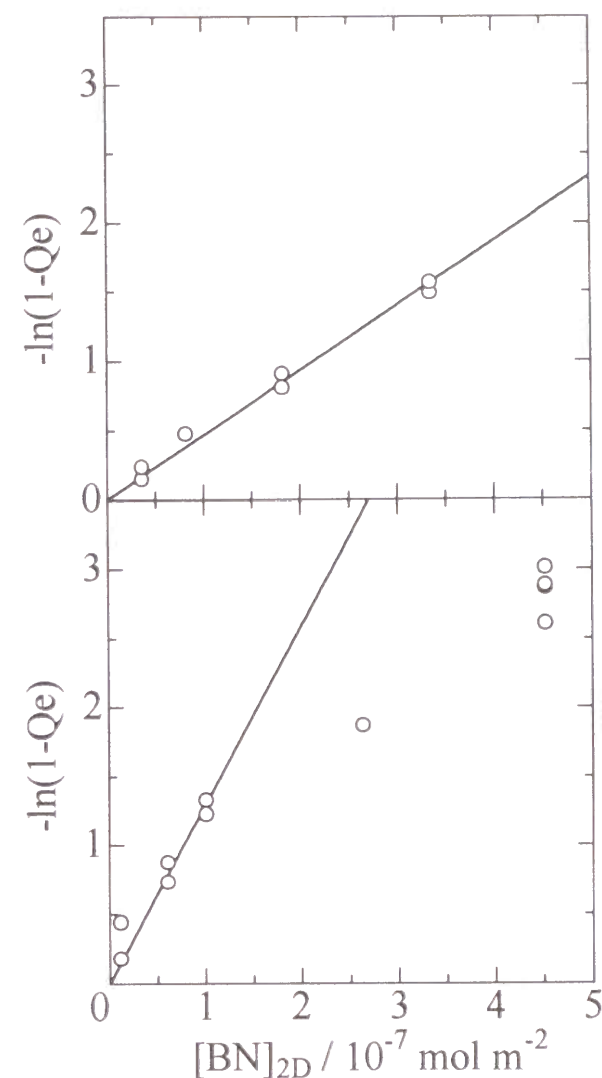
Figure 2–8. Perrin plot for the quenching efficiency of carbazole phosphorescence at 77 K: (a) P(CN-OD)5-*n* LB films; (b) P(CN-OD)15-*n* LB films.

chromophores arrange in a two-dimensional plane with the range of a few angstroms.

When the carbazole content is 15 mol %, a Perrin plot does not give a straight line (Figure 2–8b). The active radius was estimated from the initial slope: R_A = 2.55 nm. The active radius is much greater than the previous value because in this system carbazole triplets are quenched by a dynamic process, *i.e.*, a few steps of energy migration among the donors, and then followed by an energy transfer to the acceptor. In the active sphere model, we presume that there is no diffusion of chromophores and excitons. So this model cannot be applied to P(CN-OD)15-*n* LB films because efficient energy migration takes place. To analyze this high donor content system, time evolution of energy trapping processes in a two-dimensional plane will be simulated in the next chapter, by solving the differential equations relevant to the energy migrations and the energy transfers.

2.4. Conclusion

Triplet energy transfer between carbazole and bromonaphthalene moieties was measured in a two-dimensional plane made by LB films of poly(octadecyl methacrylate). When the carbazole content was 5 mol %, the dependence of the quenching efficiency of the carbazole triplet upon the bromonaphthalene density was represented by the active sphere model assuming a planar chromophore distribution. This indicates that the chromophores in LB films of poly(octadecyl methacrylate) situate in a planar distribution within the range of a few angstroms. Therefore the LB technique using such a preformed polymer allows us to construct molecular systems involving a triplet energy transfer process. The triplet energy transfer is mechanistically equivalent to the electron transfer because it takes place through electron exchange interaction. This suggests that the LB film made from this polymer is able to regulate an electron transfer process, too. High crystallinity of the alkyl side chain plays an important role in the regulation of chromophore distribution.

References

1   H. Ringsdorf, G. Schmidt, and J. Schneider, *Thin Solid Films*, **152**, 207 (1987).

2   H. Kuhn, *Thin Solid Films*, **178**, 1 (1989).

3   G. Wegner, *Ber-Bunsen. Ges. Phys. Chem.*, **95**, 1326 (1991).

4   H. Kuhn, D. Möbius, and H. Bücher, *"Physical Methods of Chemistry"*, A. Weissberger, and B. W. Rossiter, Wiley, New York, 1972, Vol. 1, Part 3B, p577.

5   Th. Förster, *Z. Naturforsch.*, **4A**, 321 (1949).

6   T. Yamazaki, N. Tamai, and I. Yamazaki, *Chem. Phys. Lett.*, **124**, 326 (1986); N. Tamai, T. Yamazaki, and I. Yamazaki, *J. Phys. Chem.*, **91**, 841 (1987); *Chem. Phys. Lett.*, **147**, 25 (1988); I. Yamazaki, N. Tamai, and T. Yamazaki, *J. Phys. Chem.*, **91**, 3572 (1987); I. Yamazaki, N. Tamai, T. Yamazaki, A. Murakami, M. Mimuro, and Y. Fujita, *J. Phys. Chem.*, **92**, 5035 (1988).

7   K. B. Blodgett, *Phys. Rev.*, **55**, 391 (1939).

8   E. Stenhagen, *Trans. Faraday Soc.*, **34**, 1328 (1938).

9   G. L. Gaines, and R. W. Robert, *Nature (London)*, **197**, 787 (1963).

10   C. Naselli, J. F. Rabolt, J. D. Swalen, *J. Chem. Phys.*, **82**, 2136 (1985); *Thin Solid Films*, **134**, 173 (1985).

11   G. Duda, A. J. Schouten, T. Arndt, G. Lieser, G. F. Schmidt, C. Bubeck, and G. Wegner, *Thin Solid Films*, **159**, 221 (1988); A. J. Schouten and G. Wegner, *Makromol. Chem.*, **192**, 2203 (1991); T. Arndt, A. J. Schouten, G. F. Schmidt, and G. Wegner, *Makromol. Chem.*, **192**, 2215 (1991).

12   C. S. Winter, R. H. Tredgold, A. J. Vickers, E. Khoshdel, and P. Hodge, *Thin Solid Films*, **134**, 49 (1985); R. H. Tredgold, *Thin Solid Films*, **152**, 223 (1987).

13   K. Shigehara, Y. Murata, N. Amiya, A. Yamada, *Thin Solid Films*, **179**, 287 (1989).

14   A. Laschewsky, H. Ringsdorf, G. Schmidt, and J. Schneider, *J. Am. Chem. Soc.*, **109**, 788 (1987); C. Erdelen, A. Laschewsky, H. Ringsdorf, J. Schneider, and A. Schuster, *Thin Solid Films*, **180**, 153 (1989).

15   K. Oguchi, T. Yoden, K. Sanui, and N. Ogata, *Polym. J.*, **18**, 887 (1986); M. Watanabe, Y. Kosaka, K. Sanui, N. Ogata, K. Oguchi, and T. Yoden, *Macromolecules*, **20**, 452 (1987); M. Watanabe, Y. Kosaka, K. Oguchi, K. Sanui, and N. Ogata, *Macromolecules*,

21, 2997 (1988).

16 L. M. Hayden, B. L. Anderson, J. Y. S. Lam, B. G. Higgins, P. Storoeve, S. T. Kowel, *Thin Solid Films*, **160**, 379 (1989).

17 M. Shimomura, K. Song, and J. F. Rabolt, *Langmuir*, **8**, 887 (1992).

18 W. Jark, T. P. Russel, G. Comelli, J. Stohr, *Thin Solid Films*, **199**, 161 (1991).

19 K. Naito, *J. Colloid. Interface Sci.*, **131**, 218 (1989).

20 T. Miyashita, T. Yatsue, Y. Mizuta, and M. Matsuda, *Thin Solid Films*, **179**, 439 (1989); T. Miyashita, T. Yatsue, and M. Matsuda, *J. Phys. Chem.*, **95**, 2448 (1991); T. Mizuta, M. Matsuda, and T. Miyashita, *Macromolecules*, **24**, 5459 (1991); T. Miyashita, M. Matsuda, M. Van der Auweraer, and F. C. De Schryber, *Macromolecules*, **27**, 513 (1994).

21 S. Ito, H. Okubo, S. Ohmori, and M. Yamamoto, *Thin Solid Films*, **179**, 445 (1989); S. Ohmori, S. Ito, M. Yamamoto, Y. Yonezawa, and H. Hada, *J. Chem. Soc., Chem. Commun.*, **1989**, 1293.

22 S. Ohmori, S. Ito, and M. Yamamoto, *Macromolecules*, **23**, 4047 (1990).

23 J. Schneider, H. Ringsdorf, and J. F. Rabolt, *Macromolecules*, **22**, 205 (1989); J. Schneider, C. Erdelen, H. Ringsdorf, and J. J. Rabolt, *Macromolecules*, **22**, 3475 (1989).

24 S. J. Mumby, J. F. Rabolt, and J. D. Swalen, *Thin Solid Films*, **133**, 161 (1985).

25 S. J. Mumby, J. D. Swalen, and J. F. Rabolt, *Macromolecules*, **19**, 1054 (1986).

26 S. Ito, S. Ohmori, and M. Yamamoto, *Macromolecules*, **25**, 185 (1992).

27 A. Shiotani and K. Okimoto, *Jpn. Kokai Tokkyo Koho*, JP 01 113 354, 1989: *Chem. Abst.*, **111**, 153383n (1989).

28 J. C. Seferis, *"Polymer Handbook 3rd Ed."*, J. Brandrup and E. H. Immergut Eds., Wiley, New York, 1989, Chapter VI, p 459.

29 S. Ito, H. Katayama, and M. Yamamoto, *Macromolecules*, **21**, 2456 (1988).

30 H. Katayama, K. Hisada, M. Yanagida, S. Ohmori, S. Ito, and M. Yamamoto, *Thin Solid Films*, **224**, 253 (1993); K. Hisada, H. Katayama, S. Ito, and M. Yamamoto, *J. Photopolym. Sci. Technol.*, **6**, 105 (1993).

31 V. L. Ermolaev, *Sov. Phys. —Dokl. (Engl. Transl.)*, **6**, 600 (1962).

32 H. Katayama, S. Ito, and M. Yamamoto, *J. Phys. Chem.*, **96**, 10115 (1992).

33 Jordan, E. F. Jr.; Feldeisen, D. W.; Wrigley, A. N. *J. Polym. Sci. A–1*, **9**, 1835 (1971).

34 H. W. S. Hsieh, B. Post, and H. Morawetz, *J. Polym. Sci. Polym. Phys. Ed.*, **14**, 1241 (1976).

Chapter 3

Sensitized Triplet Energy Transfer in a Two-Dimensional
Plane of Polymeric Langmuir–Blodgett Films

3.1. Introduction

In the previous chapter, the chromophore distribution in LB films of PODMA was studied by phosphorescence spectroscopy. The chromophores in the LB films were placed in a planar distribution whose deviation is a few angstroms in the direction of plane normal. However, the active sphere model[1] adopted in Chapter 2 could not be applied to the high chromophore density films in which triplet excitons migrate among the donors. To analyze such a high chromophore density system, a model taking into account the hopping process of excitons is necessary. For the singlet energy transfer in two-dimensional (2D) systems, Klafter and Blumen derived similar analytical solutions when the acceptor groups were distributed in a 2D plane with a fractal dimension $\overline{d}$.[2] In this theory, an analytical equation was obtained also for the case in which both energy migration and transfer take place (multistep trapping). The direct trapping of the exciton depends on the fractal dimension $\overline{d}$ while the multistep trapping is expressed in terms of another dimension called a spectral dimension $\widetilde{d}$. Sisido *et al.* simulated the time evolution of the distribution of the excited state on a 2D square lattice, taking into account both energy migration and energy transfer.[3]

P(CN-OD)*m-n*
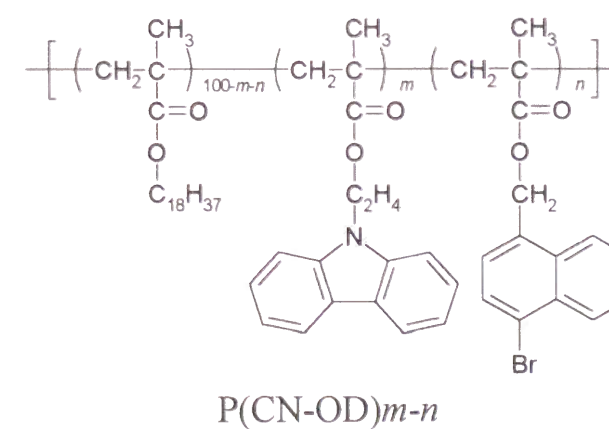
In this chapter, triplet exciton diffusion on a 2D square lattice is simulated by solving the differential equations relevant to energy migration and transfer. The rate constants for both energy migration and energy transfer were obtained from Dexter's formula. By the simulation, we derived the time profile of survival probability of the excited donor and the quantum efficiency of energy transfer to acceptors. The dynamic processes of energy migration and transfer as well as direct energy transfer from a donor to an acceptor (static process) could be described by this simulation.

3.2. Experimental Section

3.2.1. Materials

Poly[2-(9-carbazolyl)ethyl methacrylate-*co*-4-bromo-1-naphthylmethyl methacrylate-*co*-octadecyl methacrylate] (P(CN-OD)) was prepared by the copolymerization of octadecyl methacrylate with 2-(9-carbazolyl)ethyl methacrylate (CzEMA) and (4-bromo-1-naphthyl)methyl methacrylate (BNMMA). Detailed preparative methods for PODMA, P(CN-OD) and PVO were described in Chapter 2. The composition of copolymers and the chromophore densities in a plane for the LB films are listed in Table 3–1. We prepared two

Table 3–1. Compositions of Poly(octadecyl methacrylate) Copolymers and Chromophore Densities in the LB Films

Sample	CzEMA mol % [a]	BNMMA mol % [a]	$[Cz]_{2D}$ 10^{-7} mol m^{-2} [b]	$[BN]_{2D}$ 10^{-8} mol m^{-2} [b]
P(CN-OD)L-1	5.3	0	3.87	–
P(CN-OD)L-2	5.2	0.47	3.98	3.62
P(CN-OD)L-3	5.1	1.1	4.00	8.17
P(CN-OD)L-4	5.0	2.1	4.32	18.2
P(CN-OD)L-5	5.2	4.1	4.26	33.5
P(CN-OD)H-1	15.7	0	13.1	–
P(CN-OD)H-2	15.4	0.14	12.9	1.18
P(CN-OD)H-3	15.3	0.75	13.2	6.09
P(CN-OD)H-4	15.2	1.3	11.7	10.1
P(CN-OD)H-5	14.7	3.4	11.5	26.4

[a] Determined by UV absorbance. [b] Chromophore density in the surface films (mol m^{-2}) at deposition.
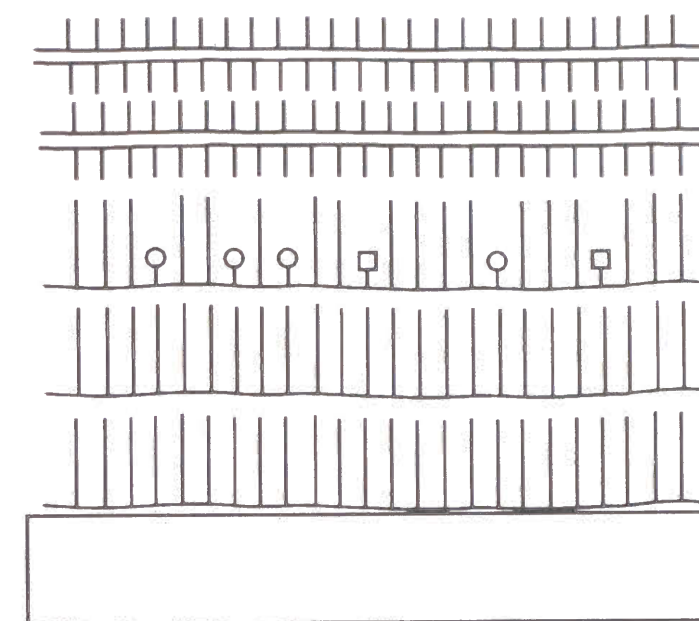
Figure 3–1. Schematic illustration of single chromophoric layer sandwiched by protective layers for emission measurements. Circles represent carbazole chromophores, and squares represent bromonaphthalene chromophores.

series of octadecyl methacrylate copolymers with a fixed content of CzEMA ($x \sim 5$ and 15) but with various contents of BNMMA, abbreviated as P(CN-OD)L-n ($n = 1$–5) and P(CN-OD)H-n ($n = 1$–5), respectively. We assumed that the chromophore density is maintained during the deposition procedure. The chromophore density at the surface pressure of the deposition was employed as that in the LB film. It is a reasonable assumption because the LB films of P(CN-OD) maintains a highly order structure due to the crystallization of alkyl side chain.

3.2.2. Sample Preparation

Water in the subphase was deionized, distilled, and passed through a water purification system (Barnstead Nanopure II). The sample was spread on the surface of pure water from a dilute benzene solution (*ca.* 0.1 g L^{-1}) at 20 °C, and then the solvent was allowed to evaporate. The surface film was compressed at a rate of 15 cm^2 min^{-1} and transferred vertically onto a substrate at a surface pressure of 20 mN m^{-1} for PODMA and PVO and of 17.5 mN m^{-1} for P(CN-OD). For PODMA and P(CN-OD), the deposition rate was 15 mm min^{-1} in the down mode and 2 mm min^{-1} in the up mode. For PVO, the rate was 15 mm min^{-1} in both up and down modes. A quartz plate used as a substrate was cleaned in sulfuric acid containing a small amount of potassium permanganate, dipped in 10% hydrogen peroxide solution, and then

rinsed with water. The transfer ratio was nearly unity and the transfer mode was in Z-type for PODMA and P(CN-OD), and in Y-type for PVO.

Figure 3–1 illustrates the structure of the LB films for the spectroscopic measurements. On quartz, polymeric layers were deposited in the following order: (1) two layers of PODMA; (2) a layer of P(CN-OD); (3) four layers of PVO. Note that P(CN-OD) takes a Z-type deposition, then the intralayer interaction of chromophores is dominant. The layers of PODMA and PVO were deposited to remove the effects of the interface.

3.2.3. Measurements

The phosphorescence spectra were recorded with a Hitachi 850 spectrophotometer equipped with a phosphorescence attachment. All the emission spectra were recorded with an excitation wavelength of 340 nm; this wavelength could excite the carbazole chromophore selectively. The lowest singlet state of bromonaphthalene is at a higher energy level than that
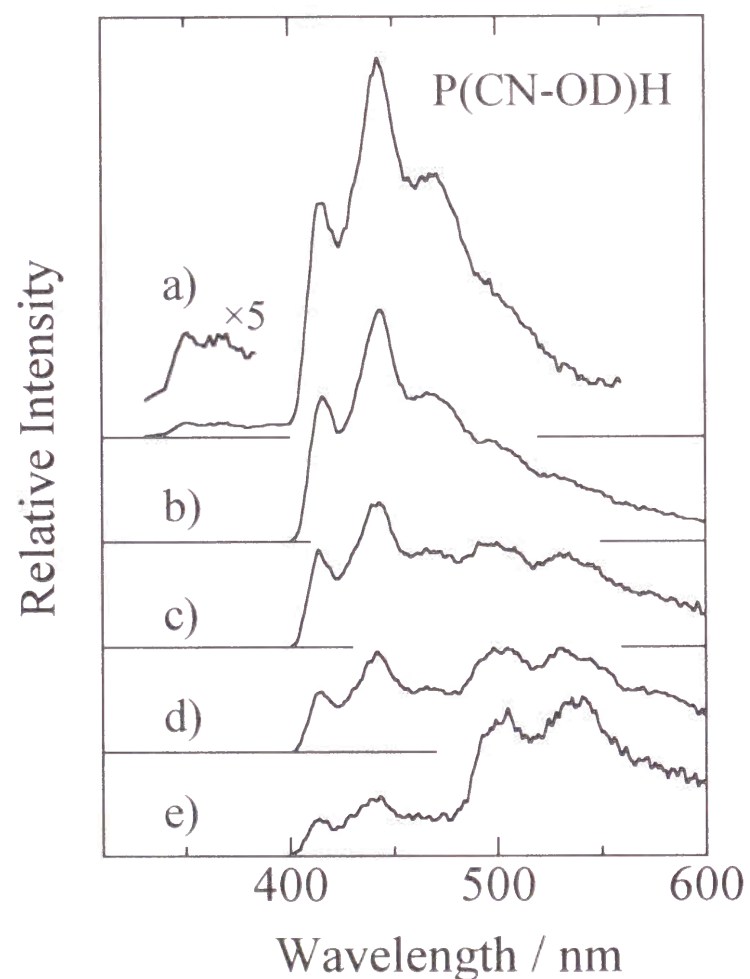

Figure 3–2. Delayed emission spectra for the LB films of P(CN-OD)H copolymers.

of carbazole, so that bromonaphthalene does not quench the singlet excited state of carbazole. The phosphorescence decays were measured with a phosphorimeter assembled in our laboratory. Details of the system have been described by Ito *et al.*[4] The LB films were immersed into liquid nitrogen in a quartz Dewar vessel for the emission measurements.

3.3. Results and Discussion

3.3.1. Delayed Emission Spectra

The delayed emission spectra of polymeric LB films are summarized in Figure 3–2. The intensity was normalized by the carbazole fluorescence intensity at 365 nm measured without the rotating light chopper. This procedure effectively reduces the errors in the phosphorescence intensity measurement due to the difference of optical geometry. The emission band with peaks at 412, 440, and 460 nm is the carbazole phosphorescence and that
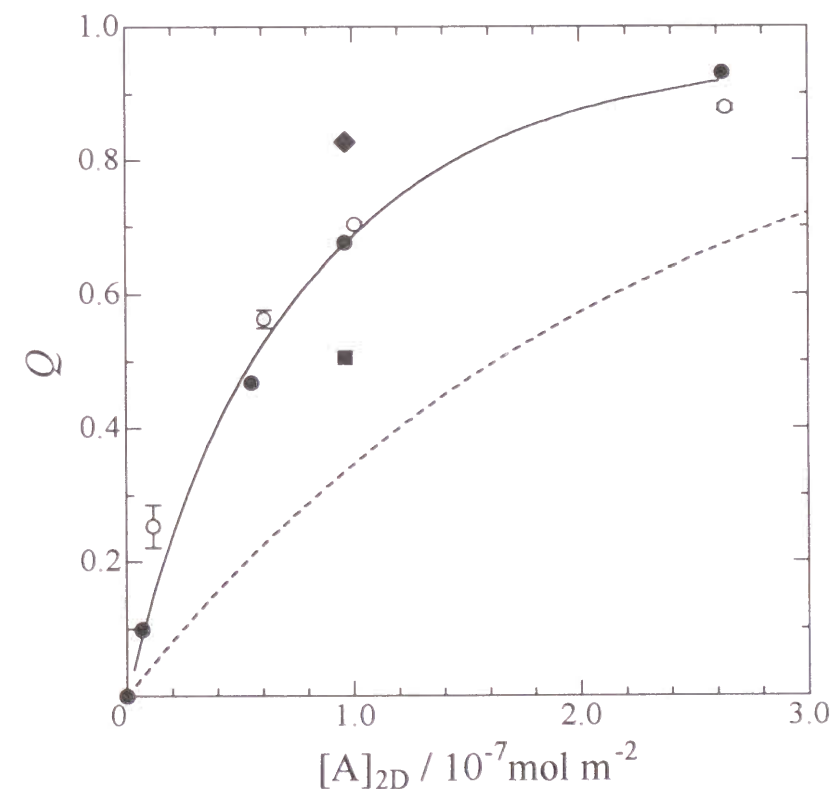

Figure 3–3. Acceptor density dependence of the quenching efficiency of carbazole phosphorescence for P(CN-OD)H LB films. Simulated quenching efficiencies with energy migration are compared with the experimental results (○). The simulation made for L_{da} was 0.086 nm (■), 0.094 nm (●) and 0.101 nm (◆). Quenching efficiency curve estimated from the active sphere model (------) is also illustrated ($R_A = 1.57$ nm).

with peaks at 500 and 535 nm is the bromonaphthalene phosphorescence. With the increase of bromonaphthalene content, the carbazole phosphorescence was quenched by the acceptor and the intensity of the bromonaphthalene phosphorescence increased. The quenching efficiency of carbazole phosphorescence (Q) was determined from the phosphorescence intensity at 412 nm compared with the fluorescence intensity.

Figure 3–3 provides a plot of Q against the 2D acceptor density in a plane, $[A]_{2D}$. The quenching efficiency observed (Q_{obsd}) increased with $[A]_{2D}$ and was larger than the estimated value from the active sphere model in which the quenching radius of the active sphere (R_A) was assumed to be 1.57 nm.[2] The LB film of P(CN-OD)H-1 shows both phosphorescence and delayed fluorescence around 360 nm. These findings indicate that in this system a carbazole triplet is quenched by a dynamic process, *i.e.*, a few steps of energy migration among the donors followed by energy transfer to an acceptor. The active sphere model cannot be applied to such a high donor content system involving the diffusion of triplet excitons. To analyze this
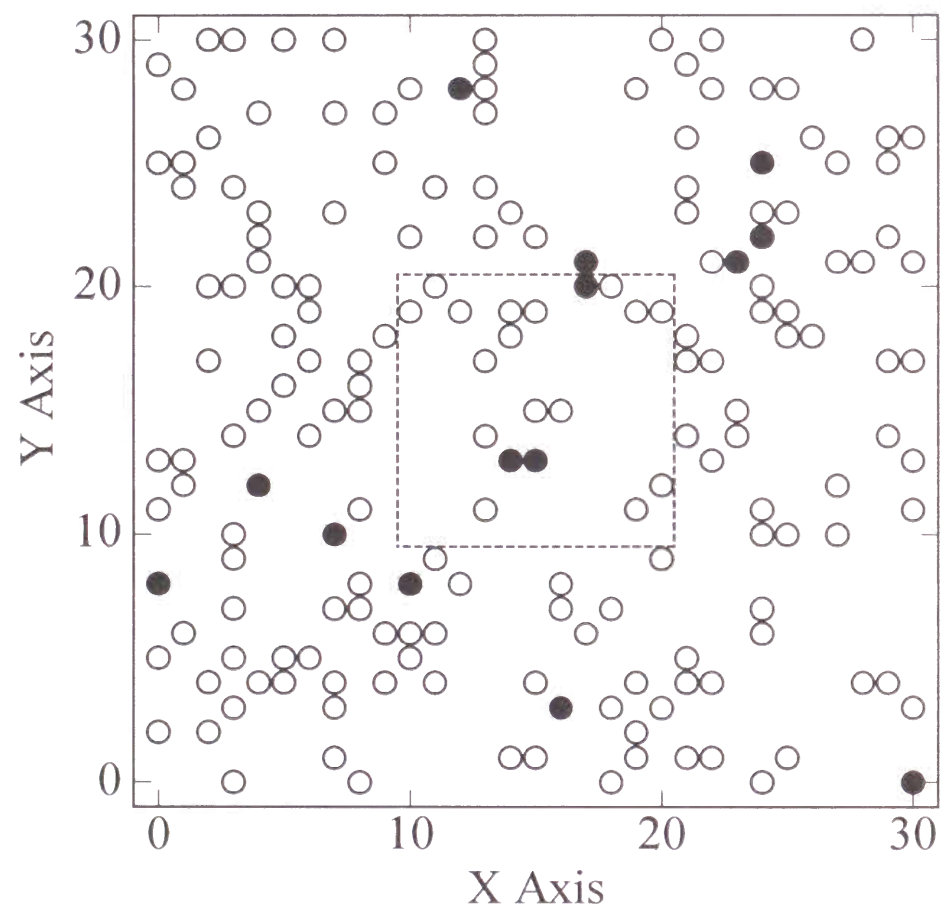
Figure 3–4. Schematic illustration of chromophore distribution in a 2D lattice: $[D]_{2D} = 1.2 \times 10^{-6}$ mol m^{-2} and $[A]_{2D} = 9.7 \times 10^{-8}$ mol m^{-2}. Open circles and filled circles represent the donors and the acceptors, respectively.

system, we simulated time evolution of the triplet energy diffusion process in a 2D plane by solving the differential equations relevant to the energy migration and the energy transfer. The simulation procedure is described below.

3.3.2. Computer Simulation for Triplet Energy Migration and Triplet Energy Transfer

Both the donors and the acceptors were randomly distributed in a square lattice as Figure 3–4 shows. The position of each chromophore was fixed, at least during the lifetime of the excited donor. The lattice interval was taken to be 0.5 nm, which was estimated from the unit size of P(CN-OD)H monolayer at the deposition. The surface pressure–area isotherms of P(CN-OD)H are shown in Figure 2–2.

All distances between the donors and the acceptors were calculated. The energy-migration rates and the energy-transfer rates at the distances, R_{ji} and R_{si}, are given by the Dexter formula,[5]

$$k_{ji} = v_{dd} \exp\left(-\frac{2R_{ji}}{L_{dd}}\right) \tag{3-1}$$

$$k_{si} = v_{da} \exp\left(-\frac{2R_{si}}{L_{da}}\right) \tag{3-2}$$

where k_{ji} is the energy-migration rate from ith donor to jth donor, k_{si} the energy transfer rate from ith donor to sth acceptor, v_{dd} and v_{da} the prefactor constants, L_{dd} and L_{da} the constants called the effective average Bohr radii.

To calculate the probability of a donor in the excited state, the following simultaneous differential equations were solved.

$$\frac{dp_i}{dt} = -\left(\sum_j k_{ji}\right)p_i - \left(\sum_s k_{si}\right)p_i + \sum_j \left(k_{ij}p_j\right) \tag{3-3}$$

$$\frac{dp_s}{dt} = \sum_i \left(k_{si}p_i\right) \tag{3-4}$$

where p_i (p_s) is the survival probability for the ith (sth) donor (acceptor). The intrinsic lifetime of donor $\tau_d = k_{ii}^{-1}$ was taken to be 6.4 s, which was the value of 9-ethylcarbazole in a 2-methyltetrahydrofuran rigid solution at 77K.[6] The values v_{da} and L_{da} are 1.3×10^{12} s^{-1} and 0.117 nm for the intramolecular triplet energy transfer from carbazole to naphthalene at 77K.[6]

In this chapter, the parameters ν_{da} and L_{da} for the triplet energy transfer from carbazole to bromonaphthalene are assumed to be equal to that from carbazole to naphthalene. For many triplet donors, such as benzophenone and phenanthrene, the radius of active sphere is insensitive to the kind of acceptor, *e.g.*, whether it is naphthalene or 1-bromonaphthalene.[7] Since the value of R_A is reflected on ν_{da} and L_{da}, the parameters ν_{da} and L_{da} take similar values for the triplet energy transfer from a donor to naphthalene or 1-bromonaphthalene. The parameters for the energy migration, ν_{dd} and L_{dd}, are unknown. In this study, we employed the same value of ν both for the energy transfer and energy migration processes ($\nu_{dd} = \nu_{da}$). On this assumption, L_{dd}, the only variable, was used as an adjustable parameter for the following fitting procedure.

The simultaneous differential equations, eqs 3-3 and 3-4, can be expressed in the following form:

$$\frac{d\mathbf{p}}{dt} = \mathbf{k}\mathbf{p} \qquad (3-5)$$

where $\mathbf{p}$ is a column vector consisting of p_i and p_s, and $\mathbf{k}$ is the matrix of rate constants. The
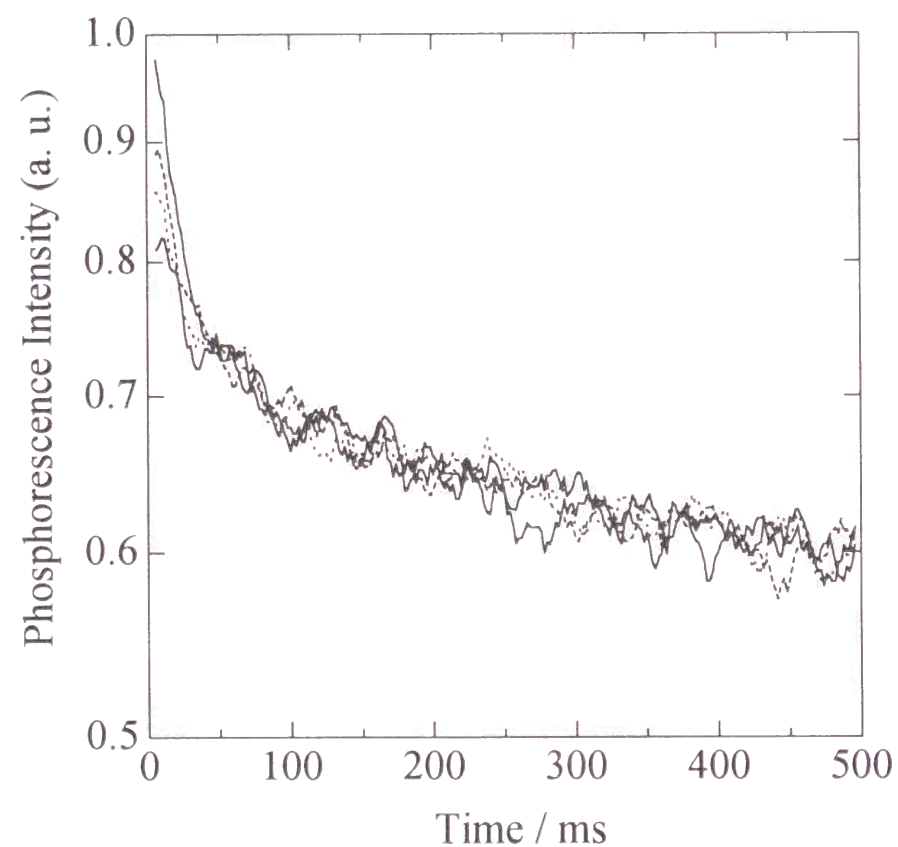
Figure 3–5. Phosphorescence decay curves for the LB films of P(CN-OD)H at 77 K: $n = 2$ (——), $n = 3$ (------), $n = 4$ (– – – –) and $n = 5$ (– - – - –).

set of differential equations, eq 3–5, has a formal solution that includes the eigenvalues of the rate constant matrix k_i:

$$p_i(t) = \sum_i A_i \exp(-k_i t) \qquad (3-6).$$

The pre-exponential factors A_i can be calculated from the eigenvector of the matrix. Practically, the differential equations were solved directly by numerical integration for the reduction in computation time.[8] In this simulation, a square lattice of $31 \times 31 = 961$ lattice points was assumed and the number of chromophores was set from the real chromophore density in each LB film.

The simulation yields the trapped probability $p_s(t)$ of excitons for each acceptor at position s. The summation of all $p_s(t)$ values gives the population of trapped excitons at time t. This value was divided by the initial number of triplet excitons, giving the quenching efficiency at time t, $Q(t)$. These calculations were repeated for 5–12 patterns of random distribution of chromophores to obtain a statistical average. The obtained $Q(t)$ vs t curves were added and the sum was normalized by the number of initially excited chromophores. The calculation was performed until 4 ms after excitation. Figure 3–5 shows the phosphorescence decay curves observed for the LB films of P(CN-OD)H. Each phosphorescence decay has a similar time profile after 10 ms. This indicates that the exciton capture by acceptors was finished within this period. Although the major quenching process was expressed by the above simulation, a minor portion of quenching occurs after the calculation time. To reduce the computation time, the time profile of $Q(t)$ for the longer times was approximated by triexponential curves with eq 3–7,

$$Q(t) = Q_\infty - \sum_{i=1}^{3} A_i \exp\left(-\frac{t}{R_i}\right) \qquad (3-7)$$

where Q_∞ is the probability that triplet excitons are trapped by acceptors during the intrinsic lifetime, R_i the apparent lifetime of donor exciton. Using eq 3–7, the phosphorescence decay curve is expressed as eq 3–8.

$$I(t) = I_0 \{1 - Q(t)\} \exp\left(-\frac{t}{\tau_d}\right)$$

$$= I_0 \left\{1 - Q_\infty + \sum_{i=1}^{3} A_i \exp\left(-\frac{t}{R_i}\right)\right\} \exp\left(-\frac{t}{\tau_d}\right) \qquad (3-8)$$
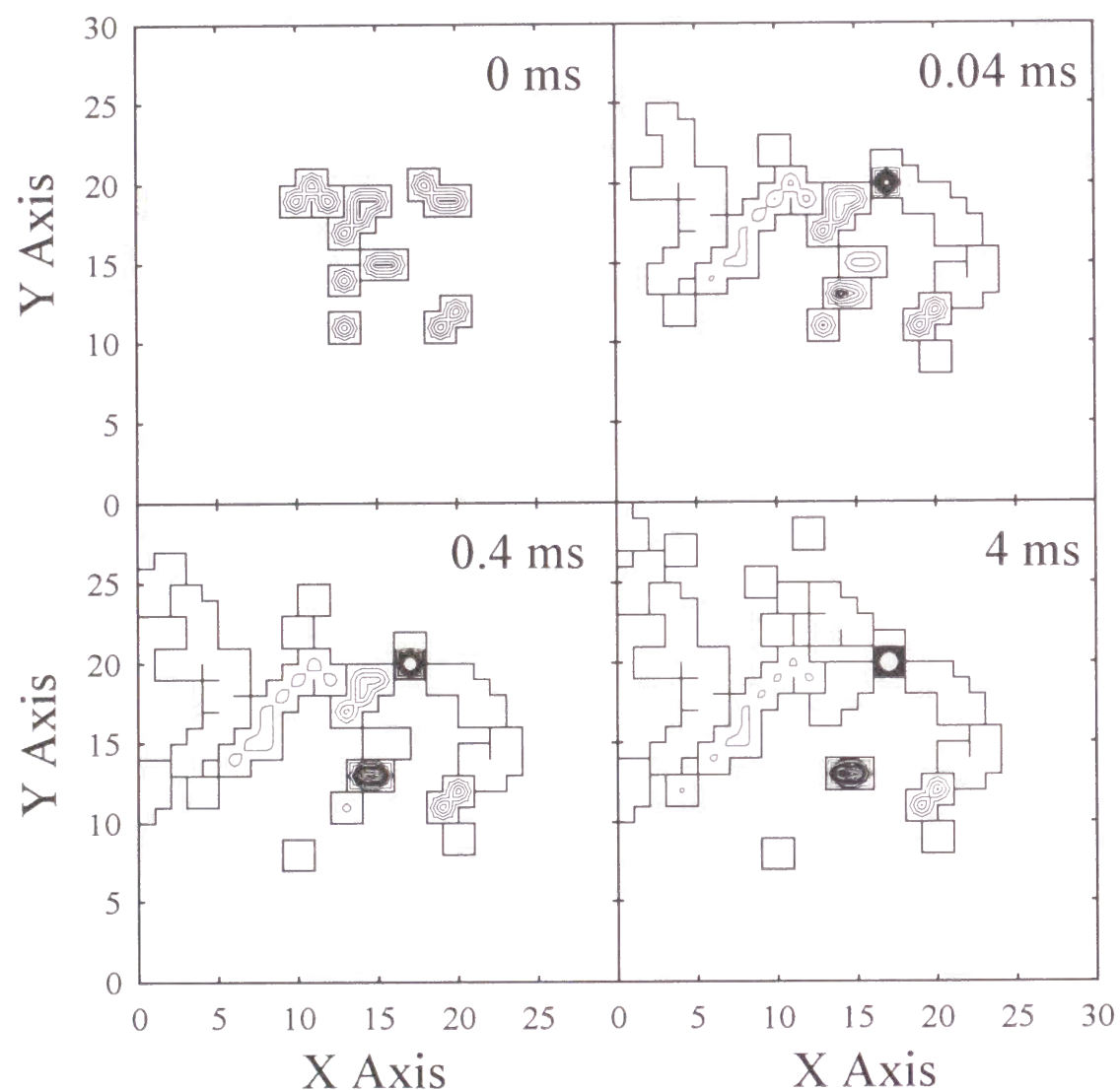
When the apparent lifetime R_i is much smaller than the intrinsic lifetime ($R_i \ll \tau_d$), eq 3–9 holds.

$$\int_0^\infty I(t)\,dt \approx \int_0^\infty I_0(1-Q_\infty)\exp\left(-\frac{t}{\tau_d}\right)dt = I_0(1-Q_\infty)\tau_d \qquad (3\text{–}9)$$

Then total quenching efficiency, Q_{calcd}, is obtained as eq 3–10.

$$Q_{calcd} = 1 - \frac{\int_0^\infty I(t)\,dt}{\int_0^\infty I_0\exp(-t/\tau_d)\,dt} = Q_\infty \qquad (3\text{–}10)$$

The obtained Q_{calcd} value was compared with the quenching efficiency, Q_{obsd}, experimentally observed.

Figure 3–6. Time evolution of the population of triplet exciton in a 2D square lattice: $[D]_{2D} = 1.2 \times 10^{-6}$ mol m^{-2} and $[A]_{2D} = 9.7 \times 10^{-8}$ mol m^{-2}. The chromophore distribution was the same as that in Figure 3–4. The interval of the contour line is 0.2.

Figure 3–6 shows an example of time evolution for the triplet excited state. At the initial stage, donors at 11×11 lattice points around the center were excited ($p_i(t) = 1$). Triplet excitons are spread over the plane and trapped by the acceptors. At first, the acceptor near the initially excited donors, e.g., $(x,y) = (17,20)$ and $(17,21)$, trap the excitons. The population of triplet excitons on the acceptors located on the route of triplet diffusion, e.g., $(x,y) = (4,12)$, grows with the elapse of time.

Figure 3–7 shows the time profile of the calculated $Q(t)$, and the solid lines are the exponential expression with eq 3–7. Each time profile was expressed by the triexponential function. First, the simulation was made at $[A]_{2D} = 9.7 \times 10^{-8}$ mol m^{-2} for three different L_{dd} (0.086, 0.094 and 0.101 nm). When L_{dd} is 0.094 nm, Q_{calcd} is in agreement with the experimentally observed value as given in Figure 3–3. Next, Q_{calcd} was calculated for a wide range of acceptor densities keeping $L_{dd} = 0.094$ nm. The simulation reproduced the experimentally observed quenching efficiencies at various acceptor densities in a fairly good manner. Although the simulated value is smaller than the observed one at a low acceptor density, this deviation probably comes from the experimental error in the phosphorescence
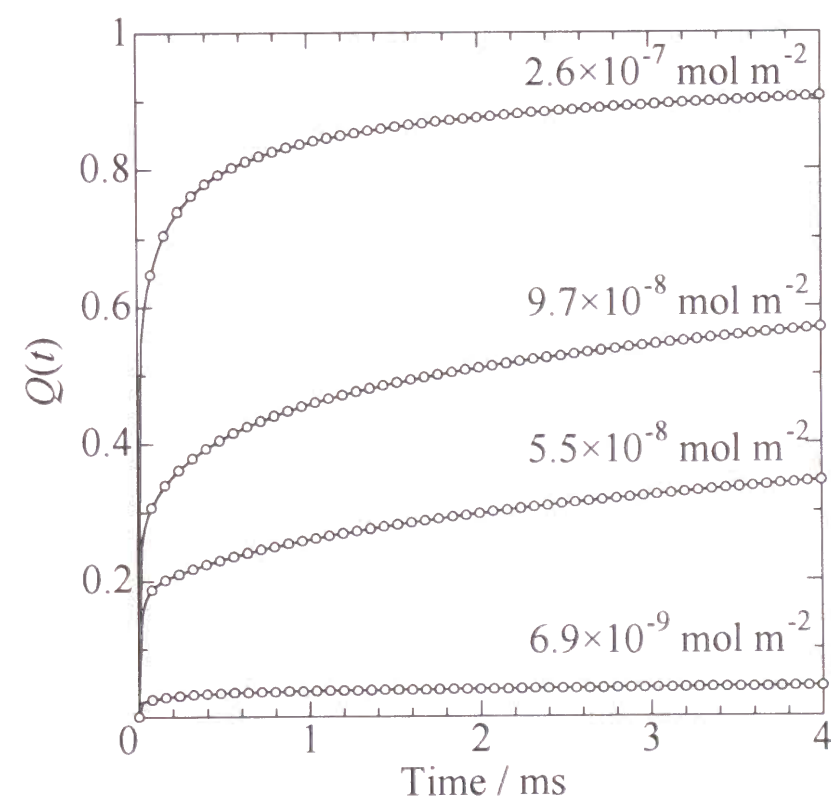
Figure 3–7. Plot of the simulated quenching efficiencies as a function of time. Solid lines are the curves calculated by eq 3–6. The donor density in a plane is fixed to be 1.2×10^{-6} mol m^{-2} and acceptor densities in a plane are indicated in the figure.

intensity measurements, because the intensity difference between P(CN-OD)H-1 film and P(CN-OD)H-2 film is small at the low [A]$_{2D}$.

3.3.3. Computer Simulation for One-Step Triplet Energy Transfer in a 2D Plane

To confirm the validity of parameters, L_{da} and ν_{da}, the data for the low donor densities ([Cz] ~ 4 × 10^{-7} mol m^{-2}) were also simulated. As described in Chapter 2, the [A]$_{2D}$ dependence of Q_{obsd} for the LB films of P(CN-OD)L can be explained by an active sphere model.[1] When chromophores are distributed exactly in one plane, the quenching efficiency was calculated from eq 3–11,

$$Q = 1 - \exp\left\{-\left(\pi R_A\right)^2 N_A [A]_{2D}\right\} \qquad (3-11)$$

where R_A is a quenching radius of an active sphere and N_A is Avogadro's number. Quenching efficiency was also obtained by the Monte Carlo simulation. For this system, the energy-
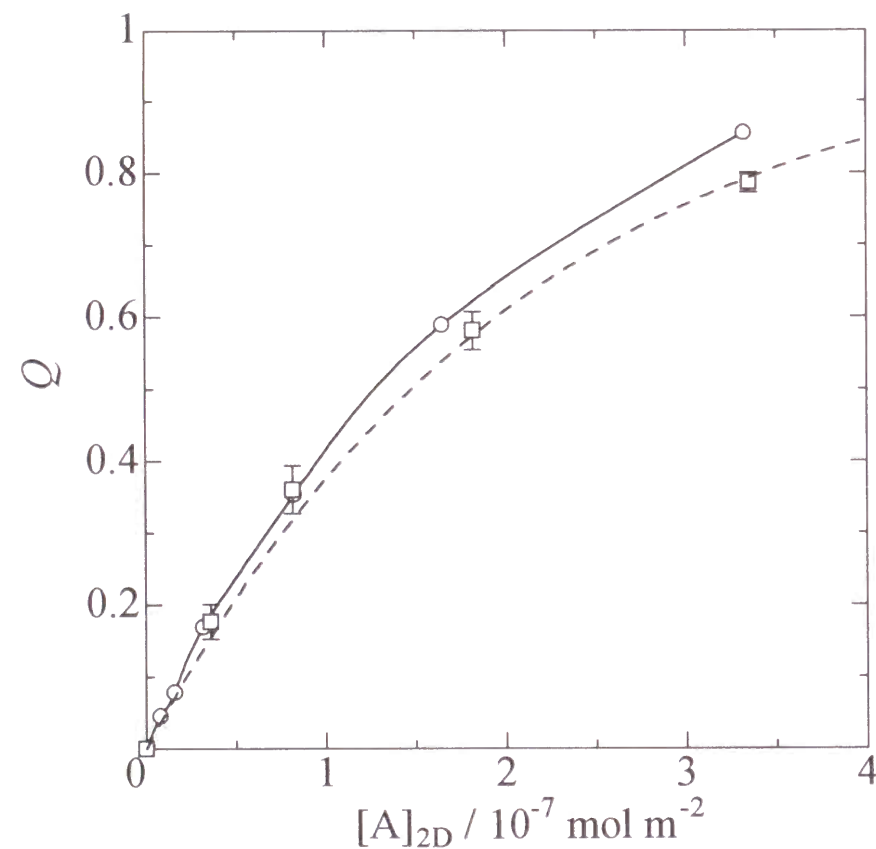

Figure 3–8. Comparison of experimentally observed quenching efficiency ($\square$) with the simulated one without energy migration ($\bigcirc$) for P(CN-OD)L copolymers. Quenching efficiency curve estimated from active sphere model (------) is also illustrated. The radius of active sphere for the triplet energy transfer in this system is 1.57 nm.

migration term in eq 3–3 can be omitted because the donor densities in the LB films were low. To calculate the probability of a donor in the excited state, the following simultaneous differential equations were solved.

$$\frac{\mathrm{d}p_i}{\mathrm{d}t} = \sum_s \left(k_{si}\right)p_i \qquad (3-12)$$

$$\frac{\mathrm{d}p_s}{\mathrm{d}t} = \sum_i \left(k_{si}p_i\right) \qquad (3-13)$$

Figure 3–8 shows that Q_{obsd} was also reproduced by this simulation. From this result, we confirmed the validity of energy transfer parameters, ν_{da} and L_{da}. This means that the triplet energy transfer in the polymeric LB films takes place in a similar manner to that in the three dimensional (3D) system although the LB film is a highly ordered system. In other words, the orientation of chromophores in the LB films is not restricted in a 2D plane and gives the averaged parameters L_{da} and ν_{da} in analogy with 3D system. Therefore, the triplet energy transfer in the polymeric LB films can be simulated by the Dexter formula. Then, by using such a simulation we can predict Q for other donor–acceptor pairs in the LB film.
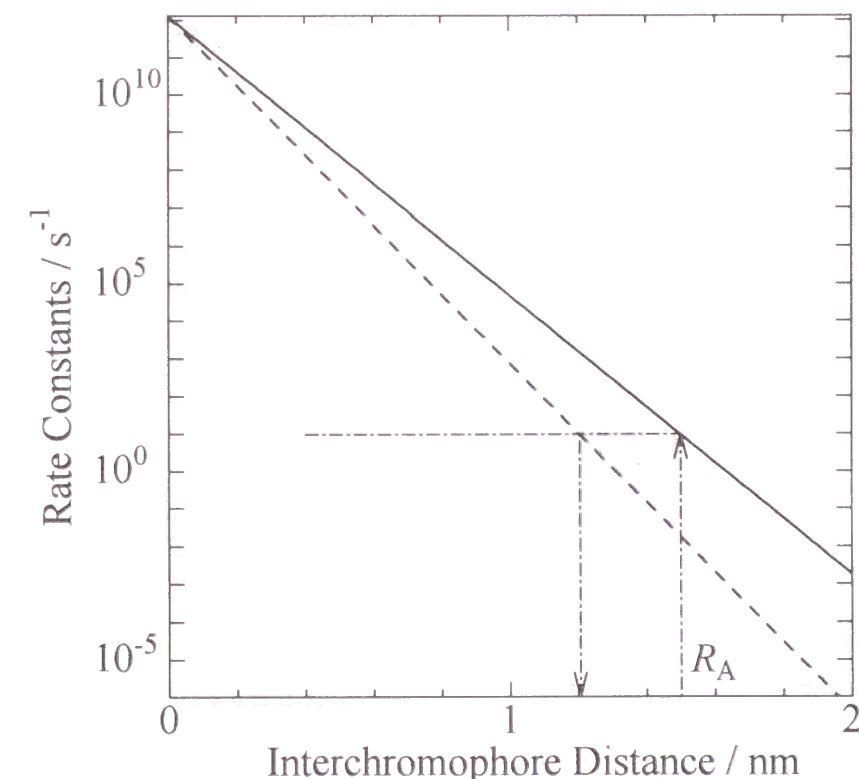
Figure 3–9. The dependence of the rate constants upon the interchromophore distances: $\nu_{da} = 1.3 \times 10^{12}$ s^{-1} and $L_{da} = 0.117$ nm (———), $\nu_{dd} = 1.3 \times 10^{12}$ s^{-1} and $L_{dd} = 0.094$ nm (— — —). The radius of active sphere for the triplet energy transfer from carbazole to bromonaphthalene (R_A) is indicated in the figure.

As described by eqs 3-1 and 3-2, the rates of triplet energy migration and transfer decrease with the increase of interchromophore distance. Figure 3–9 illustrates the dependence of the rates of triplet energy migration and transfer on the interchromophore distances: The parameters were $L_{dd} = 0.094$ nm and $\nu_{dd} = 1.3 \times 10^{12}$ s^{-1} for the triplet energy migration between carbazole chromophores, $L_{da} = 0.117$ nm and $\nu_{da} = 1.3 \times 10^{12}$ s^{-1} for the triplet energy transfer. For the energy transfer from carbazole to naphthalene, R_A is known to be 1.5 nm.[6,9] When the interchromophore distance is 1.2 nm, the rate constant of energy migration is approximately equal to that for the energy transfer at 1.5 nm. This means that the distance 1.2 nm is regarded as the critical distance for the migration process among carbazole chromophores. Previously, the critical distance for triplet energy migration between carbazole chromophores was obtained as 1.0–1.2 nm for the system of carbazole chromophores in polymer films at various concentrations.[4,10] The similar results for the energy migration distance assures that the value of the parameter L_{dd} used in the present simulation is reasonable. The triplet energy migration and transfer in PODMA LB films were well expressed by the present simulation on the assumption of a planar distribution of chromophores, because of this high quality of LB film.

3.4. Conclusion

Triplet exciton capture in a 2D plane was simulated by solving the differential equations relevant to energy migration and energy transfer. The calculated results well reproduced the quenching efficiencies obtained experimentally for both P(CN-OD)L and P(CN-OD)H LB films. This indicates that the triplet energy migration and transfer in a 2D plane can be described by the mechanism described in the above simulation. The best-fit parameters were $L_{dd} = 0.094$ nm and $\nu_{dd} = 1.3 \times 10^{12}$ s^{-1} for the triplet energy migration between carbazole chromophores, and $L_{da} = 0.117$ nm and $\nu_{da} = 1.3 \times 10^{12}$ s^{-1} for the triplet energy transfer from carbazole to bromonaphthalene. The triplet energy transfer process is mechanistically equivalent to the electron transfer process because it takes place through the electron exchange interaction. Therefore similar molecular systems involving an electron transfer process can be built by using polymeric LB films.

References and Notes

1 F. Perrin, *Compt. rend.*, **178**, 1978 (1924).

2 J. Klafter and A. Blumen, *J. Chem. Phys.*, **80**, 875 (1984).

3 M. Sisido, H. Sasaki, and Y. Imanishi, *Langmuir*, **7**, 2788 (1991).

4 S. Ito, H. Katayama, and M. Yamamoto, *Macromolecules*, **21**, 2456 (1988).

5 D. L. Dexter, *J. Chem. Phys.*, **21**, 836 (1953).

6 H. Katayama, S. Ito, and M. Yamamoto, *J. Phys. Chem.*, **96**, 10115 (1992).

7 J. B. Birks, *"Photophysics of Aromatic Molecules"*, Wiley, New York, 1970, p605.

8 The differential equations were solved numerically according to the Runge–Kutta–Verner method. The subroutine IVPRK included in the IMSL mathematical library (IMSL, Inc., Houston, TX) was used.

9 V. L. Ermolaev, *Sov. Phys. Dokl.*, **6**, 600 (1962).

10 K. Hisada, H. Katayama, S. Ito, and M. Yamamoto, *J. Photopolym. Sci. Technol.*, **6**, 105. (1993); H. Katayama, K. Hisada, M. Yanagida, S. Ohmori, S. Ito, and M. Yamamoto, *Thin Solid Films*, **224**, 253 (1993).

11 S. J. Mumby, J. F. Rabolt, and J. D. Swalen, *Thin Solid Films*, **133**, 161 (1985); S. J. Mumby, J. D. Swalen, and J. F. Rabolt, *Macromolecules*, **19**, 1054 (1986).

12 T. Arndt, A. J. Schouten, G. F. Schmidt, and G. Wegner, *Makromol. Chem.*, **192**, 2215 (1991).

Chapter 4

Intramolecular Triplet Energy Transfer. A Carbazole–Naphthalene System Having a Flexible Alkyl Spacer Doped in Poly(methyl methacrylate) Matrices.

4.1. Introduction

Triplet–triplet (T–T) energy transfer has been observed in various photochemical and photobiological systems.[1] Dexter formulated the transfer rate using an electron-exchange mechanism,[2] which requires the overlap of the electron clouds of both the triplet donor and acceptor chromophores. It is assumed that the transfer rate decreases exponentially as the distance between the donor and the acceptor increases.

Dexter's mechanism has been studied thoroughly using model compounds such as D–spacer–A.[3] The nature of this spacer unit ranges from flexible alkyl chains to rigid cyclohexane rings. Two main mechanisms, involving *through-bond* transfer or *through-space* transfer, have been proposed depending on the type of spacer units used. Close *et al.*,[4] Speiser *et al.*,[5] and Paddon-Row[6] have shown that for compounds with rigid spacer units, the rate of triplet energy transfer and electron transfer can be modeled in terms of the *through-bond* mechanism. Close *et al.* suggested that the transfer rate is dependent not only on the separation distance but also on the orientation of donor and acceptor.[4] Recently, other laboratories have shown that the *through-space* mechanism represents the long-distance triplet energy transfer.[7,8] Wagner reported that triplet energy transfer proceeds predominantly *through-space* rather than *through-bond* for compounds with flexible spacer units exceeding five atoms.[9]

Katayama *et al.* have used compounds with a flexible spacer on the studies of intramolecular triplet energy transfer.[3,10,11] Their studies on compounds containing carbazole (Cz) as a donor and naphthalene (Np) as an acceptor have shown that the transfer rate can be modeled by the *through-space* mechanism when the chromophores are connected by an alkyl

chain.[10,11] These studies were based on computational determination of the distribution of interchromophore distances between Cz and Np. By incorporating this distribution into Dexter's equation, they have been able to simulate the decay of the phosphorescence[10] and the transient absorption of Cz.[11] In the earlier paper dealing with longer spacer compounds ($n = 8-12$), R_i, the interchromophore distance, was defined as the distance between the centers of Cz and Np.[10] For the shorter spacer compounds ($n = 4-8$), however, two sets of distances and probabilities were calculated and the results were combined by giving equal weight to each of the calculated sets.[11] The first set was calculated using a center-to-center distance, while the second set was calculated by defining R_i as the distance between the closest atoms of Cz and Np, to be referred to as the edge-to-edge separation. In both cases, the parameters in Dexter's equation were different and this discrepancy remained unsettled.

This chapter is concerned with intramolecular triplet energy transfer in a series of bichromophoric compounds separated by alkyl chains of various lengths with 4 to 12 methylene units. Dexter's equation was again applied as the model neglecting *through-bond* coupling between Cz and Np. Computation provided a distribution of edge-to-edge distances, and the transfer rate was determined from the decay of phosphorescence and transient absorbance for Cz at room temperature. Temperature dependence of intramolecular T–T transfer was also investigated.
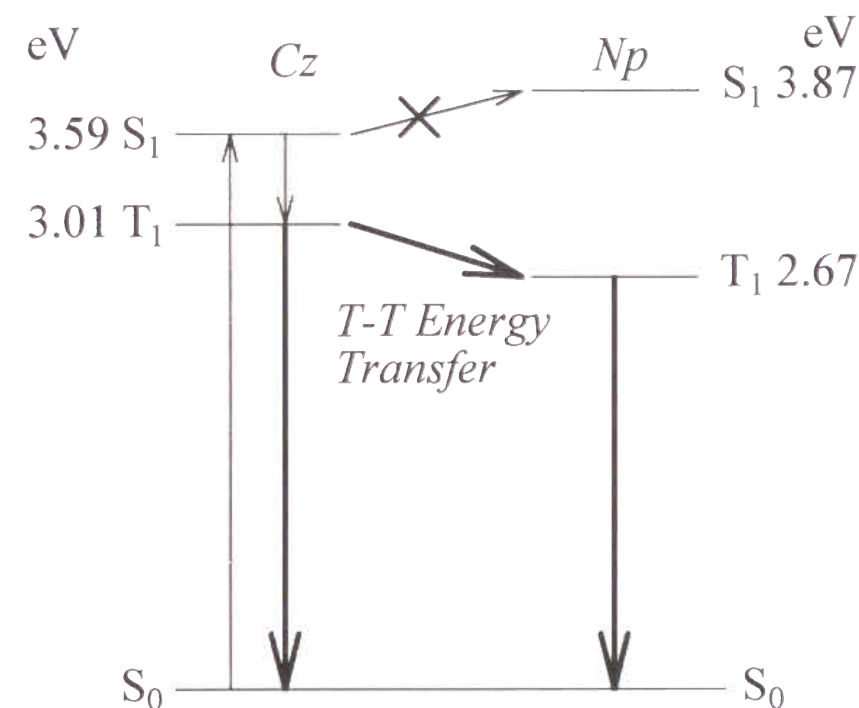
Cz-*n*-Np
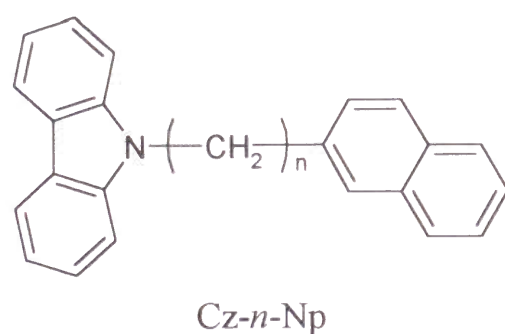
4.2. Experimental Section

4.2.1. Materials

A series of polymethylene compounds having a carbazole group and a naphthalene group as the chain terminals were synthesized by the Grignard reaction of 9-(ω-bromoalkyl)carbazole

with 2-(bromomethyl)naphthalene. Details of the synthetic method have been described elsewhere.[10,11] These bichromophoric compounds are denoted by Cz-*n*-Np ($n = 4-12$), each numeral representing the number of methylene units for each alkyl chain. The excitation and emission processes of Cz-*n*-Np are summarized in Figure 4–1. In this system, the S_1 state energy for the Cz chromophore is lower than that for the Np chromophore, and inversely the T_1 state energy is higher for the carbazole chromophore than for the naphthalene chromophore. Excitation by a nitrogen laser (337 nm) or a XeF excimer laser (351 nm) induces the energy transfer from Cz to Np in the triplet state.

4.2.2. Sample Preparation

Before the sample preparation, the bichromophoric compounds (Cz-*n*-Np) were repurified by liquid chromatography (Japan Spectroscopic Co. Ltd.) to remove any trace amount of impurity. The samples doped in PMMA bulk were prepared as follows: Cz-*n*-Np was dissolved in methyl methacrylate that was purified by distillation at a reduced pressure. After addition of a small amount of azobis(isobutyronitrile), the solution in a Pyrex cell ($10 \times 10 \times 30$ mm) was degassed by several freeze-pump-thaw cycles and then polymerized for 12 h at 60 °C and further for 12 h at 120 °C. To remove residual monomers, the PMMA block was

Figure 4–1. Energy level diagram for carbazole (Cz) and naphthalene (Np) in compound Cz-*n*-Np, selective excitation of Cz was done at 337 or 351 nm.

evacuated for 10 h at 120 °C.   PMMA film samples were also prepared by casting a solution of PMMA in a small quantity of 1,2-dichloroethane (spectrophotomeric grade; Dojindo Laboratories).   Cz-*n*-Np was added to the casting solution.   After the solvent evaporated, the film was dried *in vacuo* for more than 10 h at room temperature and at 110 °C, respectively. The concentration of Cz-*n*-Np in both samples was adjusted to be 1×10^{-3} mol L^{-1} to avoid the intermolecular interaction.

4.2.3.   Measurements

Steady-state emission spectra were recorded with a Hitachi 850 spectrofluorophotometer. Phosphorescence decay curves were measured with a phosphorimeter assembled in our laboratory.   A nitrogen laser (NDC Co., JH-500) was used as the pulsed excitation light source for the measurements.   To avoid damage to the detector by the intense excitation light, a gated photomultiplier (Hamamatsu, R1333) was used.   Details of the system have been described elsewhere.[12]

Transient absorbance decays were collected using a cross beam alignment.   An excimer laser (Lambda Physik EMG101MSC) was used as the excitation source.   The excitation wavelength was 351 nm (XeF).   The probe beam source (Hamamatsu C2178, 150W) was collimated and passed through the front edge of the sample.   The monochromator (Ritsu Oyo Kogaku MC-10N) was placed 25 cm away from the sample in order to reduce the collection of the emission from the sample.   A photomultiplier tube (Hamamatsu R928) was placed at the exit of the monochromator.   The data were collected on a digital oscilloscope (250 MHz, Hewlett Packard 54510A) and transferred to a personal computer.

The transient absorption spectra were measured using the same excitation and probe beam source as in the kinetic measurements.   The probe beam was collected by an optical fiber and directed into the detection parts of an optical multichannel analyzer (Unisoku USP-500).

The temperature of film sample was varied by a closed cycle liquid helium system (Iwatani Plantech Co., CRT 510).   It consists of a low heat leak helium transfer line and a cryotip to which a sample holder is attached.   Onto the sample holder made of copper, the quartz sample plate and its cover plate were placed and fixed with another copper block with a hole.   Indium foil was used between the quartz plates and the copper blocks to keep efficient thermal conductivity.   A radiation shield and shroud, the interior of which was evacuated during operation, surrounded the film holder.   A tip heater was used to counter the cooling action and the temperature was maintained within ± 0.1 K by a temperature control unit (Iwatani Plantech Co., TCU-4).   A calibrated thermocouple (Au + 0.07 % Fe / chromel) was connected to the copper block in the neighborhood of the sample to provide temperature as close to the area of observation as possible.

4.2.4.   Computation

Conformational analysis was performed by an empirical potential energy calculation,[13-17] in which the van der Waals interaction energy between nonbonded atoms and the intrinsic torsional potential energy associated with the rotation about C-C bonds were taken into account.

We calculated the potential energy applying the t-g rotational isomer model to the alkyl spacer. $N + 1$ rotational angles ϕ_1, ϕ_2, ..., ϕ_{n+1}, were taken into account to generate a given conformation for the Cz-*n*-Np compound (Scheme).   The van der Waals energies were calculated by a Lennard-Jones type function and given as the sum over all pairs of nonbonded atoms including the terminal chromophores.   The distance between Cz and Np was calculated by defining R_i as the distance between the closest carbon atoms of Cz and Np, to be referred to as the edge-to-edge separation.

Dexter's equation was used to model the T–T energy transfer rate.   For each R_i, a corresponding T–T energy transfer rate (k_i) is given as

$$k_i = k_0 \exp\left(-\frac{2R_i}{L}\right) \qquad (4\text{--}1)$$
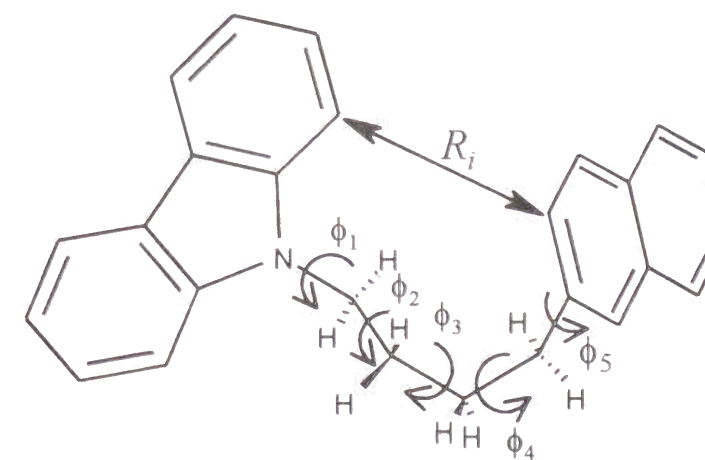
Scheme.   The parameters of Cz-*n*-Np using for conformational analysis.

where L and k_0 are the effective average Bohr radius and a constant, respectively. The emission intensity and the absorbance of carbazole triplet are proportional to the time-dependent concentration of the donor triplets, $\alpha(t)$. When R_i has a distribution, $\alpha(t)$ will decay according to the equation

$$\alpha(t) = \alpha(0)\left[x\exp\left(-\frac{t}{\tau_1}\right) + (1-x)\exp\left(-\frac{t}{\tau_2}\right) \right]\sum_{i=1}^{n} p_i \exp\left(-k_i t\right) \qquad (4\text{--}2)$$

where p_i is the probability of separation distance equal to R_i, τ_1 and τ_2 are the lifetimes of donor in the absence of acceptor. Each lifetime was estimated from the lifetime of 9-
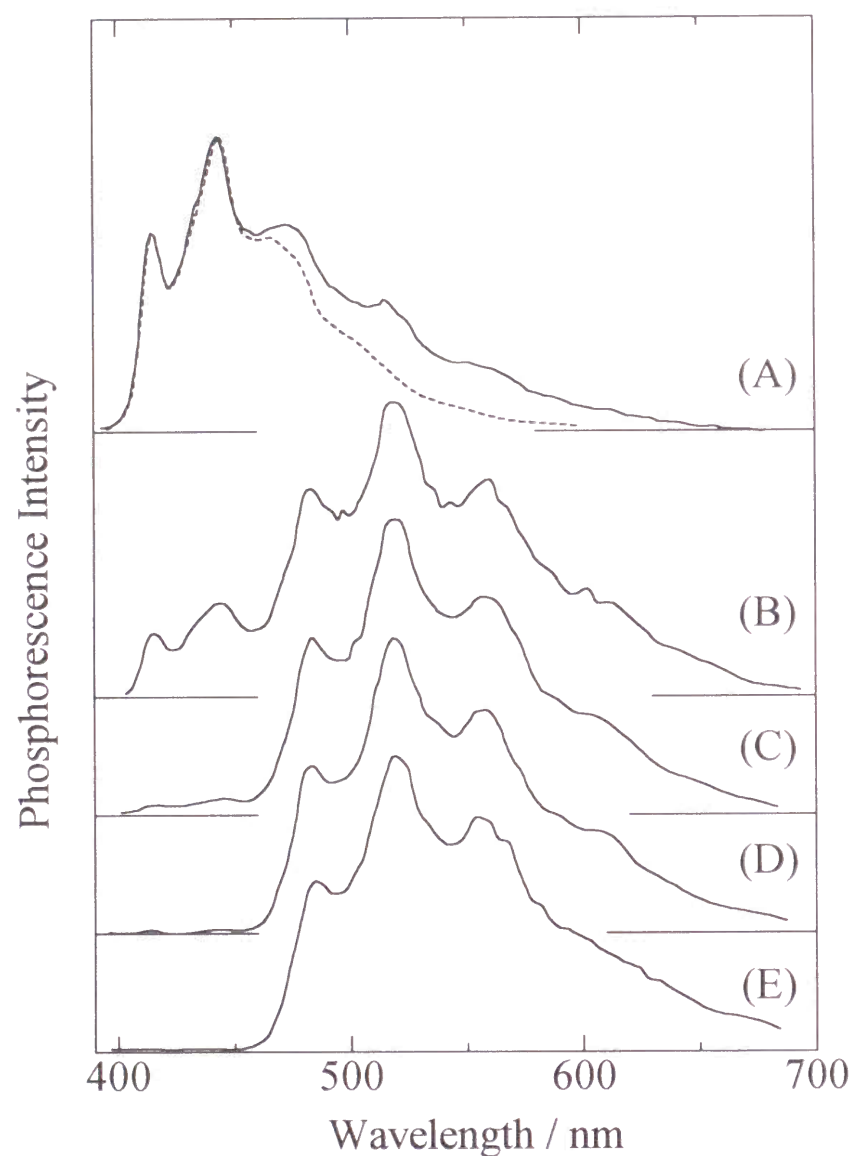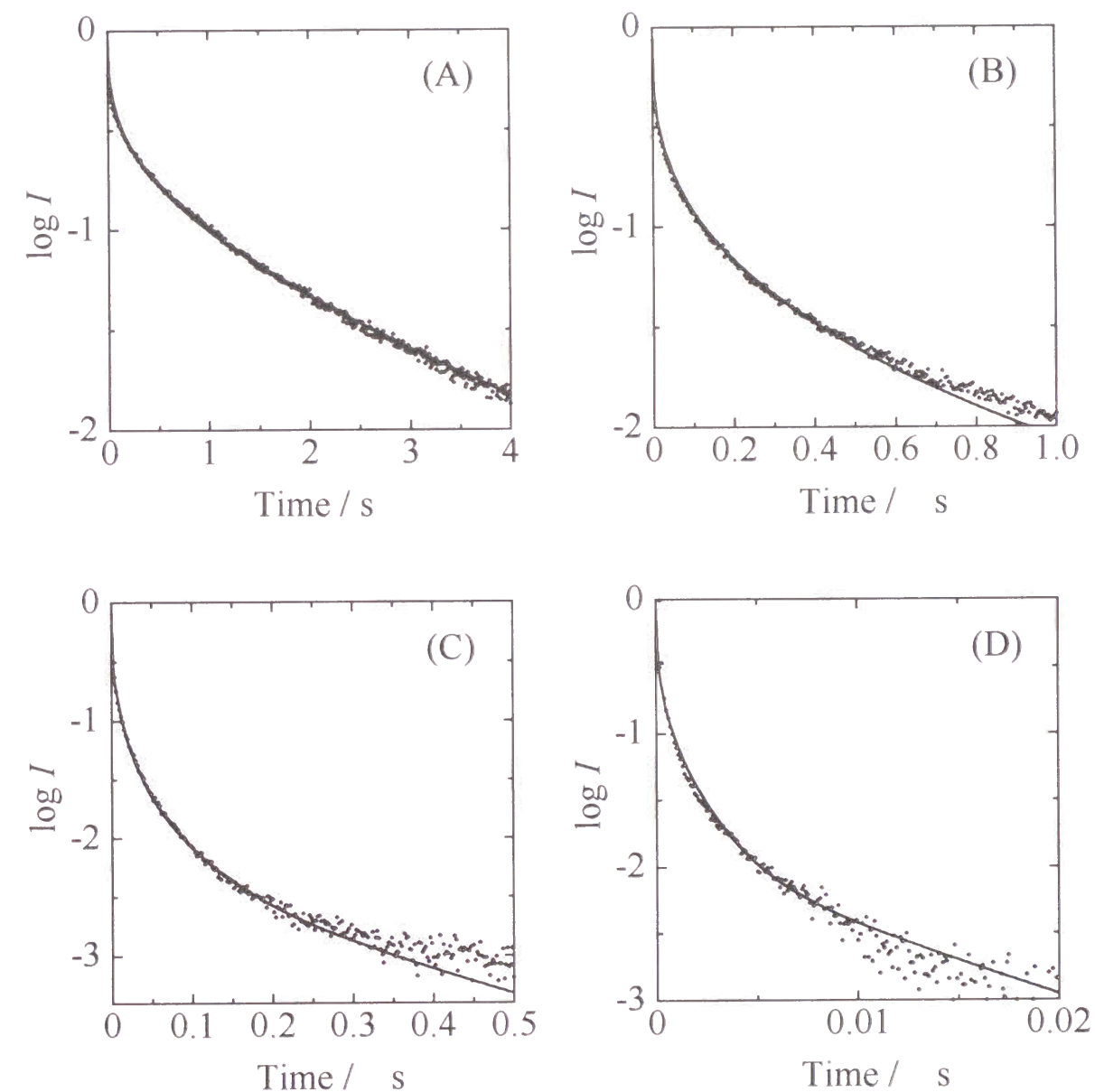

Figure 4–2. Phosphorescence spectra of Cz-*n*-Np in PMMA at room temperature: (A) Cz-12-Np; (B) Cz-10-Np; (C) Cz-9-Np; (D) Cz-8-Np; (E) Cz-6-Np. The broken line in (A) indicates the phosphorescence spectrum of EtCz. Spectra are normalized at the maximum of each spectrum peak.

ethylcarbazole (EtCz) in the same condition.

4.3. Results and Discussion

### 4.3.1. Phosphorescence Measurement

Absorption spectra of Cz-*n*-Np compounds were found to be the same as that of EtCz

Figure 4–3. Phosphorescence decay curves of Cz-*n*-Np in PMMA matrix at room temperature: (A) Cz-12-Np; (B) Cz-10-Np; (C) Cz-9-Np; (D) Cz-8-Np. Experimental data are represented by the dots. The solid lines represent the results of simulation with $L = 0.107$ nm and $k_0 = 2.5 \times 10^{10}$ s^{-1} (A), 3.0×10^{10} s^{-1} (B), 7.0×10^{10} s^{-1} (C) and 2.0×10^{11} s^{-1} (D).

with respect to carbazole moiety. No specific ground-state interaction between Cz and Np appeared to be present.

Figure 4–2 shows the normalized phosphorescence spectra for bichromophoric compounds of n = 8, 9, 10, and 12 at photostationally conditions. Emission from Np was observed for all samples. These spectra shown in Figure 4–2 indicate that energy transfer from Cz to Np occurs for all samples. The quantum yield of naphthalene phosphorescence is much smaller ($\Phi = 0.060$)[18] than that of carbazole ($\Phi = 0.21$)[19] in MTHF at 77 K. Therefore, for Cz-12-Np, for example, the quenching efficiency of carbazole phosphorescence is more than 0.9, although the intensity of naphthalene phosphorescence is weaker than that of carbazole.
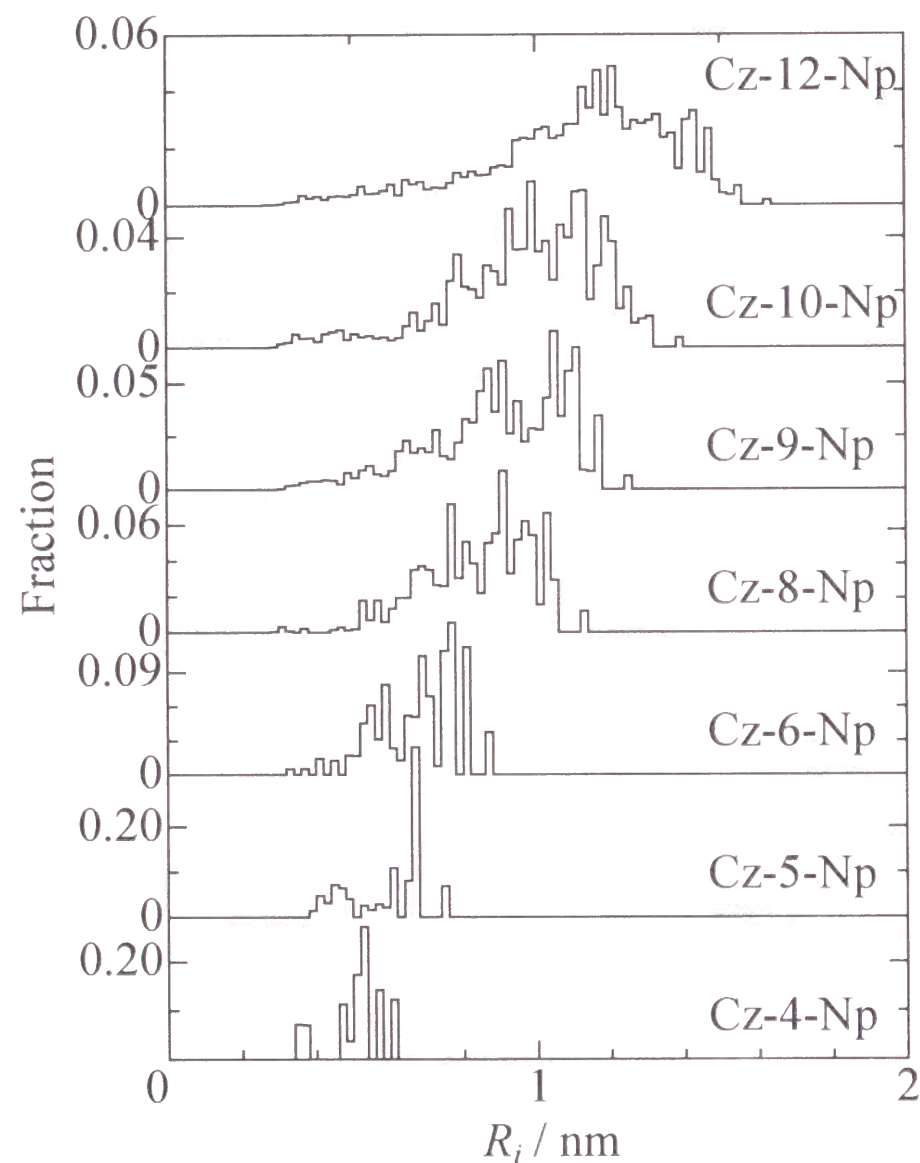

Figure 4–4. Distribution function of R_i for the Cz-n-Np compounds. The distance resolution between successive marks on the abscissa is 0.02 nm.

The efficiency that a Cz triplet was quenched by an Np in another molecule (Q) was estimated using Perrin's equation.

$$Q = 1 - \exp\left[-\frac{4}{3}\pi R_A^3 N_A C\right] \qquad (4-3)$$

where R_A is the critical radius of phosphorescence quenching, N_A Avogadro's number, C the concentration of bichromophoric compound. The critical radius of phosphorescence quenching between carbazole and naphthalene was reported to be 1.5 nm.[20] Using this R_A, Q was calculated to be 8.5×10^{-3}. For the present chromophore concentration (1×10^{-3} mol L^{-1}), it is safely said that most of the carbazole in triplet state (^{3}Cz*) is quenched intramolecularly by naphthalene. Therefore, intermolecular energy transfer is negligible here.
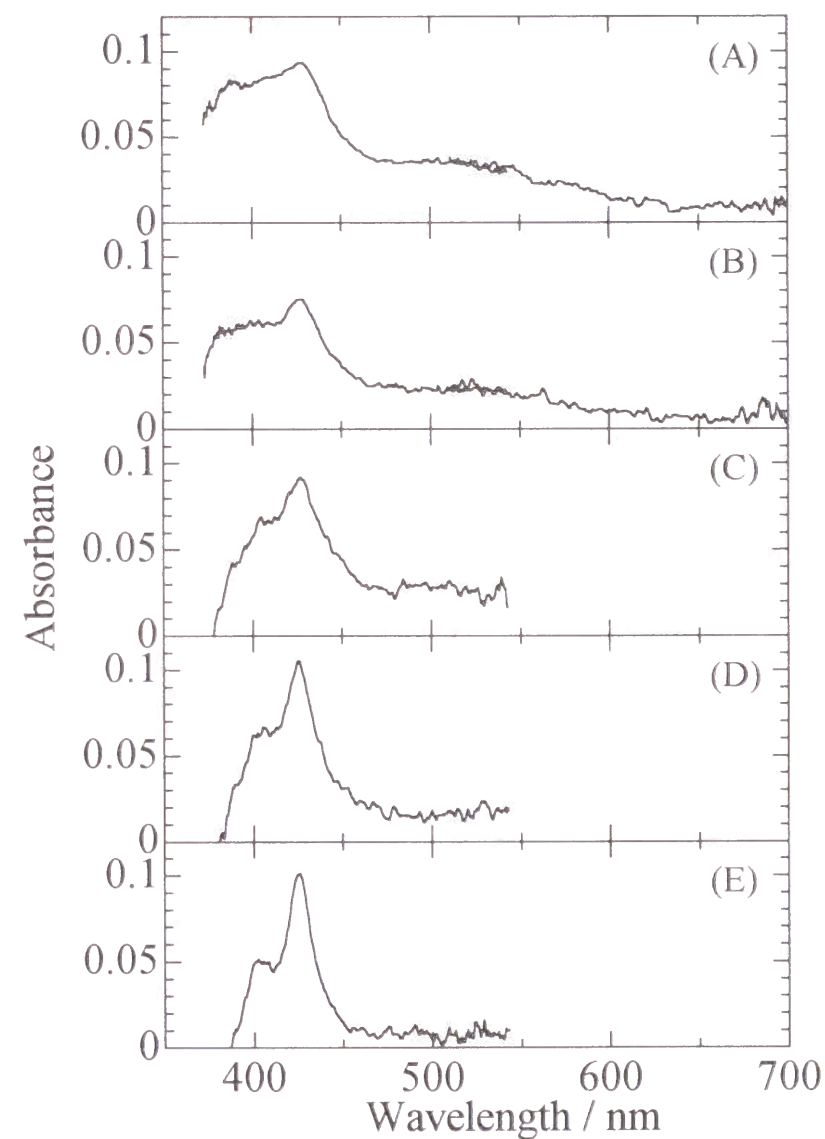
Figure 4–5. Transient absorption spectra in PMMA matrix at room temperature with a delay time of 72 ns for (A) EtCz, (B) Cz-8-Np, (C) Cz-6-Np, (D) Cz-5-Np and (E) Cz-4-Np.

Figure 4–3 shows the decay curves of carbazole phosphorescence for the Cz-n-Np compounds (n = 8–12). The carbazole chromophore was selectively excited by a nitrogen laser (337 nm) for phosphorescence decay measurements. All these decay profiles were nonexponential and strongly depended on the chain length. These nonexponential decay curves were analyzed with Dexter's equation as described in the Experimental Section. Figure 4–4 shows R_i and p_i obtained by the potential energy calculation. From this distribution function, eq 4–2 was fitted to the phosphorescence decay curves using k_0 as the fitting parameter. The solid lines indicate the calculated decay curves, and the dots indicate the observed points. The calculated curves are in good agreement with the experimental data.
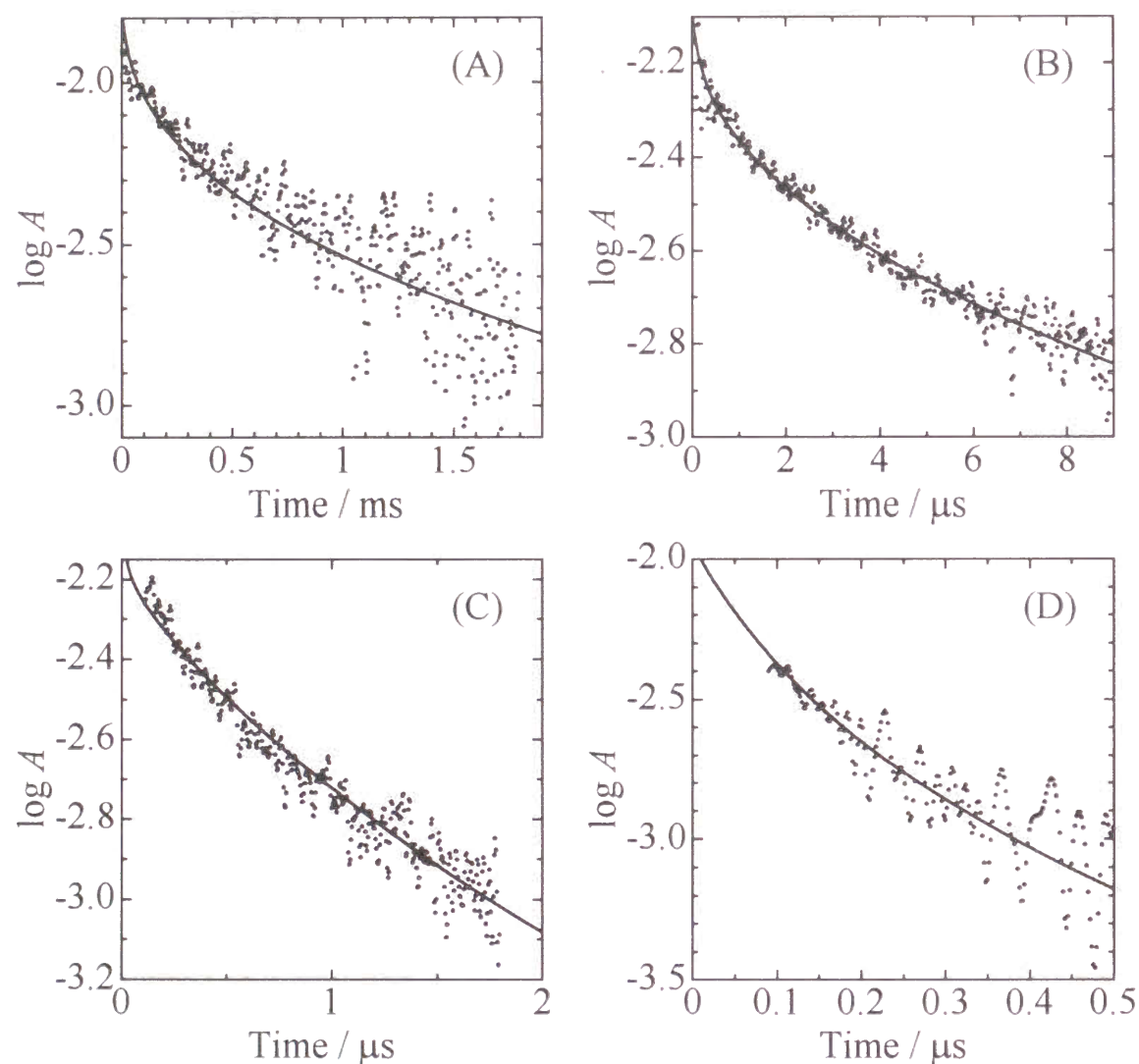

Figure 4–6. Transient absorbance decay at 500 nm of Cz-n-Np in PMMA matrix at room temperature: (A) n = 8; (B) n = 6; (C) n = 5; (D) n = 4. Experimental data are represented by the dots. The solid lines represent the results of simulation with L = 0.107 nm and k_0 = 1.2×10^{11} s^{-1} (A), 2.2×10^{11} s^{-1} (B), 3.5×10^{11} s^{-1} (C) and 2.5×10^{11} s^{-1} (D).

4.3.2. Transient Absorption Measurement

Transient absorption spectra were collected for Cz-n-Np; n = 4–8. A 351-nm laser pulse was used as the excitation source, which selectively excited the Cz chromophore. Figure 4–5 shows transient absorption spectra of EtCz and Cz-n-Np (n = 4–8) in PMMA matrix at room temperature with a delay time of 72 ns. The top spectrum was attributed to ^{3}Cz*,[21] whereas the bottom spectrum was attributed to the Np triplet state[22] produced by the energy transfer from Cz. It is clear that the triplet energy of Cz is being transferred to Np, and the transfer rate can be observed by monitoring the 500-nm absorbance; at 500 nm, only the ^{3}Cz* absorbance is present in this particular experiment.

Absorbance decays at 500 nm are shown in Figure 4–6, where the points are the collected data and the solid lines are the calculated decay curves. All the decays were nonlinear or a semilogarithmic scale showing a nonexponential character. The transient absorbance decay
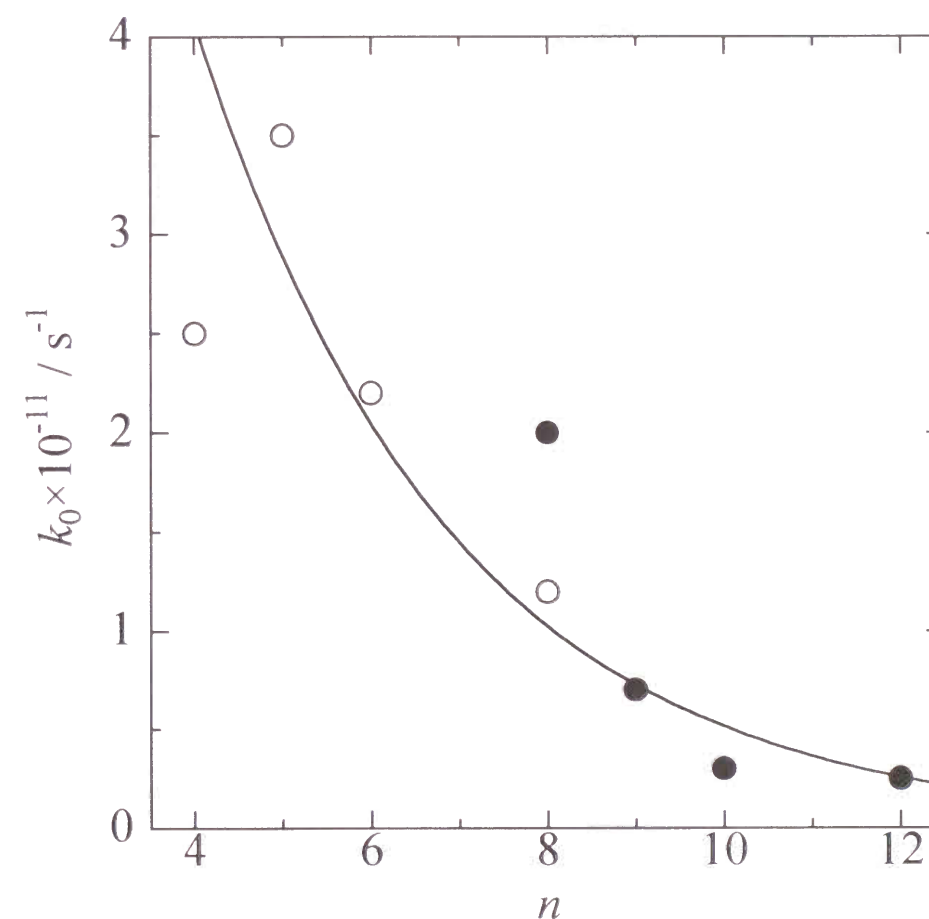
Figure 4–7. Pre-exponential factor k_0 for triplet energy transfer as a function of the number of atoms connecting Cz and Np. The value was estimated from phosphorescence decay (●) and transient absorption decay (○).

curve was also collected for Cz-9-Np. The decay curve well corresponded to the phosphorescence decay shown in Figure 4–3 (C). This means that two-photon ionization of Cz is negligible[23] and does not affect the decay profile in this system. Similar to phosphorescence decay fitting, eq 4–2 was fitted to the absorbance decays by using k_0 as the fitting parameter. The fitting procedure gave reasonable k_0 and L values and succeeded in reproducing the data for Cz-n-Np; n = 4–8. In Figure 4–6, Fourier transform smoothing was applied to the decay curves of transient absorbance in order to reduce the high-frequency RF noise from excimer laser. The value of L is fixed to 0.107 nm according to the previous report by Strambini and Galley.[24]

In Figure 4–7, the obtained pre-exponential factors k_0 are plotted as a function of the number of carbon atoms connecting Cz and Np. The value of k_0 decreased with the increase of spacer length exponentially. For longer spacer samples, the value k_0 is acceptable in comparison with the previous results obtained for intermolecular T–T energy transfer by
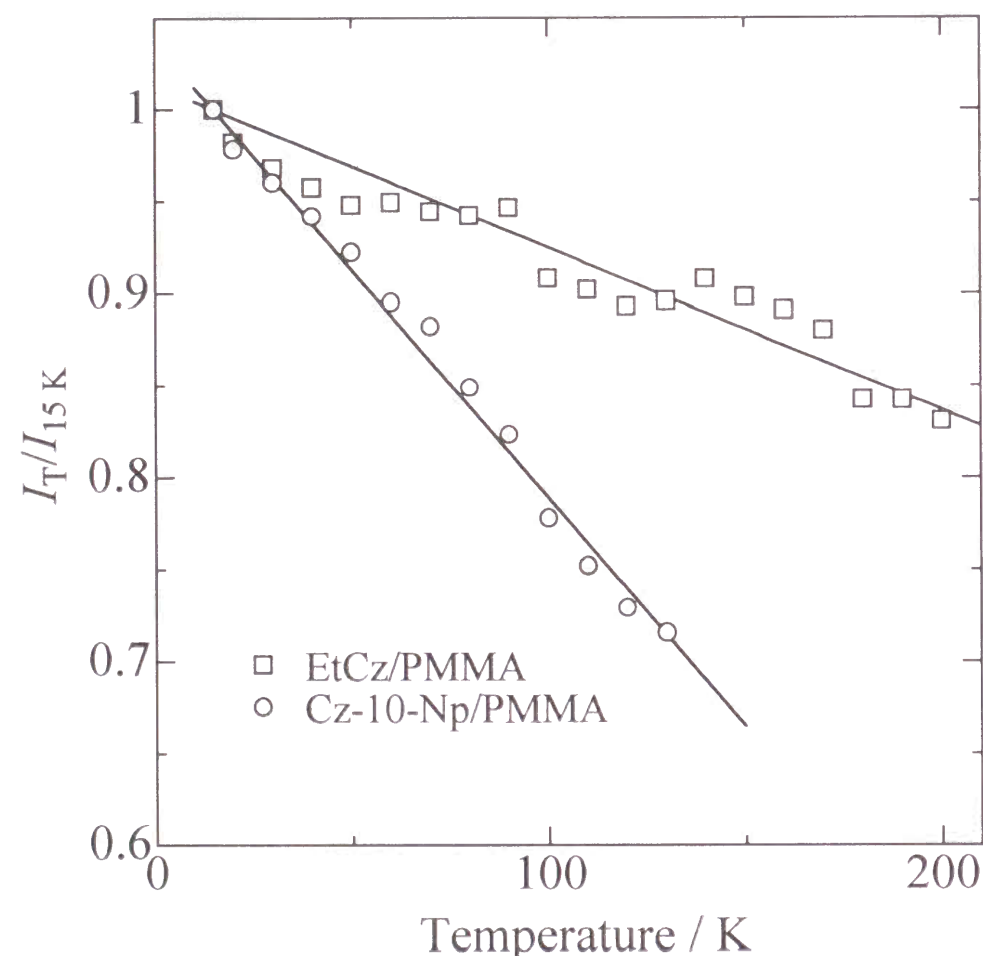
Figure 4–8. Normalized intensity of phosphorescence from Cz moiety at 440 nm as a function of temperature: (A) EtCz (□) and (B) Cz-10-Np (○) in PMMA film.

Strambini and Galley.[24] This means that the *through-space* mechanism governs the T–T energy transfer of Cz-n-Np with a long flexible spacer. The reason why k_0 becomes large at a shorter spacer is not obvious. Two explanations are possible. One is that Dexter's equation that assumes point chromophores having exponential decay of electric charge clouds does not hold for the energy transfer through a short distance, especially in the case of large plate-like aromatic chromophores. Another reason is that with increasing fraction of all trans conformation, the *through-bond* mechanism starts to contribute to the energy transfer.
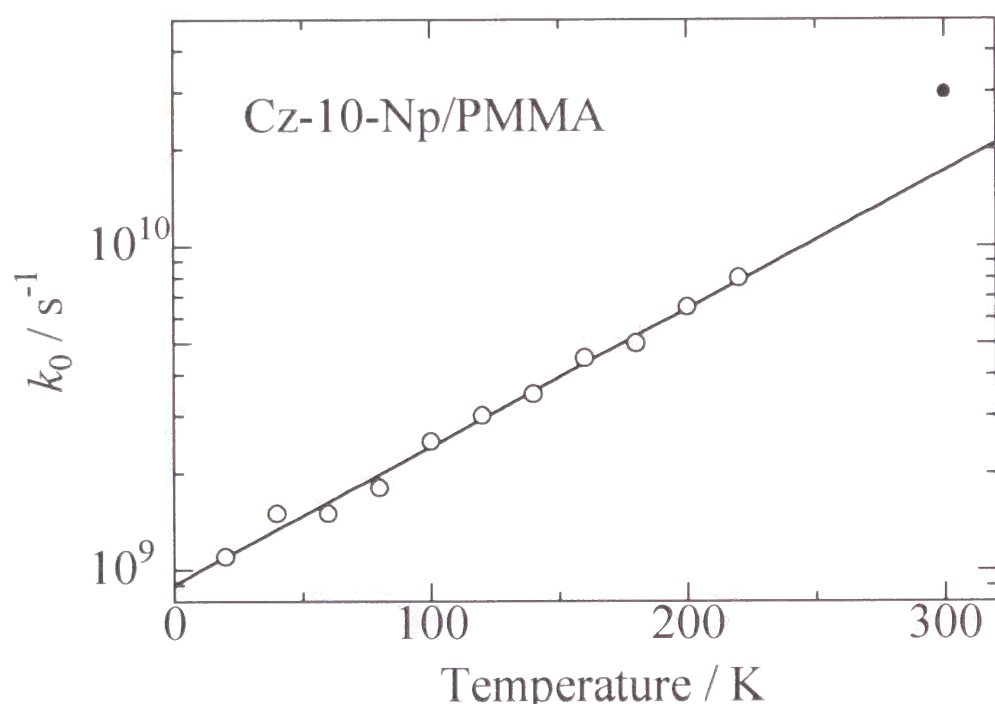
4.3.3. Temperature Dependence
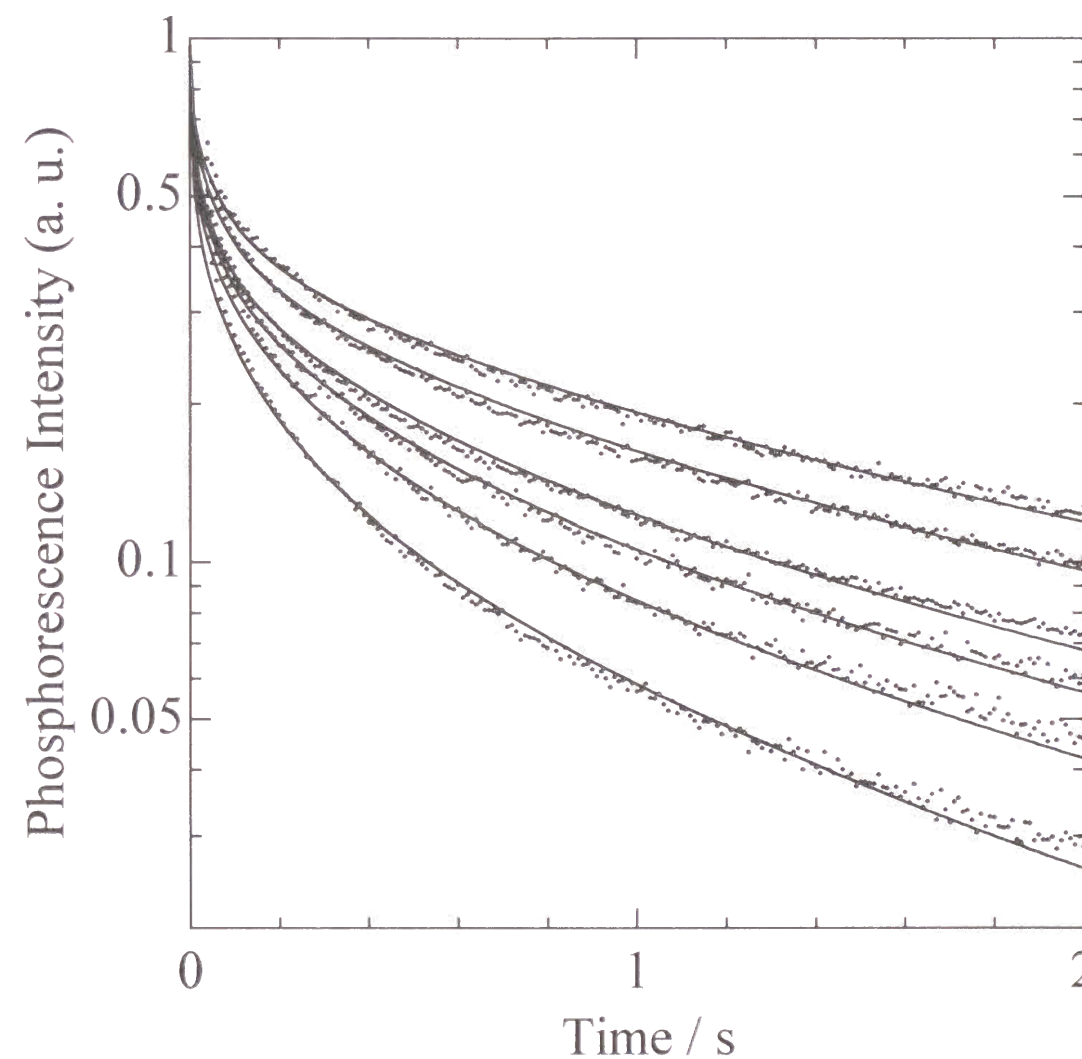
Figure 4–9. Phosphorescence decay curves of Cz-10-Np in PMMA film. Sample temperature was changed from 20 K (top) to 220 K (bottom) by every 40 K separation. Experimental data are represented by the dots. The solid lines represent the results of simulation with L = 0.107 nm and k_0 = 1.0 × 10⁹ s⁻¹ (20 K), 1.5 × 10⁹ s⁻¹ (60 K), 2.5 × 10⁹ s⁻¹ (100 K), 3.5 × 10⁹ s⁻¹ (140 K), 5.0 × 10⁹ s⁻¹ (180 K) and 8.0 × 10⁹ s⁻¹ (220 K).

Figure 4–8 shows the temperature dependence of the intensity of phosphorescence from Cz chromophore at 440 nm for EtCz and Cz-10-Np. The intensities were normalized by the intensity at 15 K for each compound. The intensity of phosphorescence for Cz-10-Np decreased with increasing temperature and the amount of decrease is larger than that of EtCz. The temperature dependence of non-radiative deactivation rates is equal for both compounds but that of the triplet energy transfer to Np must be different, resulting in a larger temperature dependence in phosphorescence intensity. This result shows that intramolecular triplet energy transfer is accelerated with temperature in this system.

Figure 4–9 shows the phosphorescence decay curves of Cz-10-Np at 440 nm in the temperature range from 20 to 220 K. The Cz phosphorescence decays faster at higher temperatures. As seen in the phosphorescence intensity, the temperature dependence of Cz-10-Np was larger than that of EtCz. These decay curves were analyzed with Dexter's equation as for the decay curves at room temperature. In the present analysis, the parameter L is fixed to 0.107 nm and the pre-exponential factor k_0 is used as a fitting parameter. In Figure 4–9, the solid lines indicate the calculated decay curves and are in good agreement with the experimental data.

The temperature dependence of k_0 is plotted in Figure 4–10 and k_0 increased

Figure 4–10. Temperature dependence of pre-exponential factor k_0 of triplet energy transfer for Cz-10-Np in PMMA film (○). The data at room temperature are also indicated (●).

exponentially with increasing temperature. The value of k_0, which was obtained in Figure 4–3 (B), is also shown in Figure 4–10. The procedure of sample preparation is different for both samples; one is made by film casting and the other is bulk polymerization. The value k_0 at room temperature is on the extrapolation of the semilogarithmic k_0 vs temperature plot at low temperatures. This means the value is not dependent on the procedure of sample preparation and is intrinsic to compound Cz-10-Np in PMMA matrix. In the present fitting, we assumed that only k_0 is dependent on temperature. However, the temperature dependence may be explained by the vibration or rotation of chromophores. When a chromophore can move within its lifetime and Cz and Np approach one another, triplet energy could be transferred faster. If the value k_0 apparently increases due to the variation of interchromophore distance, the chromophores have to move in the distance of 0.8 Å at room temperature. However, at temperatures much below the glass transition temperature of the matrix, the distance 0.8 Å is too large. Furthermore, if the motion within the lifetime of Cz triplet causes the increase of the energy transfer rate, some discontinuity should be observed around the transition temperature of matrix polymer in Figure 4–10 as it was done in the phosphorescence lifetime studies.[25-27] However, no discontinuity was observed in the temperature range from 20 to 220 K. From these results, we conclude that high frequency vibration of chromophores is coupled with the energy transfer process through the increase of the electron coupling element or the Franck Condon factor, which was detected as acceleration of k_0.

4.4. Conclusion

The intramolecular T–T energy transfer of bichromophoric compounds connected with a flexible alkyl chain was directly analyzed by phosphorescence decay measurements and transient absorption decay measurements. The distribution of donor-acceptor distances was calculated by a conformational analysis, and the decay profile was simulated using Dexter's equation. The result of simulation was in fairly good agreement with the experimental value. The present study reconfirms our previous report that the *through-space* mechanism governs the intramolecular T–T energy transfer in D–A molecules with a flexible long spacer. However, when the spacer length became shorter, the pre-exponential factor k_0 increased apparently by deviating the ideal *through-space* mechanism described by Dexter's model. Temperature dependence of the intramolecular T–T energy transfer was also studied for Cz-

10-Np. The rate of energy transfer rose exponentially with the increase of temperature.

References

1   N. J. Turro, *"Modern Molecular Photochemistry"*, Benjamin, Menlo Park, CA, 1978, p. 296; J. B. Birks, *"Photophysics of Aromatic Molecules"*, Wiley, New York, 1970, p. 518; J. E. Guillet, *"Polymer Photophysics and Photochemistry"*, Cambridge University Press, Cambridge, U. K., 1985; S. C. Webber, *"Polymer Photophysics"*, D. Phillips Ed., Chapman and Hall, New York, 1985; J. M. Pearson and M. Stolka, *"Poly(N-vinylcarbazole)"*, Gordon and Breach Sci. Pub., New York, 1981.

2   D. L. Dexter, *J. Chem. Phys.*, **21**, 836 (1953).

3   H. Katayama, S. Maruyama, S. Ito, Y. Tsujii, A. Tsuchida, and M. Yamamoto, *J. Phys. Chem.*, **95**, 3480 (1991).

4   G. L. Closs, M. D. Johnson, J. R. Miller, and P. Piotrowiak, *J. Am. Chem. Soc.*, **111**, 3751 (1989); G. L. Closs, P. Piotrowiak, J. M. MacInnis, and G. R. Fleming, *J. Am. Chem. Soc.*, **110**, 2652 (1988).

5   S. Speiser, S. Hassoon, and M. B. Rubin, *J. Phys. Chem.*, **90**, 5085 (1986).

6   M. N. Paddon–Row, *Acc. Chem. Res.*, **27**, 18 (1994).

7   S. Levy, M. B. Rubin, and S. Speiser, *J. Am. Chem. Soc.*, **114**, 10747 (1992).

8   P. J. Wagner and G. M. El–Taliawi, *J. Am. Chem. Soc.*, **114**, 8325 (1992).

9   P. J. Wagner, B. P. Giri, H. W. Freking Jr., and J. DeFrancesco, *J. Am. Chem. Soc.*, **114**, 8326 (1992).

10 H. Katayama, S. Ito, and M. Yamamoto, *J. Phys. Chem.*, **96**, 10115 (1992).

11 G. W. Haggquist, H. Katayama, A. Tsuchida, S. Ito, and M. Yamamoto, *J. Phys. Chem.*, **97**, 9270 (1993).

12 S. Ito, H. Katayama, and M. Yamamoto, *Macromolecules*, **21**, 2456 (1988).

13 T. Ikeda, B. Lee, S. Kurihara, S. Tazuke, S. Ito, and M. Yamamoto, *J. Am. Chem. Soc.*, **110**, 8299 (1988); S. Ito, K. Takami, Y. Tsujii, and M. Yamamoto, *Macromolecules*, **23**, 2666 (1990).

14 P. J. Flory, *"Statistical Mechanics of Chain Molecules"*, Wiley, New York, 1969.

15 A. J. Hopfinger, *"Conformational Properties of Macromolecules"*; Academic, New York, 1973.

16 S. Ito, M. Yamamoto, and Y. Nishijima, *Bull. Chem. Soc. Jpn.*, **55**, 363 (1982); T.

Kanaya. Y. Hatano, M. Yamamoto, and Y. Nishijima, *Bull. Chem. Soc. Jpn.*, **52**, 2079 (1979).

17 A. Takenaka and Y. Sasada, *J. Cryst. Soc. Jpn.*, **22**, 214 (1980).

18 E. H. Gilmore, G. E. Gibsum, and D. S. McClure, *J. Chem. Soc.*, **20**, 829 (1952).

19 V. L. Ermoleav, *Opt. Spectrosk.*, **11**, 266 (1961); I. B. Berlman, *J. Chem. Phys.*, **52**, 5616 (1970).

20 V. L. Ermoleav, *Sov. Phys. —Dokl. (Engl. Transl.)*, **6**, 600 (1962).

21 G. W. Haggquist, R. D Burkhart, and K. R. Naqvi, *J. Phys. Chem.*, **95**, 7588 (1991).

22 T. G. Pavlopoulos, *J. Phys. Chem.*, **53**, 4230 (1970).

23 A. Tsuchida, M. Nakano, M. Yoshida, M. Yamamoto, and Y. Wada, *Polym. Bull.*, **20**, 297 (1988).

24 G. B. Strambini and W. C. Galley, *J. Chem. Phys.*, **63**, 3467 (1975).

25 K. Horie, K. Morishita, and I. Mita, *Macromolecules*, **17**, 1746 (1984).

26 A. C. Somersall, E. Dan, and J. E. Guillet, *Macromolecules*, **7**, 233 (1974).

27 S. K. Ho and S. Siegel, *J. Chem. Phys.*, **50**, 1142 (1969).

Part II

Chapter 5

Monte Carlo Simulation for the Hopping of Triplet Excitons in Poly[(9-phenenthrylmethyl methacrylate)-*co*-(methyl methacrylate)] Film

5.1. Introduction

Light-induced processes in aromatic polymers have been well investigated during the past two decades.[1-5] One of the important processes is the excitation energy migration in polymers through the aromatic pendant groups. The electronic excited state initially produced at a chromophore by absorption of a photon has been suggested to move to the adjacent chromophore sites by the Förster or Dexter mechanism.[6,7] The Dexter type energy transfer is often utilized in photosensitive polymers in view of the long lifetime of the triplet state. However, the behavior of triplet energy transfer in polymers has not been fully elucidated, because of experimental difficulties such as weak emission due to the efficient nonradiative deactivation. The triplet energy migration involve a short-range interaction of chromophores with overlapping of electric charge clouds.[7] This means that the efficient transport of triplet excitons occurs only in concentrated chromophoric systems. In such systems, excited chromophores often form stabilized sites such as an excimer site or a trap site.[8-14]

Previously, triplet behavior of several kinds of chromophoric polymer films has been reported and the interaction between chromophores classified into two types: excimer-type and trap-type.[15-18] The copolymer film with high concentrations of phenanthrene or naphthalene chromophores, shows slightly red-shifted phosphorescence spectra compared with the films having a low concentration of chromophores. However, those spectra are maintaining the vibrational band structure.[16,18] This type of excited species is called a *triplet trap-site* (^{3}T*) to distinguish it from the triplet excimer which is often observed in the copolymer films containing carbazole or benzene chromophores compared with the films having low concentration of the chromophores.[15,17] The triplet trap sites act as shallow traps for energy migration. The

trapped exciton can be thermally released from the trap site, and it migrates through the polymer film with iterative trapping and detrapping processes. The decay profiles of phosphorescence from trap sites are characterized by multiexponential functions or stretched exponential functions. Such decay profiles are observed when the excitons diffuse in the spatially or energetically inhomogeneous matrices.[19,20]

Many workers have proposed models to describe the complicated relaxation process of excited states.[19-28] Transport properties in inhomogeneous systems are described by a distribution of microscopic (site-to-site) transfer rates (temporal disorder) and by dispersive magnitudes of interactions with the surroundings (energetic disorder). Treatment of both disorders is an arduous task, which calls for extensive numerical simulations. Spatial randomness may be modeled by fractals,[29,30] and temporal disorder can be accounted for by using a waiting-time distribution, as familiar in continuous-time random walk (CTRW),[31,32] and multiple trapping (MT)[32,33] approaches. A drastic temperature effect on excitation energy migration and trapping could not be explained by either CTRW or MT models. Bässler *et al.* analyzed the migration process of triplet excitons in organic matrices by Monte Carlo simulation.[34] They assumed that the distribution of site energies (DOS) is expressed by a Gaussian function and that an exciton hops among these sites. They also reported that this DOS model is adequate for expressing the electron transport, photophysical hole burning, singlet energy migration and thermally induced transformation of spiropyran in polymer solids.[35,36] Previously, Katayama *et al.* applied this model to chromophoric polymer systems and successfully represented the phosphorescence decay profiles by this model in the temperature range of 115–165 K.[37]
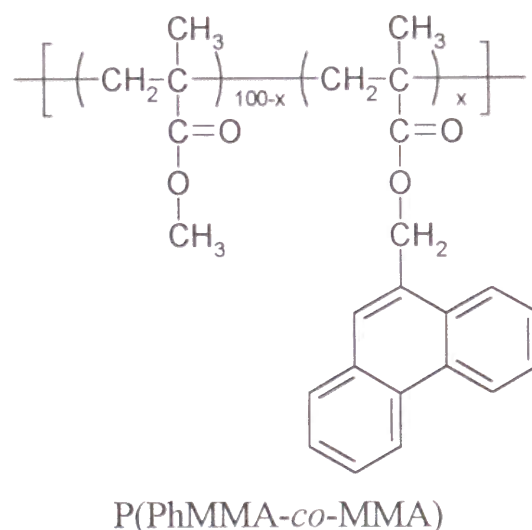
P(PhMMA-*co*-MMA)

Table 5–1. Compositions (x), Molecular Weights of P(PhMMA-*co*-MMA)s and Chromophore Concentrations ([Ph]), Average Distances Between Phenanthrene Chromophores (D) in the Films.

Sample	x mol %	Mw [a] 10^5	[Ph] mol L^{-1}	D [b] nm
P(PhMMA-*co*-MMA)L	0.78	1.30	0.09	2.63
P(PhMMA-*co*-MMA)H	18.6	1.20	1.67	1.00

[a] Determined by GPC calibrated with polystyrene standards. [b] Calculated by $D = n^{-(1/3)}$, where n is the average number of chromophores per unit volume.

In this chapter, we discuss the spectral shift of phosphorescence for the copolymer films containing phenanthrene chromophores. The spectral shift was simulated by the Monte Carlo method, and DOS of the triplet states was estimated in a temperature range of 15–100 K. The temperature dependence of the energy distribution is also discussed in terms of the thermal fluctuation of the chromophores within the free volume.

5.2. Experimental Section

5.2.1. Materials

The synthetic method for poly[(9-phenanthrylmethyl methacrylate)-*co*-(methyl methacrylate)] (P(PhMMA-*co*-MMA)) was as described previously by Katayama *et al.*[16] In the present chapter, we used two copolymers with various content of 9-phenanthrylmethyl methacrylate (x). We abbreviated lower-content copolymer (x = 0.78 mol %) as P(PhMMA-*co*-MMA)L and higher-content one (x = 18.6 mol %) as P(PhMMA-*co*-MMA)H, respectively. 1,4-Dibromonaphthalene (DBN; Tokyo Chemical Industry Co., Ltd.) recrystallized from

Table 5–2. Singlet and Triplet Energy Levels for Each Chromophore

Sample	E_S [a] kJ mol^{-1}	E_T [a] kJ mol^{-1}
P(PhMMA-*co*-MMA)L	346	260
DBN	374	237

[a] Calculated from the 0-0 transition band.

methanol was used as a triplet energy acceptor. The properties of copolymers and the energy levels of chromophores are listed in Tables 5–1 and 5–2, respectively. The energy levels for the lowest singlet state (E_S) of DBN is higher than that of phenanthrene (Ph), $i.e.$, when Ph is selectively excited at 337 nm, DBN quenches only the lowest triplet state of Ph.

5.2.2. Sample Preparation

A solid film on a quartz plate was formed by casting a solution of the copolymer in a small quantity of 1,2-dichloroethane (spectrophotomeric grade; Dojindo Laboratories). After the solvent evaporated, the film was dried $in\ vacuo$ for more than 10 h at room temperature and at 110 °C, respectively. In the same manner, DBN doped film was prepared by addition of prescribed amounts of DBN to the casting solution.

5.2.3. Measurements

Steady-state emission spectra were recorded with a Hitachi 850 spectrofluorophotometer. Time-resolved phosphorescence spectra and decay curves were measured with a phosphorimeter assembled in our laboratory. A xenon flash lamp (EG & G, FX198UV) and a nitrogen laser (NDC Co., JH–500) were used as the pulsed excitation light source for the measurements in millisecond and in microsecond time regions, respectively. To avoid damage to the detectors by the intense excitation light, a mechanical shutter and a gated photomultiplier (Hamamatsu, R1333) were used. Details of the system have been described elsewhere.[15]

The sample temperature was varied by a closed cycle liquid helium system (Iwatani Plantech Co., CRT 510) consisting of a low heat leak helium transfer line and a cryotip to which a sample holder is attached. Onto the sample holder made of copper the quartz sample plate and its cover plate were placed and fixed with another holed copper block. Indium foil was used between the quartz plates and the copper block to keep efficient thermal conductivity. The film holder is surrounded by a radiation shield and shroud, the interior of which is evacuated during operation. A tip heater was used to counter the cooling action and the temperature was maintained within ± 0.1 K by a temperature control unit (Iwatani Plantech Co., TCU–4). A calibrated thermocouple (Au + 0.07 % Fe / chromel) was connected to the copper block in the neighborhood of the sample to provide temperature as close to the area of observation as possible.

5.3. Results and Discussion

5.3.1. Spectroscopic Measurements

Figure 5–1 shows the phosphorescence spectra for the films of P(PhMMA-co-MMA). The 0–0 band of the spectra appeared at 474 nm for the 0.09 mol L^{-1} film (P(PhMMA-co-MMA)L) and 489 nm for the 1.67 mol L^{-1} film (P(PhMMA-co-MMA)H). In a glassy solution of MTHF, P(PhMMA-co-MMA)L gave a phosphorescence spectrum corresponding to the chromophores having no interaction with neighboring chromophores : the 0–0 band of the triplet state of isolated Ph appeared at 461 nm.[16] Hereafter, we will refer to the isolated species as the monomer triplet state (^{3}M*). The spectra of P(PhMMA-co-MMA) films were shifted to a longer wavelength with increasing chromophore concentration, but the band shape remained unchanged. Such shifted phosphorescence spectra have been seen in glassy
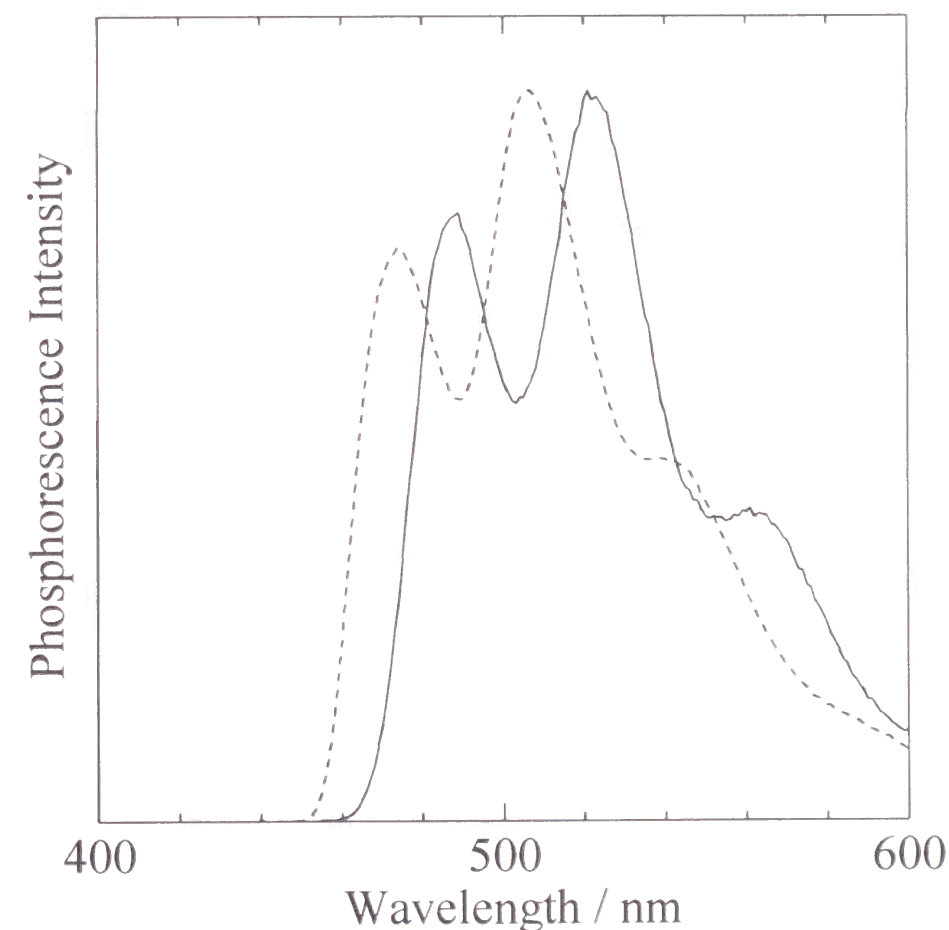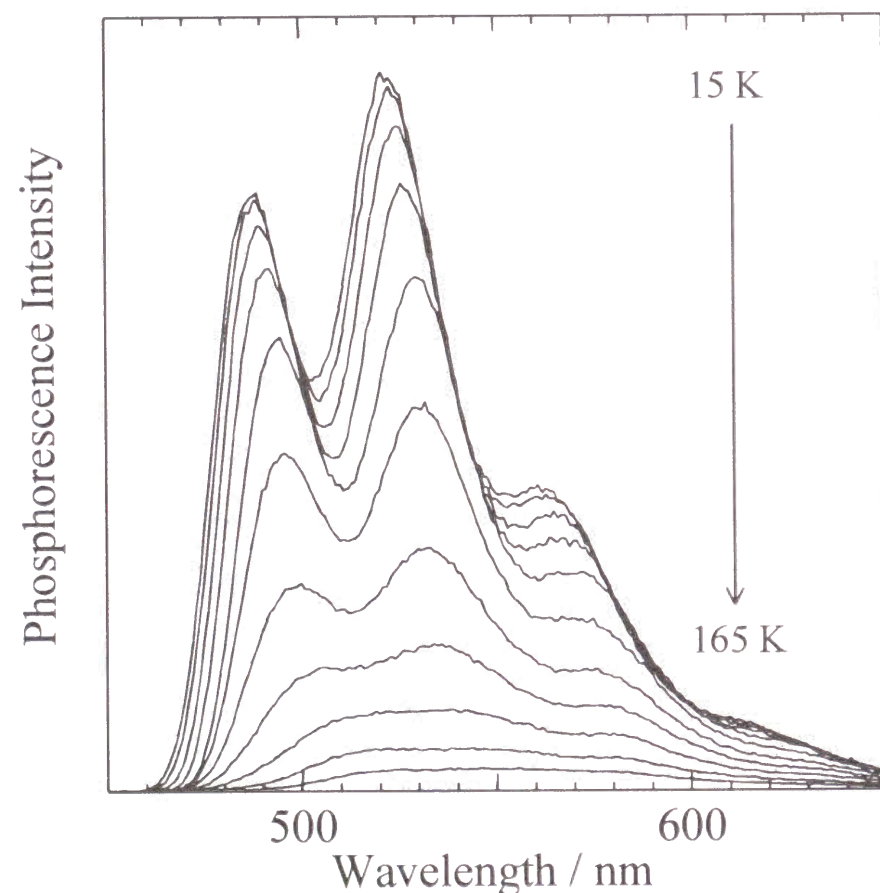

Figure 5–1. Phosphorescence spectra of P(PhMMA-co-MMA)L (------) and P(PhMMA-co-MMA)H (——) films at 15 K. Spectra are normalized at the maximum of each spectrum peak.

solutions of vinyl polymers bearing pendant aromatic groups.[38-41]   The excited triplet state is stabilized by the interactions between chromophores, but the interaction energy is not sufficient to give the spectrum a broad excimeric emission.   We will refer to this slightly stabilized state as the trap (^{3}T*) and distinguish it from the excimer which is in a strongly stabilized state.

The temperature dependence of phosphorescence spectra for P(PhMMA-co-MMA)H film is shown in Figure 5–2.   The spectra were shifted to a longer wavelength and the intensity decreased with increasing temperature, but the band shape remained the same.   This behavior resembles the dependence of the spectra on the chromophore concentration.   With elevating temperature, the free volume of the polymer film increases, and the spatial range available for the thermal vibration of the chromophore enlarges.   Then, the chromophores can form more stabilized trap sites within their excited lifetime.   The broadened spectra at high temperatures may be caused by overlapping of the emission from several trap sites of different energy levels.

Figure 5–3 shows the typical time-resolved phosphorescence spectra for P(PhMMA-co-MMA)H film, which were measured at 100 K.   The spectra were gradually shifted to longer

Figure 5–2.   Phosphorescence spectra of P(PhMMA-co-MMA)H film.   Sample temperature was changed from 15 (top) to 165 K (bottom) by every 15 K separation.

---

wavelengths with the elapse of time.   The bandwidth of the spectra became narrower simultaneously with the spectral shift as obviously observed at the 0–0 band.   Two reasons are considered for this spectral shift.   One is the dynamic formation of ^{3}T* site by the motion of the chromophores. The other is the exciton relaxation toward lower energy ^{3}T* sites through the hopping among several trap sites.   There is no clear evidence but a support for the latter is provided by the absorption spectra for P(PhMMA-co-MMA) film.

Figure 5–4 shows the temperature dependence of the absorption spectra for phenanthrene 0–0 band in P(PhMMA-co-MMA)H film.   The peak position was maintained constant below 120 K and then shifted toward the lower energy side due to increasing interchromophore interaction.   This indicates that the average energy for the Ph singlet state is maintained in the low-temperature range.   We assumed that the average energy for ^{3}T* state of the chromophores is also maintained in this temperature range.   In an amorphous polymer film,
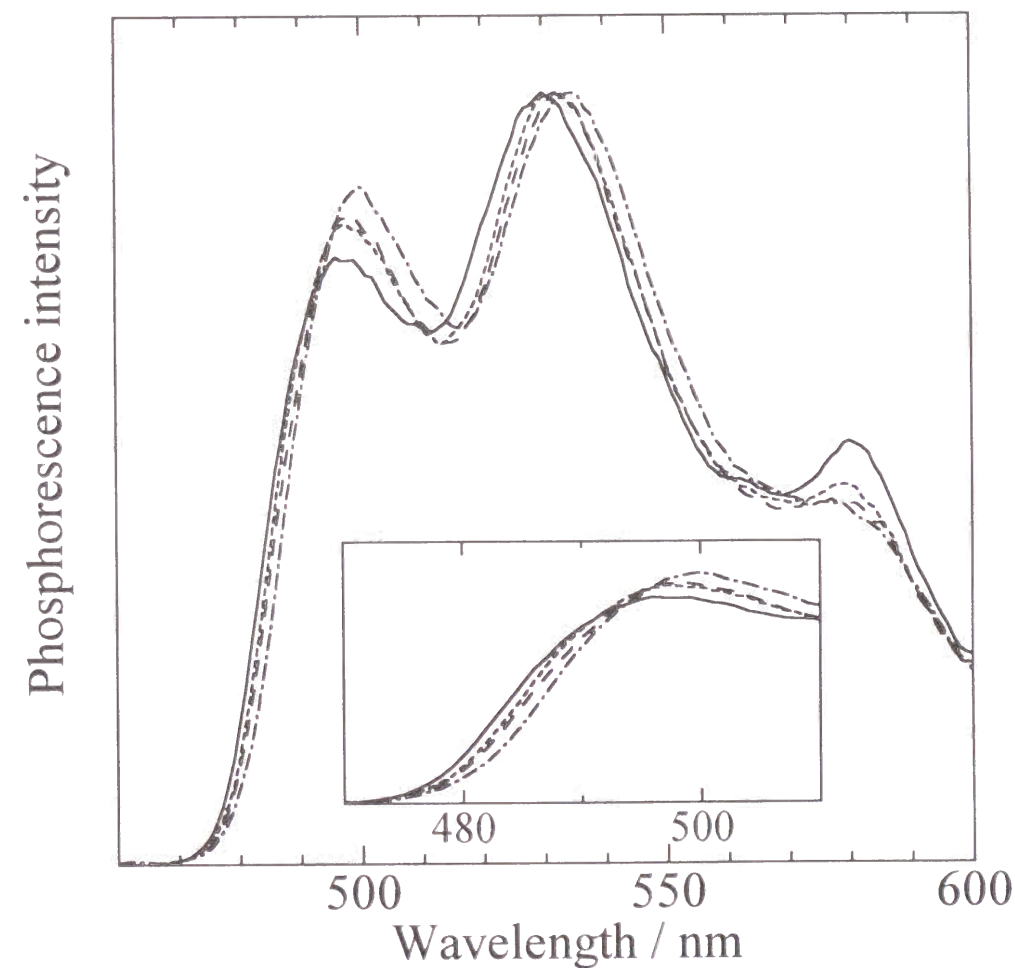
Figure 5–3.   Time resolved phosphorescence spectra of P(PhMMA-co-MMA)H films at 100 K recorded at delay time 0.8 ms (——), 17 ms (------), 33 ms (– – –) and 161 ms (– · – · –) (sampling time 8 ms).   Spectra are normalized at the maximum of each spectrum peak.
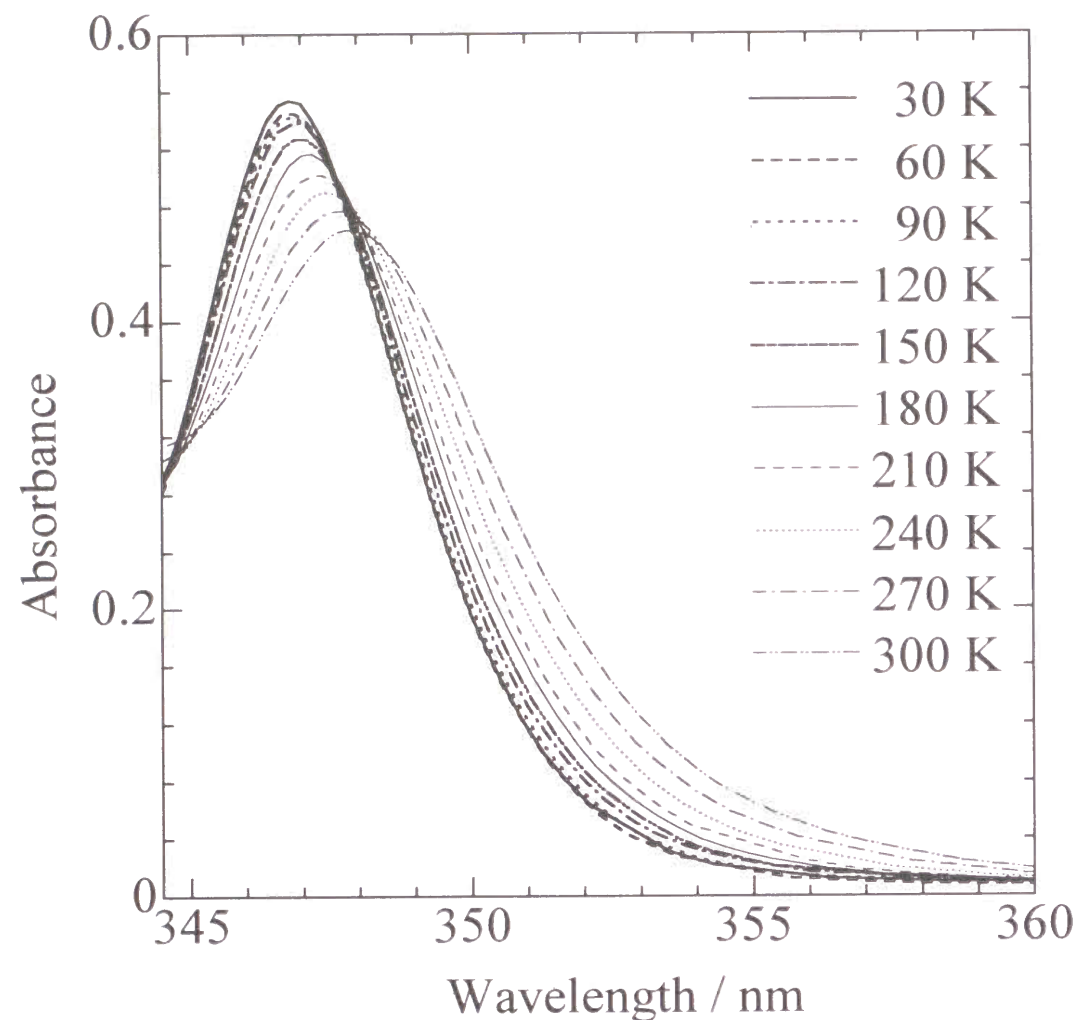
Figure 5–4. Lowest-energy absorption peak of P(PhMMA-*co*-MMA)H film. Sample temperature was changed from 30 (top) to 300 K (bottom) by every 30 K separation.

the distribution of the energy of the ^{3}T* sites becomes wider due to inhomogeneity of the environment, like the "*inhomogeneous broadening*" observed in the studies of the spectral hole-burning.[42] The triplet excitons migrate among these broad energy levels and gradually fall in lower energy sites. If the lifetime of the excited states is sufficiently long, the distribution of the triplet excitons finally obeys the Boltzmann relation. The spectral shift in Figure 5–3 can be interpreted as a result of the relaxation of the triplet excitons.

Figure 5–5 depicts the phosphorescence spectra for P(PhMMA-*co*-MMA)H film containing a small amount of DBN (5×10^{-3} mol L^{-1}). At 15 K, the phosphorescence from only the phenanthrene unit at 485, 522, and 564 nm, was observed. With increase in temperature, the Ph phosphorescence decreased, and in place of it, the DBN phosphorescence appeared at 507, 545, and 588 nm. When DBN was doped in P(PhMMA-*co*-MMA)L film, the phosphorescence only from Ph units was observed. This behavior of phosphorescence
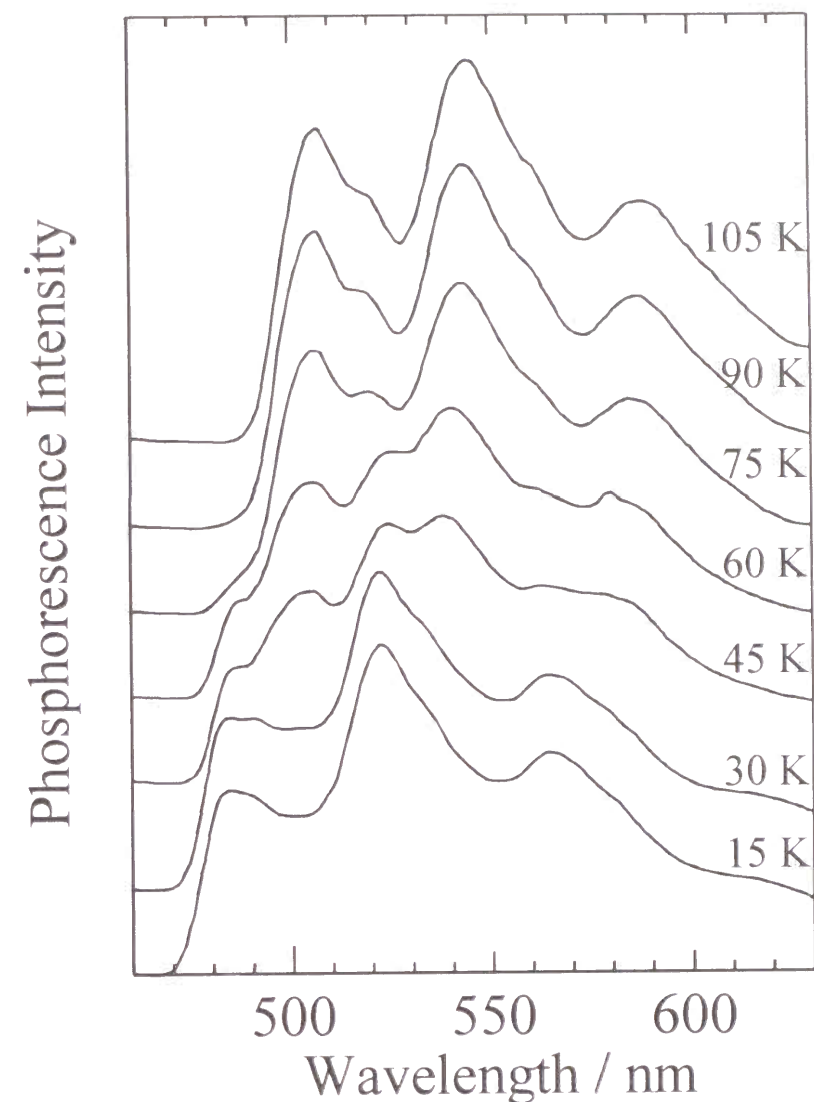
Figure 5–5. Phosphorescence spectra of the DBN doped P(PhMMA-*co*-MMA)H film at the indicated temperature. The concentration of DBN is 5×10^{-3} mol L^{-1}.

spectra can be interpreted by the mechanism as shown in scheme.

The migrating exciton is captured by a ^{3}T* site with a potential energy lower than the surrounding sites. At lower temperatures, the triplet exciton cannot overcome the energy barrier so that it is captured immediately and is able to migrate within a narrow range. At higher temperatures, the exciton may overcome the barrier and migrates over a wide range. When acceptors are doped in the film, the probability that the triplet exciton reaches the acceptor site increases with the temperature. This interpretation is also applicable for the spectral shift in Figure 5–3.

Phosphorescence decay curves at different temperatures show more direct evidence of this scheme. Figure 5–6 shows phosphorescence decay curves at different wavelengths. At

Scheme: **Schematic Illustration of the Energy Migration among the Levels with Broadly Distributed Energies** [a]
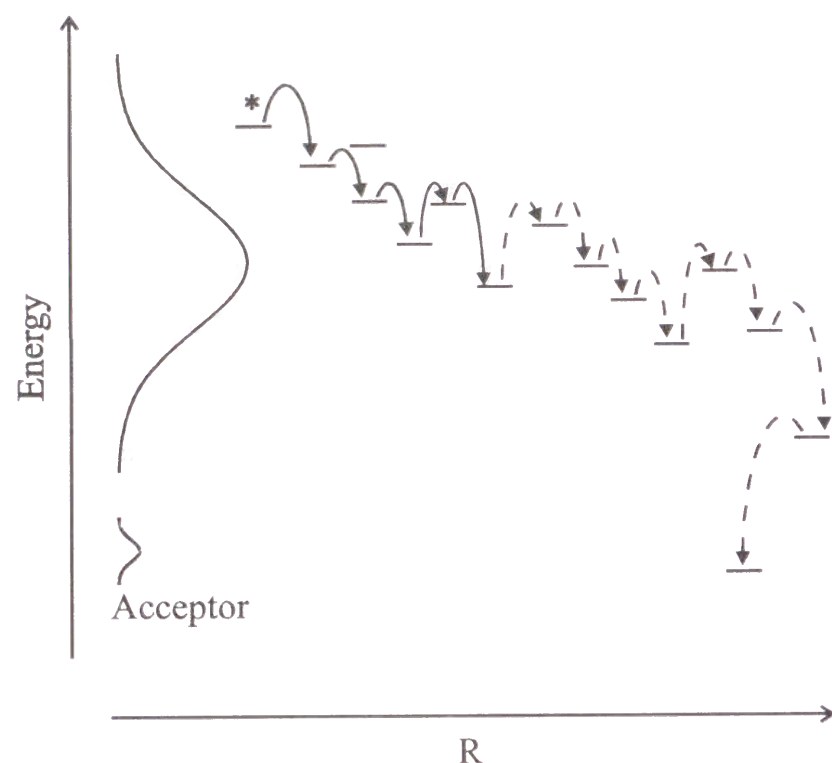
^{a} At low temperatures, an exciton ($*$) is trapped by a shallow $^3T^*$ site (——→). With increasing temperature, the exciton migrates to deeper $^3T^*$ sites (– – –→).

low temperature (15 K), phosphorescence decay profiles were similar for all wavelengths. At higher temperature (100 K), however, the higher-energy phosphorescence had decayed faster than the lower-energy one.

5.3.2. Spectral Shift due to the Energy Migration

Assuming that the DOS is a Gaussian for $^3T^*$ site of phenanthrene chromophores, very fast internal conversion and intersystem crossing produces a Gaussian distribution of phenanthrene triplet state.   The DOS, $f(\varepsilon)$, is expressed as follows:

$$f(\varepsilon) \propto \exp\left[\frac{-\left(\varepsilon - \langle\varepsilon\rangle_0\right)^2}{2\sigma^2}\right] \qquad (5\text{--}1)$$

where $\langle\varepsilon\rangle_0$ is the average transition energy with respect to the ground state and σ^2 is the site-energy dispersion.   The distribution, $g(\varepsilon)$, of excitons at $t = 0$ is the same as $f(\varepsilon)$: $g_0(\varepsilon) = f(\varepsilon)$. The distribution of excitons after thermalization is $g_\infty(\varepsilon)$ which is expressed by $f(\varepsilon)$ weighted by a Boltzmann factor:
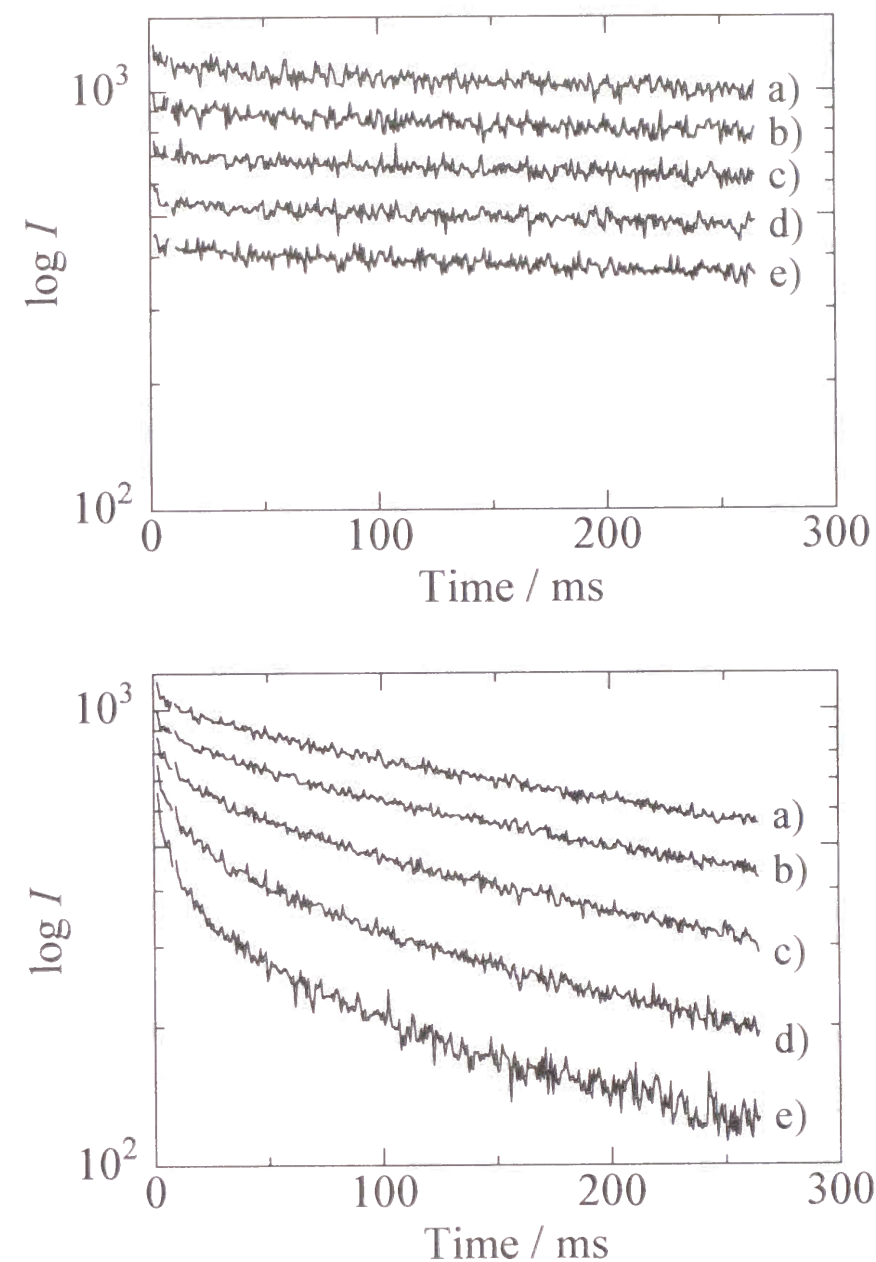
Figure 5–6.   Phosphorescence decay curves of P(PhMMA-*co*-MMA)H at 15 (top) and 100 K (bottom) : monitored at (a) 480 nm, (b) 485 nm, (c) 490 nm, (d) 495 nm, and (e) 500 nm.

$$g_\infty(\varepsilon) \propto \exp\left[\frac{-\left(\varepsilon - \langle\varepsilon\rangle_0\right)^2}{2\sigma^2}\right]\exp\left[\frac{-\left(\varepsilon - \langle\varepsilon\rangle_L\right)}{kT}\right] \qquad (5\text{--}2)$$

where $\langle\varepsilon\rangle_L$ is the lower limit of the 0–0 transition energy.   Eq 5–2 can be rewritten as a Gaussian form:

$$g_\infty(\varepsilon) \propto \exp\left[\frac{-\left(\varepsilon - \langle\varepsilon\rangle_\infty\right)^2}{2\sigma^2}\right]\exp\left[\frac{2kT\left(\langle\varepsilon\rangle_L - \langle\varepsilon\rangle_0\right) - \sigma^2}{2k^2T^2}\right]$$

$$\propto \exp\left[\frac{-\left(\varepsilon - \langle\varepsilon\rangle_\infty\right)^2}{2\sigma^2}\right] \qquad (5\text{--}3)$$

where the averaged energy, $\langle\varepsilon\rangle_\infty$, is red shifted from $\langle\varepsilon\rangle_0$ by the amount of $\sigma^2/2kT$. The Gaussian distribution given by eq 5–1 can be treated as a high temperature limit ($T \to \infty$) of eq 5–3 where no relaxation is involved. At the experimental temperature, T, the distribution function of excitons shifts continuously from the initial Gaussian $f(\varepsilon) = g_0(\varepsilon)$ toward the final
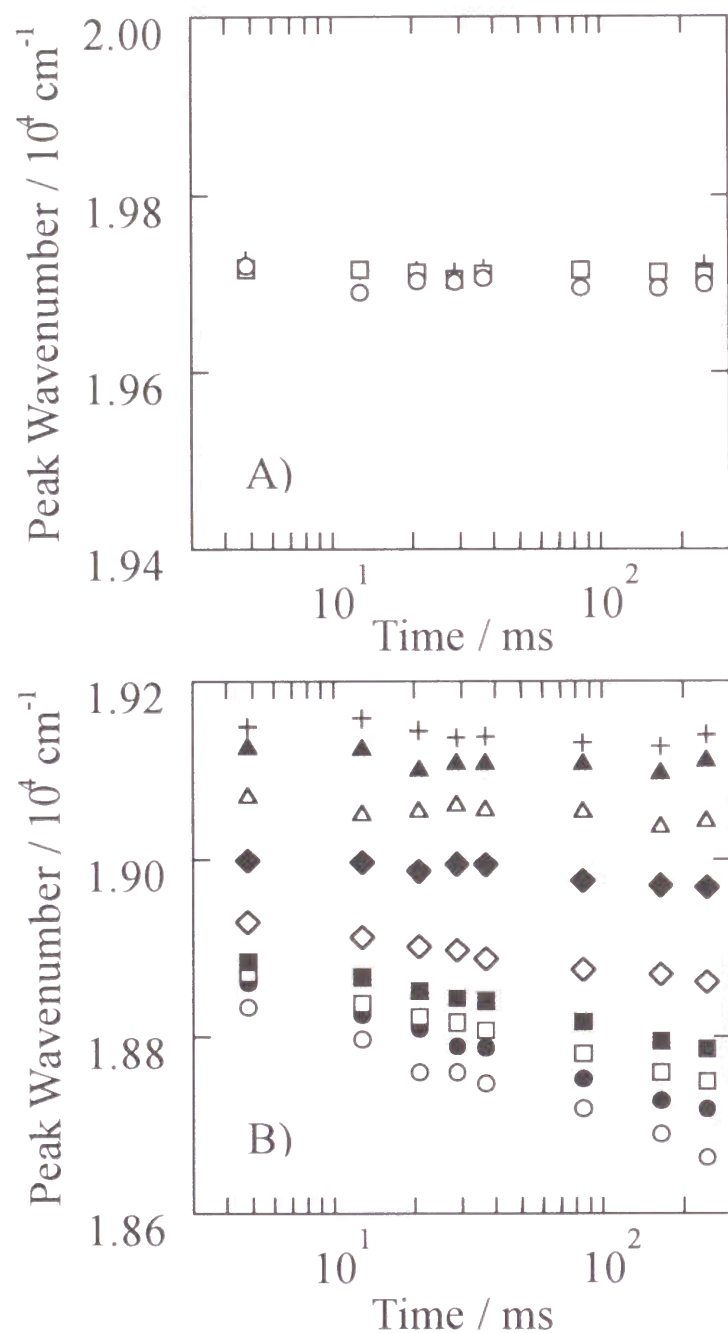
Figure 5–7. Peak wavenumber of the second phosphorescence band of P(PhMMA-*co*-MMA)L (A) and P(PhMMA-*co*-MMA)H (B) film as a function of delay time at 15 K (+), 30 K (▲), 45 K (△), 60 K (◆), 75 K (◇), 85 K (■), 90 K (□), 95 K (●), and 100 K (○).

Gaussian $g_\infty(\varepsilon)$. Therefore, the transient distribution $g_t(\varepsilon)$ during the relaxation process will be also expressed by a Gaussian shape as follows:

$$g_t(\varepsilon) \propto \exp\left[\frac{-\left(\varepsilon - \langle\varepsilon\rangle_t\right)^2}{2\sigma^2}\right] \qquad (5\text{--}4)$$

where the center position $\langle\varepsilon\rangle_t$ and the width σ are both dependent on time. This equation suggests that the mean energy can be monitored by the peak energy of phosphorescence band.

The mean energy of the triplet excitons, $\langle\varepsilon\rangle_t$ was estimated from the peak of the second band which is the most intense peak. Time profiles of $\langle\varepsilon\rangle_t$ were summarized in Figure 5–7. For the P(PhMMA-*co*-MMA)L film, $\langle\varepsilon\rangle_t$ remained constant in the temperature range from 15–100 K. On the other hand, $\langle\varepsilon\rangle_t$ for P(PhMMA-*co*-MMA)H film decreased logarithmically with the elapse of time; in particular, it decreased rapidly at the elevated temperatures. If the decrease in $\langle\varepsilon\rangle_t$ is only caused by the motion of chromophores, $\langle\varepsilon\rangle_t$ should decrease for both polymer films. The different time profiles for the phosphorescence spectra of two polymer films indicate that the spectral shift is due to the triplet energy migration as described above.

5.3.3. Monte Carlo Simulation Method

Bässler *et al.* analyzed the relaxation processes of electron and triplet energy in amorphous organic layers.[36] They assumed that the electron transport and the energy migration in those systems occur through the hopping among the sites that exhibit a Gaussian DOS. Stein *et al.* used a Voigt DOS to express the absorption bands of chromophores embedded in the glassy matrices of organic polymers, and those band shapes were in reasonably good agreement with the function.[43] This means that both Lorentzian homogeneous line and the Gaussian inhomogeneous line are good models for the amorphous polymer system. When the homogeneous linewidth is narrow, a Voigt distribution is similar to a Gaussian one. In this chapter, we expressed the DOS by a Gaussian function because the observation was performed at low temperatures (15–100 K).

On the basis of these considerations, we simulated the hopping of the triplet excitons among the $^3T^*$ sites by the following procedure. Figure 5–8 shows the system in this simulation schematically.

The procedure to set up a specific lattice is as follows. The lattice contains $51 \times 51 \times 51$ = 132,651 sites. The lattice space selected is 1.0 nm that corresponds to the average
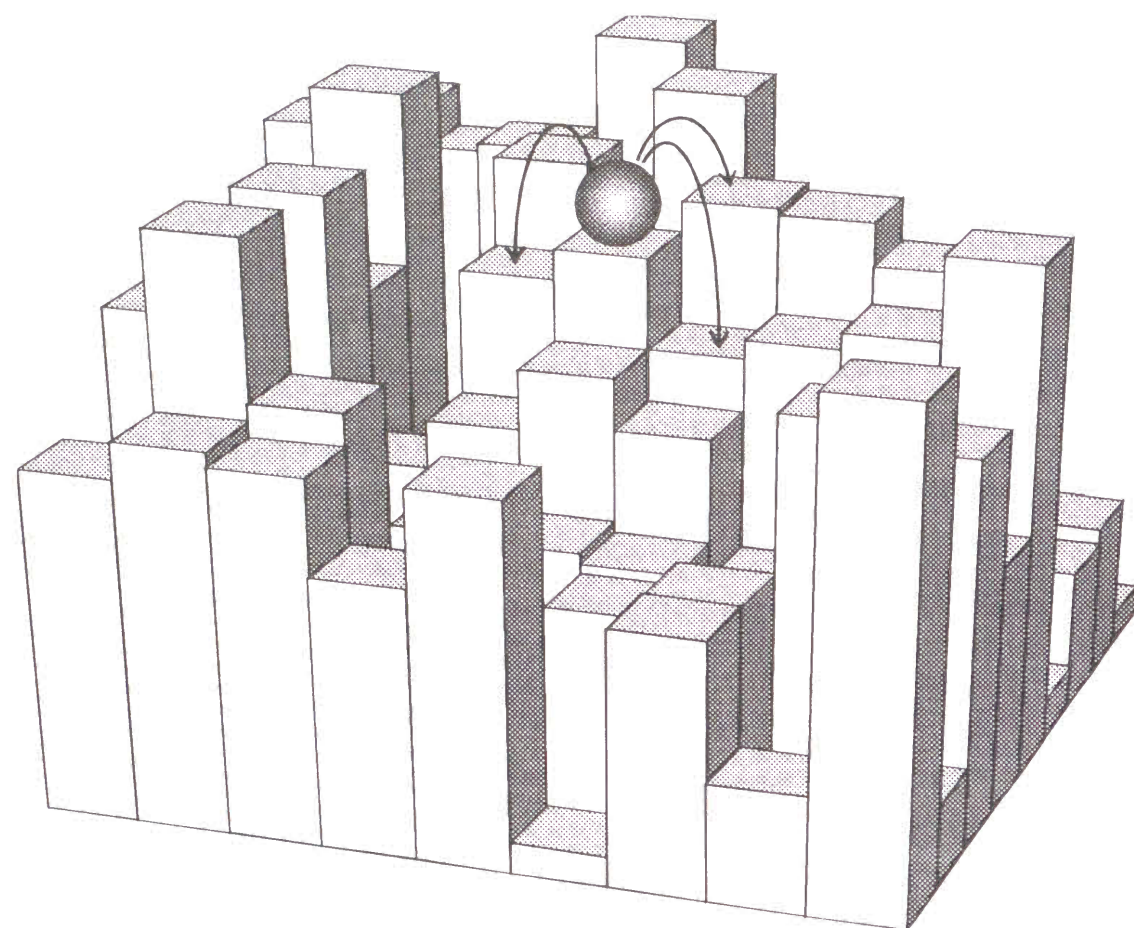
Figure 5–8. Schematic illustration of a model for the calculation with Monte Carlo method. A black ball represents the triplet exciton and arrows show the energy migration to adjacent phenanthrene units.

interchromophore distance in P(PhMMA-*co*-MMA)H film. The origin is placed at the site (25, 25, 25). The site-energy, $f(\varepsilon)$, for each of the 132,651 sites is selected at random according to a Gaussian distribution function as eq 5–5.

$$f(\varepsilon)\, \mathrm{d}\varepsilon = \frac{1}{\sqrt{2\pi\sigma^2}} \exp\left[\frac{-\varepsilon^2}{2\sigma^2}\right] \mathrm{d}\varepsilon \tag{5–5}$$

A moving particle always started from the center (25, 25, 25). The probability, P_{ij}, that the particle makes a jump from (x_i, y_i, z_i) with energy ε_i to a site (x_j, y_j, z_j) with energy ε_j is

$$P_{ij} = \frac{\nu_{ij}}{\sum_{l \neq i} \nu_{il}} \tag{5–6}$$

where

$$\nu_{il} = \nu_0 \exp\left[-\frac{2r_{il}}{L}\right] \exp\left[-\frac{(\varepsilon_l - \varepsilon_i)}{kT}\right] \tag{5–7}$$

---

providing that $\varepsilon_l - \varepsilon_i \geq 0$.

If $\varepsilon_l - \varepsilon_i < 0$, then

$$\nu_{il} = \nu_0 \exp\left[-\frac{2r_{il}}{L}\right] \tag{5–8}$$

where ν_0 is constant, r_{il} is the distance between site i and l, and L is a constant called the effective average Bohr radius. Here, $\nu_{il} \neq \nu_{li}$. This is the difference between the spatially disordered system and the energetic disordered one. While the sum over l should include all sites, for practical purpose only the nearest 26 sites are included in the calculation.

A site to which the particle jumps is chosen by a uniform random number n_u according to P_{ij}. The time for the jump, t_{ij}, is determined from

$$t_{ij} = \frac{n_{ei}}{\sum_{l \neq i} \nu_{il}} \tag{5–9}$$

where n_{ei} is a random number taken from an exponential distribution. The track of the particle is followed and its positions and the site energies are noted as a function of time. These
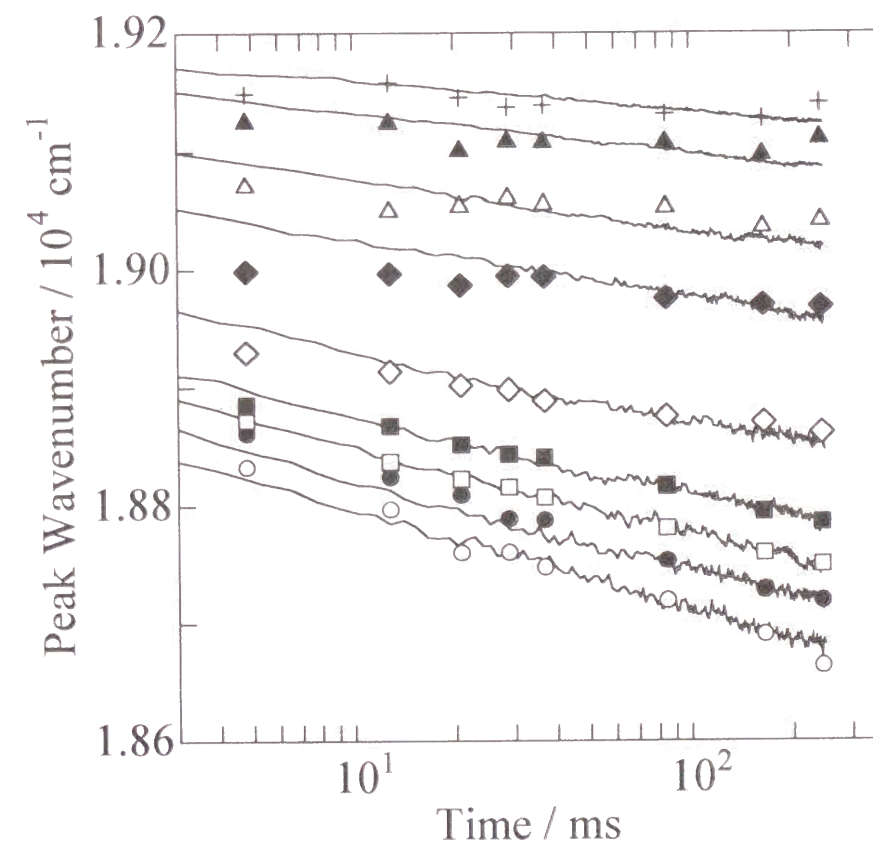
Figure 5–9. Simulation result for P(PhMMA-*co*-MMA)H film. Gaussian DOS is centered at 19,395 cm^{-1}. Data points are taken from Figure 5–7B.

procedure are continued until the time reaches 250 ms. For each configuration, a particle is sent out from the original point and the procedure is repeated 20 times. For a distribution parameter of σ, 300 different random energy configurations were considered. After obtaining the positions and the site energies as a function of time for all the 300 configurations, we obtained the root mean square diffusion length, $<r^2(t)>^{1/2}$, and the average site energy $<\varepsilon>_t$.

5.3.4. Evaluation of the Distribution of Site Energy

Figure 5–9 shows the simulation results for P(PhMMA-co-MMA)H film. The calculated lines were in agreement with the experimental values using σ and $<\varepsilon>_0$ as the fitting parameters. The center of Gaussian DOS could be maintained constant as estimated from absorption spectra. The simulated curves well reproduced the experimental data when the center energy was fixed to 19,395 cm^{-1}. The energy is lower than the average energy of triplet exciton for P(PhMMA-co-MMA)L film, 19,763 cm^{-1}, which was obtained from the second peak of the phosphorescence of the film. This means that the triplet state of Ph chromophore is stabilized by the interchromophore interaction for P(PhMMA-co-MMA)H film and the distribution of the triplet energy level shifts toward the lower energy side even at the initial stage, $t = 0$.

The parameters and the results of the simulation are summarized in Table 5–3. As shown

Table 5–3. Standard Deviation of the Trap-Energy Distribution (σ), Dispersion Parameter (α) and Root-Square-Mean Diffusion Length of Triplet Exciton ($<r(t)^2>^{1/2}$) for P(PhMMA-co-MMA)H Film

| Temperature / K	σ / cm^{-1}	σ/RT	α [a]	$<r(t)^2>^{1/2}$ / nm		
				2.5 ms	25 ms	250 ms
15	145	13.9	0.076	2.15	2.44	2.87
30	155	7.4	0.23	2.75	3.47	4.32
45	180	5.8	0.33	3.13	4.35	6.64
60	210	5.0	0.39	3.52	5.66	9.47
75	260	5.0	0.39	3.59	5.44	9.31
85	290	4.9	0.40	3.65	5.71	9.85
90	305	4.9	0.40	3.73	5.87	9.74
95	325	4.9	0.40	3.64	5.68	9.88
100	340	4.9	0.40	3.68	5.69	9.97

[a] $\alpha^{-1} = (\sigma/4RT)^2 + 1$.

in Table 5–3, σ is much larger than the thermal energy (RT) in the present temperature range. Thus, the site energy distribution must be a critical factor for the dispersive transport of the triplet excitons. Empirically, the dispersion parameter α was derived as follows,[35]

$$\alpha^{-1} = \left(\frac{\sigma}{4RT}\right)^2 + 1 \qquad (5\text{–}10)$$

The standard deviation of the trap energy distribution, σ, increased with temperature, but α saturated above 75 K. This means that energetic dispersity is constant between 75 and 100 K. The time profiles of $<r(t)^2>^{1/2}$ are also similar in this temperature range. These behaviors are in fair agreement with the previous report that the parameter α well characterizes the transport properties of a hopping system with Gaussian type of energetic disorder.[35] The standard deviation of the trap energy distribution is expressed by the superposition of homogeneous linewidth ($\Delta\omega_h$) and inhomogeneous linewidth ($\Delta\omega_i$).[44] The excited-state dephasing interaction and lifetime effect determine $\Delta\omega_h$. The site-energy shift determines $\Delta\omega_i$, which is caused by a small difference in the interaction energy of a chromophore with the
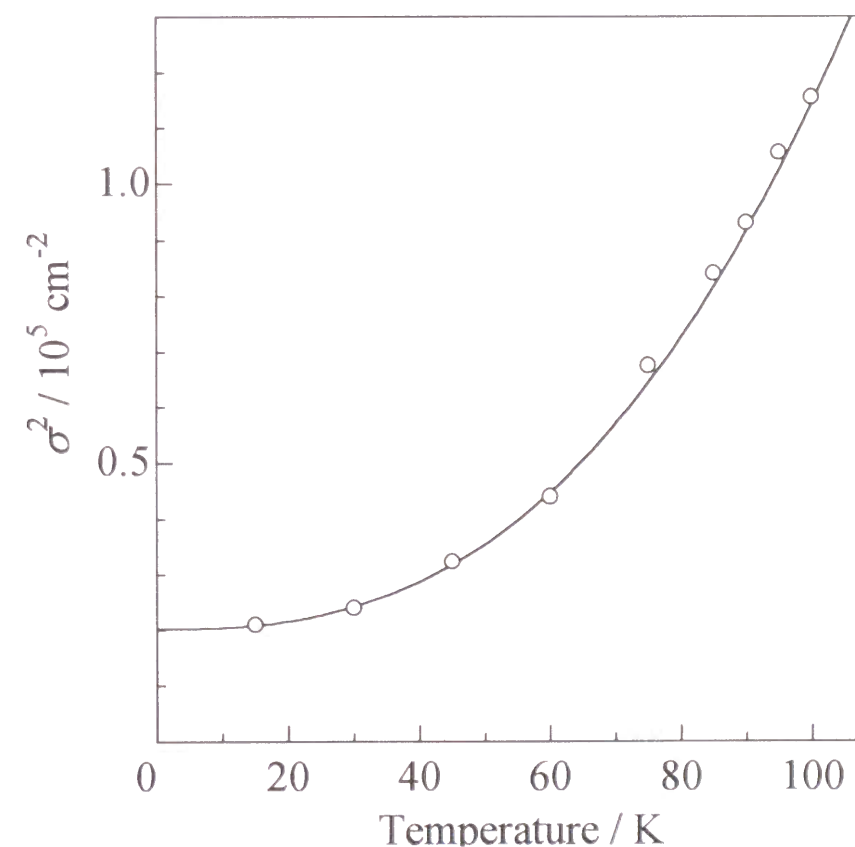
Figure 5–10. The temperature dependence of the site-energy dispersion, σ^2. The data were fitted by a function: $\sigma^2 = \Delta\omega_h{}^2 + \Delta\omega_i{}^2$, where $\Delta\omega_h = a\, T^n$. $\Delta\omega_h = 0.736 \times T^{1.31}$ cm^{-1}, $\Delta\omega_i = 142$ cm^{-1}.

environmental matrix. As Stein *et al.* adopted, the most reasonable function for DOS is the Voigt type which is a Gaussian inhomogeneous line including Lorentzian homogeneous lines for each element. However, we propose to estimate the temperature dependence of DOS profile and its influence to the transport process of the triplet exciton. Thus, we adopted the simplified model that both homogeneous and inhomogeneous lines were expressed by a Gaussian function. By this simplification, σ^2 is obtained from eq 5–11.

$$\sigma^2 = \Delta\omega_h^2 + \Delta\omega_i^2 \qquad (5\text{--}11)$$

In this study, the spectral shift was simulated at the temperatures below the γ-transition of the matrix polymer, which is associated with the rotation of the α-methyl groups of poly(methyl methacrylate). Therefore, $\Delta\omega_i$ is probably constant in the present temperature range. Assuming that $\Delta\omega_h$ follows T^n law, the temperature dependence of σ was fitted by eq 5–12.

$$\sigma^2 = \left(a\,T^n\right) + \Delta\omega_i^2 \qquad (5\text{--}12)$$

As shown in Figure 5–10, the relationship of $\Delta\omega_h \propto T^{1.3}$ holds in the temperature range from 15–100 K. This relationship has been reported to exist in many amorphous matrices.[45] Jackson *et al.* theoretically explained the temperature dependence of the hole width of molecules in soft glasses by considering a combination of two dephasing mechanisms.[46] This similarity reveals that the temperature dependence of σ is mainly attributable to the homogeneous broadening.

5.4. Conclusion

Time–resolved phosphorescence spectra were measured for the copolymer films containing Ph moieties. At a high Ph concentration, the phosphorescence spectra were shifted toward the lower energy side. This behavior was explained by the model that the population of the triplet excitons within a Gaussian DOS changes from the uniform distribution toward Boltzmann distribution. The time evolution of the standard deviation of trap energy distribution and the mean value of triplet energies were estimated by a computer simulation. The temperature dependence of the dispersity of DOS is mainly attributed to the homogeneous broadening. At low temperatures, the site energy distribution is one of the critical factors for determining the triplet energy migration.

References

1 N. J. Turro, *"Modern Molecular Photochemistry"*, Benjamin, Menlo Park, CA, 1978, p. 296; J. B. Birks, *"Photophysics of Aromatic Molecules"*, Wiley, New York, 1970, p. 518.

2 J. Mort and G. Pfister Eds., *"Electronic Properties of Polymers"*, John Wiley & Sons, New York, 1982.

3 J. E. Guillet, *"Polymer Photophysics and Photochemistry"*, Cambridge University Press, Cambridge, U. K., 1985; S. C. Webber, *"Polymer Photophysics"*, D. Phillips, Ed., Chapman and Hall, New York, 1985; I. Soutar and D. Phillips, *"Photophysical and Photochemical Tools in Polymer Science"*, M. A. Winnik Ed., Reidel, Dordrecht, The Netherlands, 1986; C. E. Hoyle and J. M. Torkelson Eds., *"Photophysics of Polymers; ACS Symposium Series 358"*, American Chemical Society, Washington DC, 1987; J. F. Rabek, *"Mechanisms of Photophysical Processes and Photochemical Reactions in Polymers"*, John Wiley & Sons, New York, 1991.

4 F. Wilkinson, *Quart. Rev.*, **20**, 403 (1966).

5 S. E. Webber, *Chem. Rev.* **90**, 1469 (1990).

6 Th. Förster, *Ann. Phys.*, **2**, 55 (1948); Th. Förster and K. Kasper, *Z. Electrochem.*, **59**, 976 (1955); Th. Förster, *Discuss. Faraday Soc.*, **27**, 7 (1959).

7 D. L. Dexter, *J. Chem. Phys.*, **21**, 836 (1953).

8 F. Hirayama, *J. Chem. Phys.*, **42**, 3163 (1965).

9 Y. Nishijima, *J. Polym. Sci. C*, **31**. 353 (1970).

10 O. L. J. Gijzeman, J. Langelaar, and J. D. W. Van Voorst, *Chem. Phys. Lett.*, **5**, 269 (1970).

11 W. Klöpffer and D. Fischer, *J. Polym. Sci. C*, **40**, 43 (1973).

12 K. Zachariasse and W. Kühnle, *Z. Phys. Chem. (Munich)*, **101**, 267 (1976).

13 S. Ito, M. Yamamoto, and Y. Nishijima, *Bull. Chem. Soc. Jpn.*, **54**, 35 (1981).

14 Y. Itoh and S. E. Webber, *Macromolecules*, **23**, 5065 (1990).

15 S. Ito, H. Katayama, and M. Yamamoto, *Macromolecules*, **21**, 2456 (1988).

16 S. Ito, N. Numata, H. Katayama, and Yamamoto, M. *Macromolecules*, **22**, 2207 (1989).

17 H. Katayama, S. Ito, and M. Yamamoto, *J. Photopolym. Sci. Technol.*, **4**, 217 (1991).

18 H. Katayama, T. Tawa, S. Ito, and M. Yamamoto, *J. Chem. Soc., Faraday Trans. 2*, **88**,

2743 (1992).

19   I. Yamazaki, N. Tamai, and T. Yamazaki, *J. Phys. Chem.*, **94**, 516 (1990); N. Tamai, T. Yamazaki, and I. Yamazaki, *Can. J. Phys.*, **68**, 1013 (1990).

20   H. Katayama, T. Tawa, G. W. Haggquist, S. Ito, and M. Yamamoto, *Macromolecules*, **26**, 1265 (1993).

21   F. E. El–Sayed, J. R. MacCallum, P. J. Pomery, and T. M. Shepherd, *J. Chem. Soc., Faraday Trans. 2*, **75**, 79 (1979).

22   G. Zumofen, A. Blumen, and J. Klafter, *J. Chem. Phys.*, **82**, 3198 (1985); *J. Chem. Phys.*, **84**, 6679 (1986).

23   J. D. Byers, M. S. Friedrichs, R. A. Friesner, and S. E. Webber, *Macromolecules*, **21**, 3402 (1988); J. D. Byers, W. S. Parsons, R. A. Friesner, and S. E. Webber, *Macromolecules*, **21**, 3402 (1988).

24   E. J. Janse van Rensburg, J. E. Guillet, and S. G. Whittington, *Macromolecules*, **22**, 4212 (1989).

25   Y. Lin, M. C. Nelson, and D. M. Hanson, *J. Chem. Phys.*, **86**, 1586 (1987); Y. Lin, R. C. Dorfman, and M. D. Fayer, *J. Chem. Phys.*, **90**, 159 (1989).

26   L. A. Harmon and R. Kopelman, *J. Phys. Chem.*, **94**, 3454 (1990); C. S. Li and R. Kopelman, *Macromolecules*, **23**, 2223 (1990).

27   K. Sienicki and G. Durocher, *Macromolecules*, **24**, 1102 (1991).

28   S. H. Kost and H. D. Breuer, *Ber. Bunsenges. Phys. Chem.*, **95**, 480 (1991).

29   B. B. Mondelbrot, *"The Fractal Geometry of Nature"*, Freeman, San Francisco, 1982.

30   A. Blumen, J. Klafter, and G. Zumofen, *Phys. Rev. B*, **27**, 6112 (1983); J. Klafter, A. Blumen, and G. Zumofen, *J. Stat. Phys.*, **36**, 561 (1984).

31   H. Scher and M. Lax, *Phys. Rev. B*, **7**, 4491 (1973); *Phys. Rev. B*, **7**, 4502 (1973).

32   E. W. Montroll and M. F. Shlesinger, *"Non-Equilibrium Phenomena. II. From Stochastics to Hydrodynamics"*, J. L. Lebowitz and E. W. Montroll Ed., North–Holland, Amsterdam, 1984, p. 1.

33   M. F. Shlesinger and E. W. Montroll, *Proc. Natl. Acad. Sci. U. S. A.*, **81**,1280 (1984).

34   R. Richert, B. Richert, and H. Bässler, *Philos. Mag. B*, **49**, L25 (1984); R. Richert and H. Bässler, *J. Chem. Phys.*, **84**, 3567 (1986).

35   H. Bässler, *Phys. Status Solidi B*, **107**, 9 (1981).

36   G. Schönherr, H. Bässler, and M. Silver, *Phil. Mag. B*, **44**, 47 (1981); R. Richert, A. Elshner, and H. Bässler, *Z. Phys. Chem. NF.*, **149**, 63 (1986).

37   H. Katayama, T. Tawa, G. W. Haggquist, S. Ito, and M. Yamamoto, *Macromolecules*, **26**, 1265 (1993).

38   R. B. Fox, T. R. Price, R. F. Cozzens, and W. H. Echols, *Macromolecules*, **7**, 937 (1974).

39   A. Itaya, K. Okamoto, and S. Kusabayashi, *Bull. Chem. Soc. Jpn.*, **50**, 52 (1977).

40   S. Ito, S. Nishimoto, M. Yamamoto, and Y. Nishijima, *Rep. Prog. Polym. Phys. Jpn.*, **26**, 483 (1983).

41   D. A. Holden and A. Safarzadeh–Amiri, *Macromolecules*, **20**, 1588 (1987).

42   K. K. Rebane and L. A. Rebane, *"Persistent Spectral Hole-Burning: Science and Applications"*, W. E. Moerner Ed., Springer–Verlag, Berlin, 1988, Chapter 2.

43   A. D. Stein, K. A. Peterson, and M. D. Fayer, *J. Chem. Phys.*, **92**, 5622 (1990).

44   W. E. Moerner, *"Persistent Spectral Hole-Burning: Science and Applications"*, W. E. Moerner, Ed., Springer–Verlag, Berlin, 1988, Chapter 1.

45   H. P. H. Thijssen, R. van den Berg, and S. Völker, *Chem. Phys. Lett.*, **97**, 295 (1983).

46   B. Jackson and R. Silbey, *Chem. Phys. Lett.*, **99**, 331 (1983).

Chapter 6

Thermally Induced Super–Trap Formation in Poly[(9-phenenthrylmethyl methacrylate)-*co*-(methyl methacrylate)] Film at Low Temperatures

6.1. Introduction

Chemical processes in a variety of photofunctional polymers can be initiated by so-called "triplet-sensitizer", which transfers the excitation energy to the reactant with a high efficiency.[1]   Furthermore, a large portion of the excitation energy, often exceeding 50 %, dissipates to the ground state *via* the triplet state.   Thus, the triplet state plays an important role in the photofunctional polymers.   The results obtained on many chromophoric polymer systems show that there are two critical factors governing the behavior of excited state in polymers at an extremely high concentration: the one is migration and transfer of triplet energy, and another factor is the formation of trap site, *e.g.*, excimer site.[2,3]

Bässler *et al.* analyzed the migration of triplet excitons in organic matrices by Monte Carlo simulation.[4]   They assumed that the distribution of site energy (DOS) is expressed by Gaussian function and the dispersity of DOS is independent of temperature.   In a previous chapter, we observed the spectral shift of phosphorescence for the copolymer films containing phenanthrene chromophores.   The spectral shift was simulated by the Monte Carlo method, and the DOS of ^{3}T* was obtained in a temperature range of 15–100 K.   However, in a soft matrix such as organic polymers, the dispersity seems to vary with temperature.   The experimental spectral shift can be reproduced by the Monte Carlo simulation when the dispersity was enlarged with temperature.   The temperature dependence of the dispersity of DOS is mainly attributed to the homogenous broadening.

This chapter deals with the phosphorescence decay profiles of poly[(9-phenenthrylmethyl methacrylate)-*co*-(methyl methacrylate)] (P(PhMMA-*co*-MMA)) films with and without acceptor.   The fitting procedure of the decay curves allowed us to evaluate

the concentration of super–traps which are the quenching sites of the trap–site phosphorescence of P(PhMMA-*co*-MMA). The relationship between the concentration of super–traps and molecular motion of the matrix polymer is discussed by measurements of the capacitance and conductance of the copolymer films.
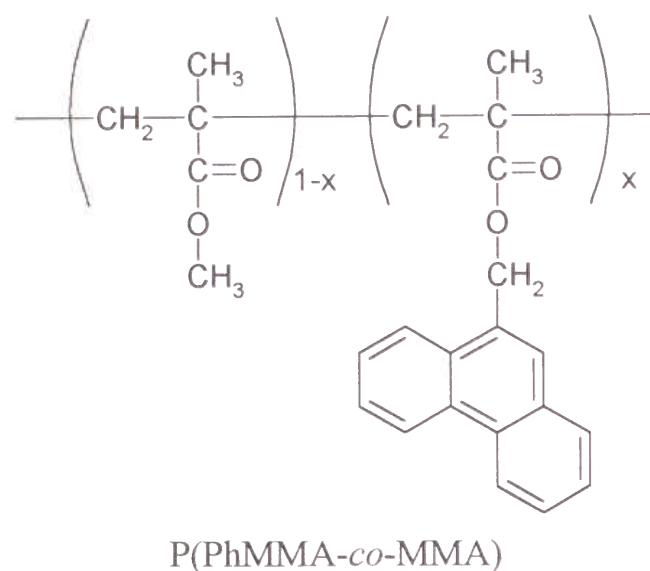
P(PhMMA-*co*-MMA)

6.2. Experimental Section

6.2.1. Materials

Synthetic methods for P(PhMMA-*co*-MMA) were described previously by Ito *et al.*[5] The properties of copolymers are listed in Table 6–1. 1,4-Dibromonaphthalene (DBN; Tokyo Chemical Industry Co., Ltd.) was recrystallized from methanol, which was used as a

Table 6–1. Compositions (*x*), Molecular Weights of P(PhMMA-*co*-MMA)s and Chromophore Concentrations ([Ph]), Average Distances between Phenanthrene Chromophores (*D*) in the Films

Sample	x mol %	Mw[a] 10^5	[Ph] mol L^{-1}	D[b] nm
P(PhMMA-*co*-MMA)L	0.78	1.30	0.09	2.63
P(PhMMA-*co*-MMA)H	18.6	1.20	1.67	1.00

[a] Determined by GPC calibrated with polystyrene standards. [b] Calculated by $D = n^{-(1/3)}$, where n is the average number of chromophores per unit volume.

triplet energy acceptor. The energy level for the lowest singlet state of DBN is higher than that of phenanthrene (Ph), *i.e.*, when Ph is selectively excited at 337 nm, only the triplet state of Ph is quenched by DBN.[6]

6.2.2. Sample Preparation

A solid film on a quartz plate was formed by casting a solution of the copolymer in a small quantity of 1,2-dichloroethane (spectrophotomeric grade; Dojindo Laboratories). After the solvent evaporated, the film was dried *in vacuo* for more than 10 h at room temperature and at 110 °C, respectively. The drying process was continued until the solvent could not be detected by UV spectrometry or IR spectrometry. In the same manner, DBN doped film was prepared by addition of prescribed amounts of DBN to the casting solution.
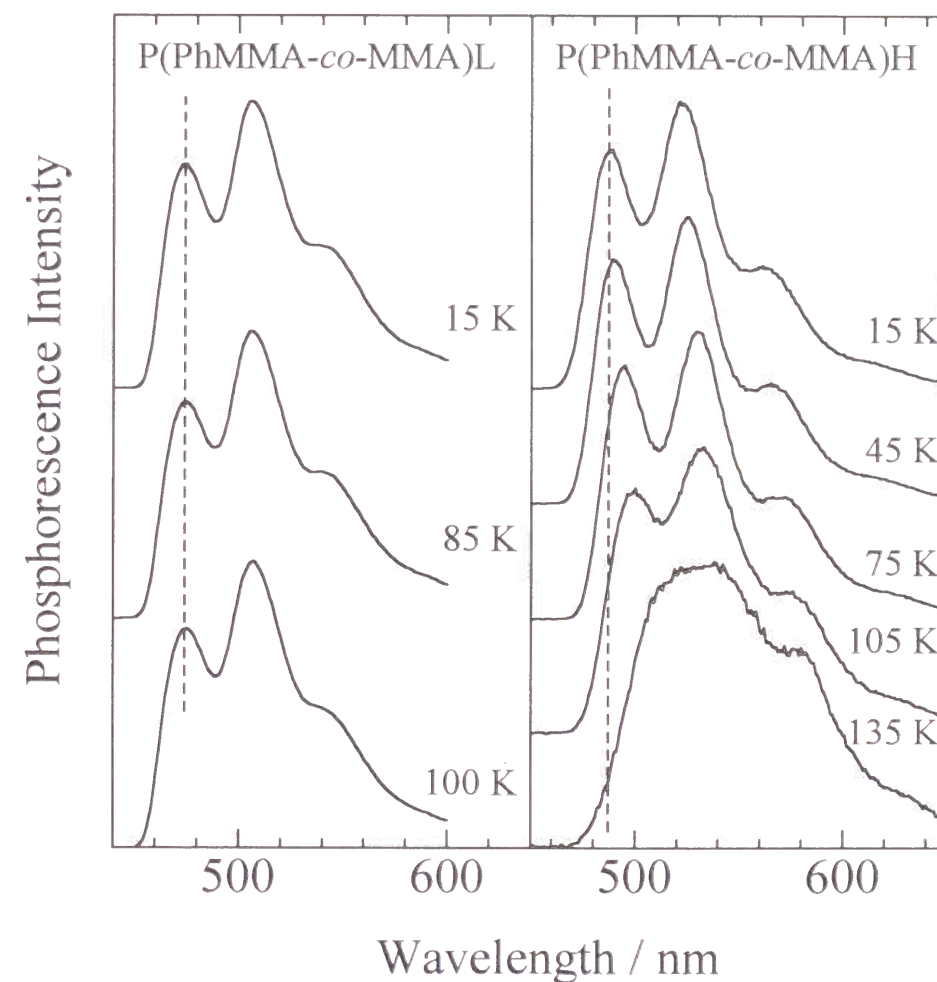
Figure 6–1. (A) Phosphorescence spectra of P(PhMMA-*co*-MMA)L film at three different temperatures. (B) Phosphorescence spectra of P(PhMMA-*co*-MMA)H film: Sample temperature was changed from 15 (top) to 135 K (bottom) by every 30 K separation. Both samples were excited at 337 nm and the spectra are uncorrected for instrumental response.

6.2.3. Measurements

Steady-state emission spectra were recorded with a Hitachi 850 spectro-fluorophotometer. Phosphorescence decay curves and time-resolved phosphorescence spectra were measured with a phosphorimeter assembled in our laboratory. A xenon flash lamp (EG & G, FX198UV) and a nitrogen laser (NDH Co., JH–500) were used as the pulsed excitation light sources for the measurements in millisecond and microsecond time regions, respectively. Details of the system have been described previously by Ito *et al.*[7] In the spectroscopic measurement, the temperature of the polymer film was varied by a closed cycle helium system (Iwatani Plantech Co., CRT 510). The temperature was maintained within ± 0.1 K by a temperature control unit (Iwatani Plantech Co., TCU–4). The temperature of sample was monitored by a calibrated thermocouple (Au + 0.07 % Fe / chromel) connected to the copper block in the neighborhood of the sample to provide a temperature as close to the area of observation as possible. Details of the temperature controlling system for the spectroscopic measurements have been described in Chapter 5.

For measurements of the capacitance and conductance of films, a three-electrode method was employed with a precision LCR Meter (ANDO Co., AG–4311B). Frequencies ranging from 100 Hz to 100 kHz were covered. The sample temperature was varied by a closed cycle liquid helium system (Daikin Co., CRYOKELVIN 204SC) between 15 K and room temperature. Measurements of capacitance and conductance were made by

Table 6–2. **Standard Deviation of the Trap Energy Distribution (σ) and Dispersion Parameter (α) for P(PhMMA-*co*-MMA)H Film and the Lifetime of Dibromonaphthalene (τ_a) in PMMA**

| Temperature / K	σ / cm^{-1}	α [a]	τ_a / ms
15	145	0.076	4.5
30	155	0.23	4.4
45	180	0.33	4.3
60	210	0.39	4.3
75	260	0.39	4.2
85	290	0.40	4.2
90	305	0.40	4.1
95	325	0.40	4.1
100	340	0.40	4.1

[a] $\alpha^{-1} = (\sigma / 4kT)^2 + 1$

maintaining the elevating rate 1–3 K min^{-1}.

6.3. Results and Discussion
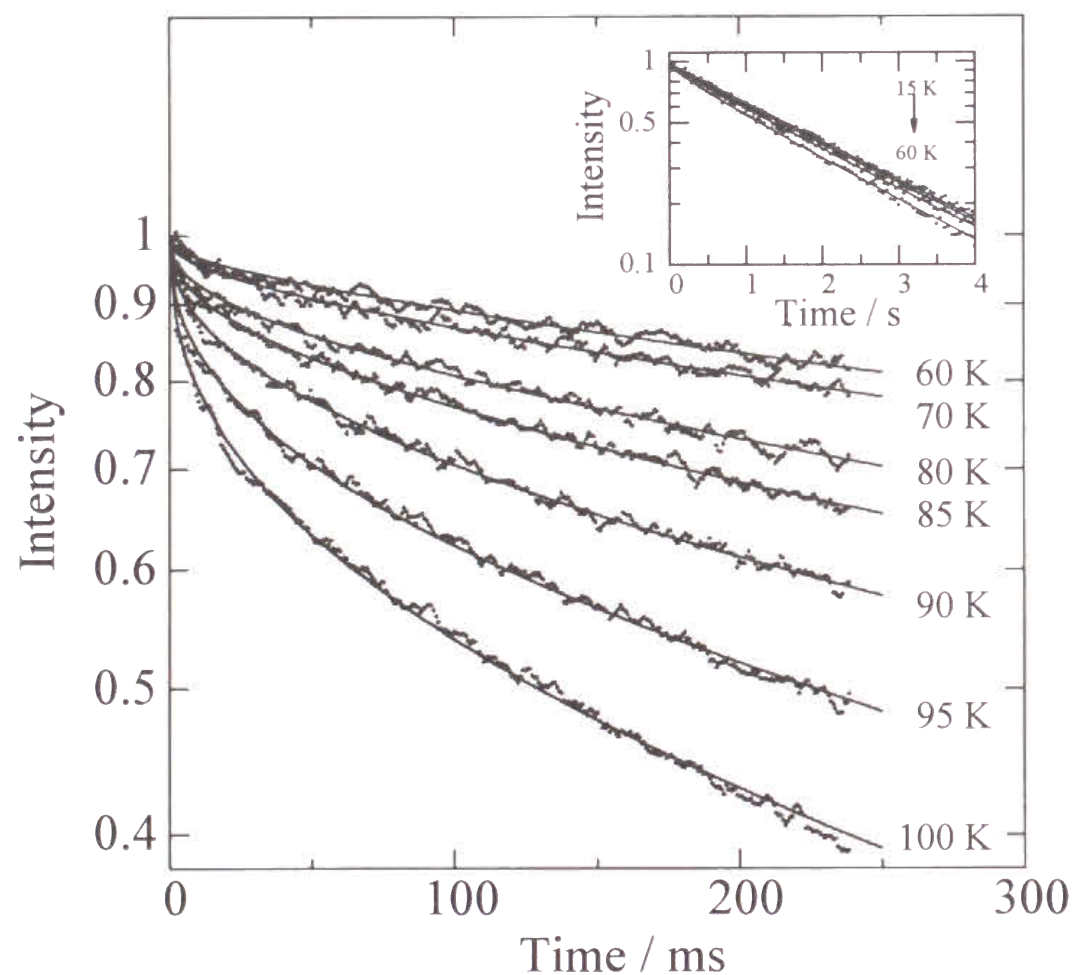
6.3.1. Spectroscopic Measurements

The temperature dependence of phosphorescence spectra for P(PhMMA-*co*-MMA) films is shown in Figure 6–1. The phosphorescence spectra of P(PhMMA-*co*-MMA)L film were independent of temperature. On the other hand, for P(PhMMA-*co*-MMA)H film, the spectra were shifted to the longer wavelength and the intensity decreased with the increase of
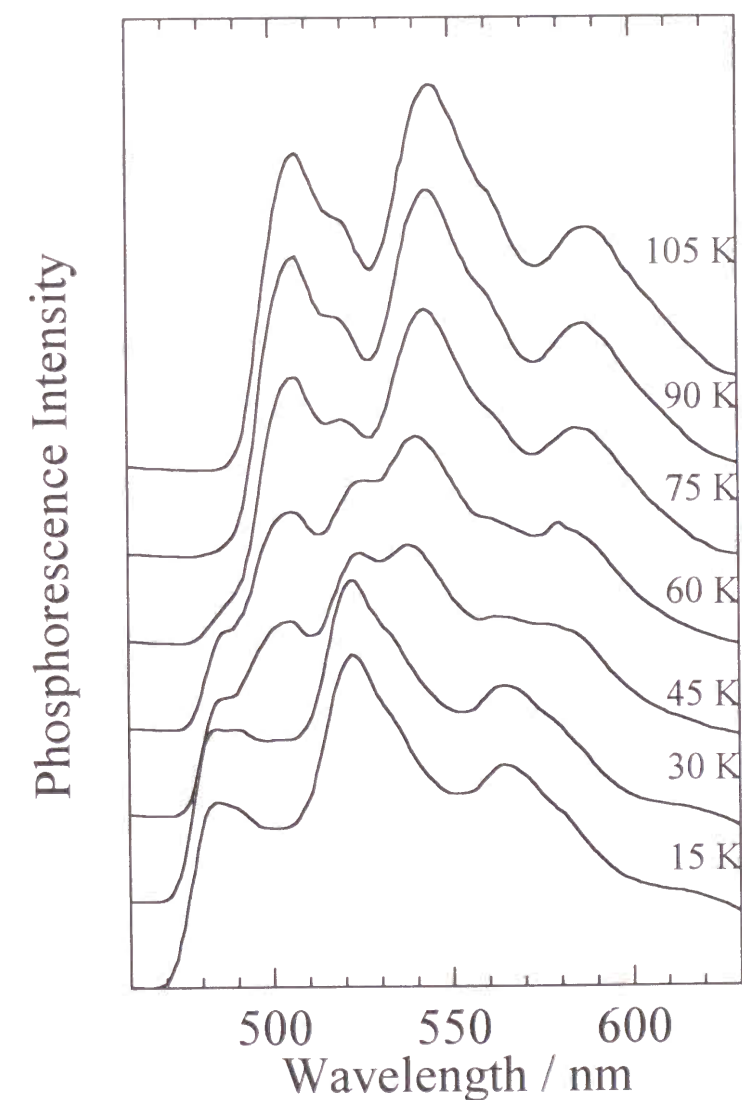
Figure 6–2. Phosphorescence spectra of the DBN doped P(PhMMA-*co*-MMA)H film excited at 335 nm. Sample temperature was changed from 15 (bottom) to 105 K (top) by every 15 K separation.

temperature, but the band shape remained the same below 105 K. The result shows that the chromophores form more stabilized $^3T^*$ sites within their excited lifetime for the polymer having a higher concentration of chromophores. The broadened spectra at high temperatures may be caused by overlapping of the emission from several $^3T^*$ sites of different energy levels. In the previous chapter, the Monte Carlo simulation of the spectral shift revealed the growth of interchromophore interaction as the enlargement of the energy dispersity of the triplet site. Table 6–2 shows the dispersion parameters, α and σ, defined in the later section.

Figure 6–2 depicts the phosphorescence spectra for P(PhMMA-*co*-MMA)H film containing a small amount of DBN (5×10^{-3} mol L^{-1}). The concentration of DBN is *ca.* 1/300 of that of Ph. At 15 K, the phosphorescence from only phenanthrene unit at 485, 522, and 564 nm, was observed. The Ph phosphorescence decreased with a rise in temperature,

and in place of it, the DBN phosphorescence appeared at 507, 545, and 588 nm. In the P(PhMMA-*co*-MMA)H film, iterative trapping–detrapping at $^3T^*$ sites and capture of the exciton to DBN result in a preferential loss of high-energy emission from these $^3T^*$ sites. At higher temperatures, the probability that the exciton reaches more stabilized sites or an acceptor site increases by the activation of detrapping process.[5] When DBN was doped in P(PhMMA-*co*-MMA)L film in which energy migration could not occur, only Ph phosphorescence was observed.

Figure 6–3 shows phosphorescence decay profiles of P(PhMMA-*co*-MMA)H film at various temperatures. The decay curves were almost single–exponential below 45 K. Above 60 K, the decay profiles became multiexponential (more than two) and the decay rate increased. For P(PhMMA-*co*-MMA)L film, the decay curves were single–exponential in the same temperature range.

The decay curves of P(PhMMA-*co*-MMA) film were fitted by a biexponential function (eq 6–1) and the average lifetime of phenanthrene triplet, $<\tau>$, was calculated by eq 6–2.

Figure 6–3. Temperature dependence of decay curves of phenanthrene phosphorescence in P(PhMMA-*co*-MMA)H film. The emission was detected at 545 nm. The solid lines represent the results of calculation based on the DOS model with $\nu_0 = 1.39 \times 10^5$ ms^{-1} and $\alpha =$ 0.076 (15 K), 0.23 (30 K), 0.33 (45 K), 0.39 (60 K), 0.39 (75 K), 0.40 (85 K), 0.40 (90 K), 0.40 (95 K), and 0.40 (100 K).
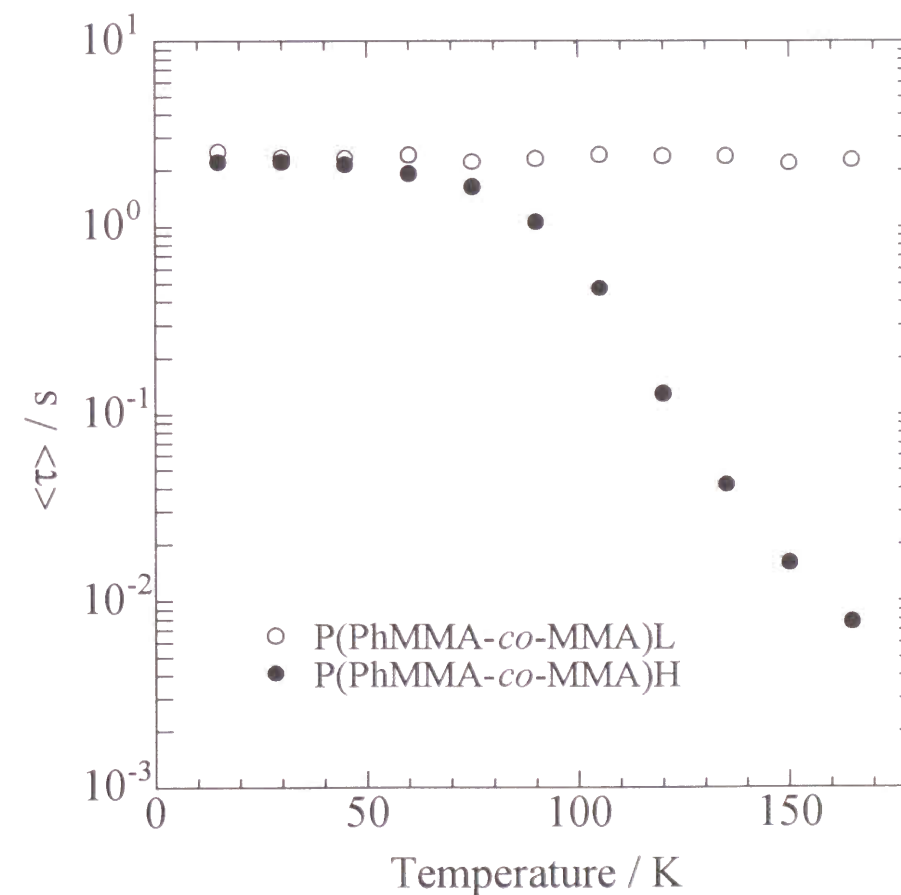
Figure 6–4. Temperature dependence of average lifetime of phosphorescence $<\tau>$: (○) P(PhMMA-*co*-MMA)L film; (●) P(PhMMA-*co*-MMA)H film.
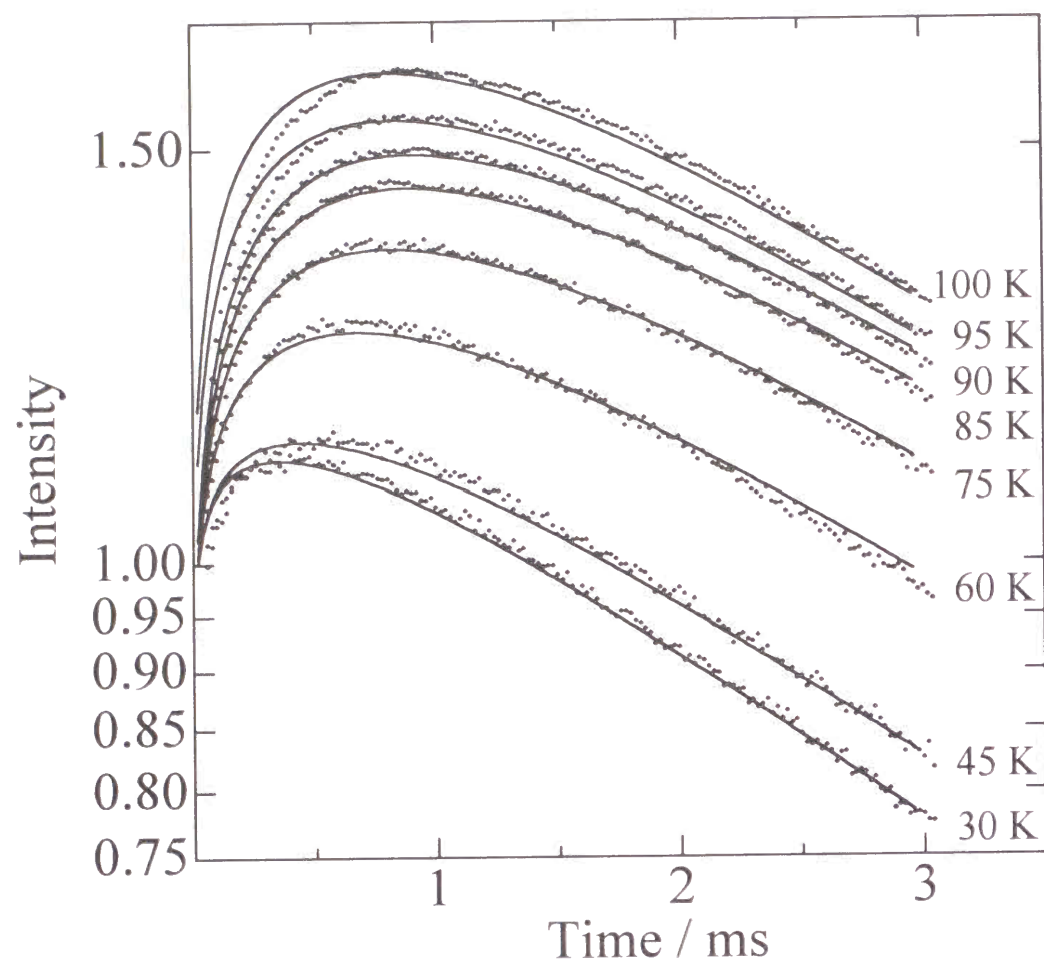
Figure 6–5. Temperature dependence of rise and decay curves of DBN phosphorescence in P(PhMMA-*co*-MMA)H film. The emission was detected at 545 nm. The solid lines represent the results of calculation based on the DOS model. The parameters of each temperature are identical to those in Figure 6–3.

$$I_d(t) = I_d(0)\left[F \exp\left(-\frac{t}{\tau_1}\right) + (1-F)\exp\left(-\frac{t}{\tau_2}\right) \right] \tag{6-1}$$

$$\langle\tau\rangle = F\tau_1 + (1-F)\tau_2 \tag{6-2}$$

The temperature dependence of $\langle\tau\rangle$ is shown in Figure 6–4. For P(PhMMA-*co*-MMA)H film, $\langle\tau\rangle$ decreased rapidly above 50 K, while $\langle\tau\rangle$ remained almost constant for P(PhMMA-*co*-MMA)L film. This indicates that the energy migration to some quenching sites is responsible for this behavior. We will refer to this quenching site as super–trap.

Figure 6–5 shows the rise and decay profiles of the acceptor (DBN) phosphorescence in the P(PhMMA-*co*-MMA)H film at various temperatures. The rise component became larger and the rise peak shifted to a longer time with increasing temperature. The behavior of phosphorescence spectra and its decay profiles can be interpreted by the thermally-accelerated
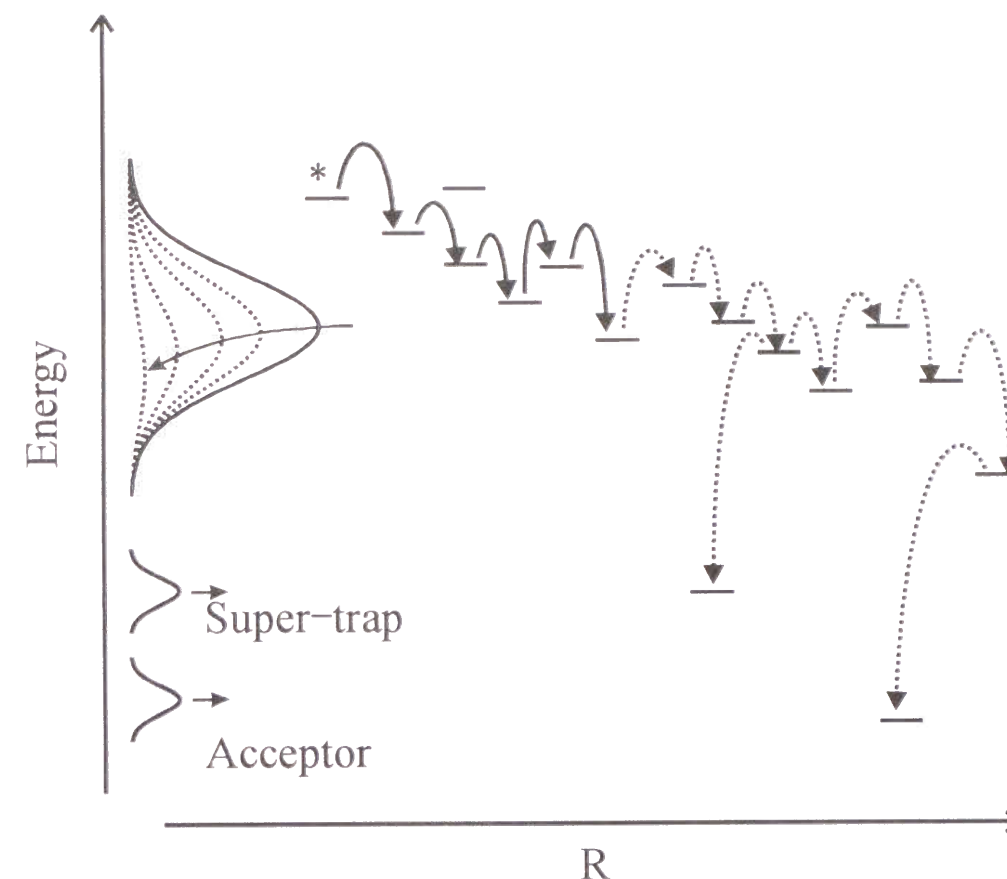
Figure 6–6. Schematic illustration of the energy migration among the levels with Gaussian energy distribution. The full curves indicate the density of state profile. Dashed curves map the distribution of excitons(*) after the excitation which populates a small fraction of sites randomly. At low temperatures, an exciton is trapped by a shallow $^3T^*$ site. With the increase of temperature, the exciton migrates to a super–trap or an acceptor site.

process as shown in Figure 6–6. The migrating exciton is captured by a $^3T^*$ site which has a potential energy lower than the surrounding sites. At lower temperatures, the triplet exciton cannot overcome the energy barrier so that it is captured immediately and migrates within a narrow range of sites. At higher temperatures, the exciton may overcome the barrier and migrates over a wide range of sites. Therefore, the probability that the triplet exciton reaches a super–trap or an acceptor site increases with the elevation of temperature.

6.3.2. Computer Simulation

For P(PhMMA-*co*-MMA) film without acceptor, the equation for the excited triplet phenanthrene chromophore is given by

$$\frac{d\,D(t)}{dt} = -\left(\tau_d^{-1} + c_E v(t)\right)D(t) \tag{6-3}$$

where $D(t)$ is the number of excited chromophores, $\nu(t)$ is the exciton hopping frequency at time t, c_E is the concentration of the super–trap, and τ_d is the intrinsic lifetime of the Ph chromophore. Bässler *et al.* analyzed the triplet energy migration in amorphous organic layers. They assumed that the energy migration occurs through exciton hopping among the sites that exhibit a Gaussian DOS. By a Monte Carlo simulation,[8] the time dependence of $\nu(t)$ is obtained as follows:

$$\nu(t) = \nu_0 \left(\frac{t}{t_0} \right)^{\alpha-1} \tag{6–4}$$

where ν_0 and t_0 are jump frequency and jump time, respectively, in an energetically discrete hopping system and α is the dispersion parameter. Empirically, α is predicted to follow the relation:

$$\alpha^{-1} = \left(\frac{\sigma}{4kT} \right)^2 + 1 \tag{6–5}$$

where σ is the width of the Gaussian distribution.[9] Then we obtained $D(t)$ from eq 6–3 and eq 6–4 as follows.

$$D(t) = D(0) \exp\left(-\frac{c_E B t^\alpha}{\alpha} - \frac{t}{\tau_d} \right) \tag{6–6}$$

where

$$B = \nu_0 t_0^{1-\alpha}.$$

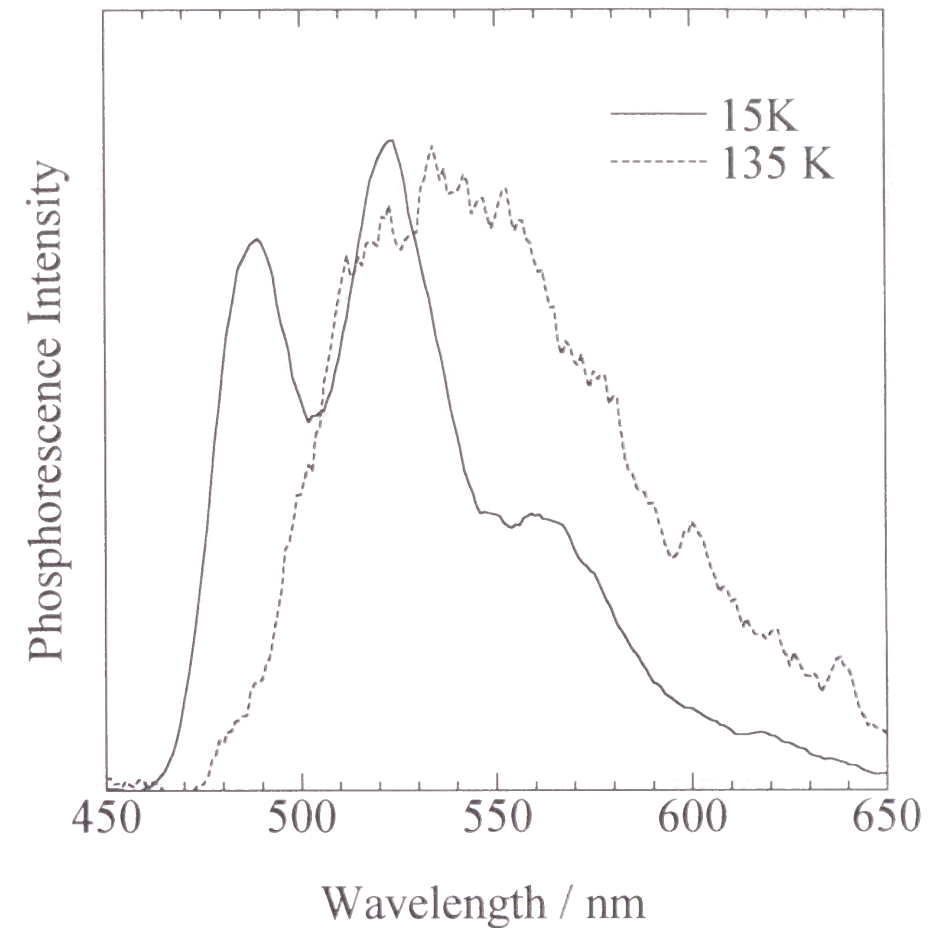When the acceptors exist in the system, eq 6–3 changes as follows.

$$D(t) = D(0) \exp\left[-\frac{(c_E + c_a) B t^\alpha}{\alpha} - \frac{t}{\tau_d} \right] \tag{6–7}$$

where c_a is the acceptor concentration. Similarly, the number of excited acceptors, $A(t)$, is written as follows:

$$\frac{dA(t)}{dt} = c_a \nu(t) D(t) - \frac{A(t)}{\tau_a} \tag{6–8}$$

where τ_a is the lifetime of acceptor. Then we obtained $A(t)$ as follows:

$$A(t) = D(0) c_a \exp\left(-\frac{t}{\tau_a} \right) \left[\int_0^t B T^{\alpha-1} \exp\left\{ -\frac{(c_E + c_a) B t^\alpha}{\alpha} \right\} \exp\left(\frac{T}{\tau_a} \right) dT \right] \tag{6–9}$$

Figure 6–7. Time-resolved phosphorescence spectra of P(PhMMA-*co*-MMA)H films observed at the time range 241–248 ms after excitation: at 15 (———) and 135 K (--------). Spectra are normalized at the maximum of each spectrum peak.

When the donor phosphorescence overlaps the acceptor phosphorescence at a monitored wavelength, the decay profiles of the phosphorescence, $I_2(t)$, is given by the sum of the donor and acceptor phosphorescence.
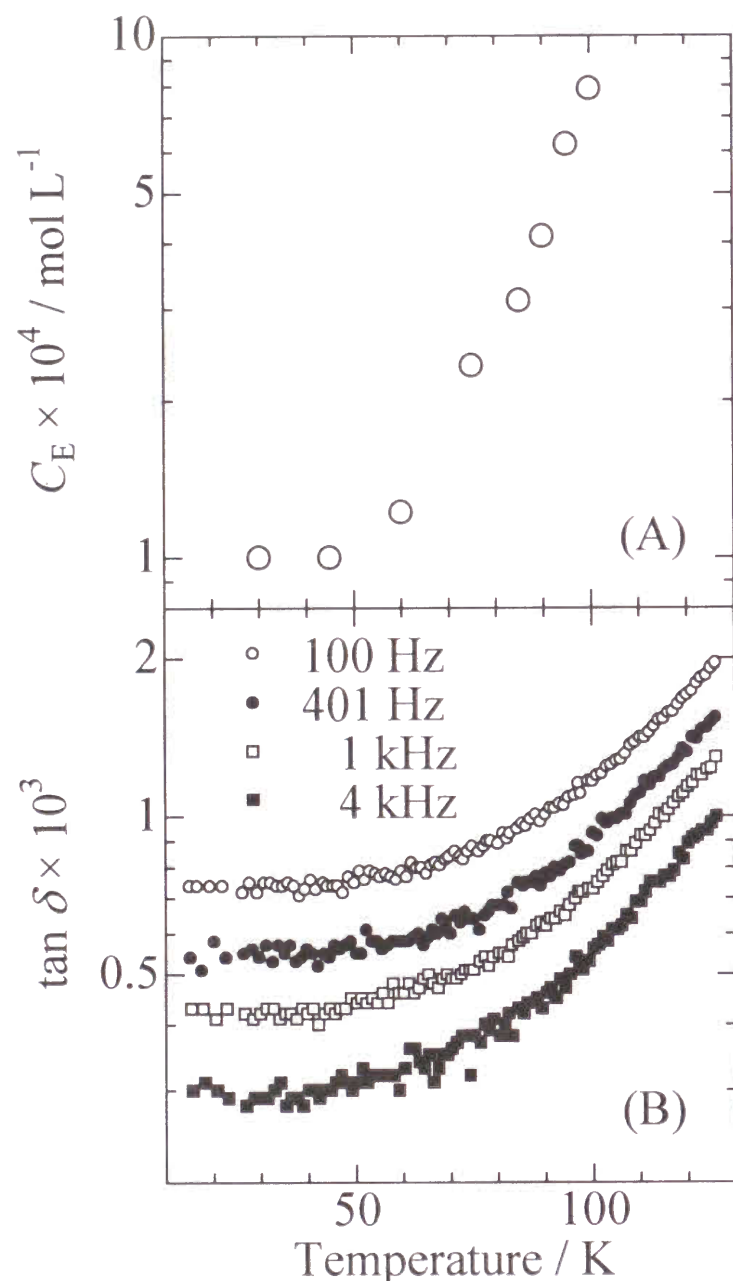
$$I_2(t) = y A(t) + (1-y) D(t) \tag{6–10}$$

where y is a fraction of the acceptor phosphorescence.

The phosphorescence decay curves of P(PhMMA-*co*-MMA)H films were fitted by using eq 6–6 with c_E, ν_0 and t_0 as the fitting parameters. We assumed that ν_0 and t_0 are independent of temperature according to Bässler's model, and are fixed to 1.39×10^8 s^{-1} and 1.55×10^9 s, respectively. The intrinsic lifetime, τ_d, was determined by the measurement of phosphorescence lifetime of P(PhMMA-*co*-MMA)L film at each temperature. The dispersion parameter, α, was calculated from the energy dispersity of the trap sites, σ, obtained in Chapter 5. The solid lines in Figure 6–3 indicate the calculated decay curves.

Next, the curve fitting was performed by use of eq 6–10 with a fraction *y* for the DBN phosphorescence in P(PhMMA-*co*-MMA)H films. The lifetime of acceptor, τ_a, was determined by the measurement of phosphorescence lifetime of DBN doped in PMMA films at each temperature (Table 6–2). Other parameters were fixed to the values that were used for the previous fitting of Ph decay curves. Figure 6–5 shows the results of the curve fitting as the solid lines. The calculated curves are in good agreement with the experimental ones.

What is the super–trap in P(PhMMA-*co*-MMA)H film. Figure 6–7 shows time-

resolved phosphorescence spectra of P(PhMMA-*co*-MMA)H film at 15 and 135 K in the time range 241–248 ms after excitation. In this time range, the energy of excitons is expected to already be relaxed in the most stable distribution. At 15 K, the spectrum is attributed to the ^{3}T* phosphorescence as obtained in a photostationary condition. At 135 K, in contrast, the time-resolved phosphorescence was broad structureless and was shifted toward the low-energy side relative to that in a photostationary condition. The spectrum at 135 K resembles that of a triplet excimer of phenanthrene that was reported previously.[10] Therefore, we assumed that the deeper trap–sites, *e.g.*, triplet excimer, act as the super–trap in P(PhMMA-*co*-MMA)H film.

The obtained concentration of the super–trap is shown in Figure 6–8(A). For poly(vinyl carbazole) film, the concentration of excimer-forming site was estimated to be *ca.* 10^{-2} mol L^{-1} at 77 K,[11] which is about two order of magnitude higher than the present c_E values in P(PhMMA-*co*-MMA)H film.

6.3.3. Dielectric Relaxation

Dielectric loss tangents (tanδ) of P(PhMMA-*co*-MMA)H film are shown in Figure 6–8(B). Similarly to the temperature dependence of c_E, tanδ increased above 50 K. The α-methyl groups in poly(alkyl methacrylate) begin to relax around this temperature.[12–14] The motion of the α-methyl groups has phenanthrene chromophores make feasible an excimer-like conformation. At a frequency higher than 4 kHz, tanδ began to increase at higher temperatures. This result indicates that the formation of a super–trap is induced by the motion of the frequency less than a few kHz.

6.4. Conclusion

Phosphorescence spectra and phosphorescence decay profiles of P(PhMMA-*co*-MMA) films were obtained at low temperatures. Phosphorescence decay profiles of P(PhMMA-*co*-MMA)H films with and without a triplet energy acceptor were fitted using a model in which the exciton hops among the sites having a Gaussian energy distribution. At the same temperature, both decay profiles were simulated by using same parameters; α, ν_0, t_0 and c_E. From the simulation, the concentrations of the super–trap in P(PhMMA-*co*-MMA)H film could be evaluated in the temperature range from 30 to 100 K. The concentration of super–

Figure 6–8. (A) Temperature dependence of the super–trap concentration in P(PhMMA-*co*-MMA)H film. (B) Dielectric loss tangent of P(PhMMA-*co*-MMA)H at four different frequencies.

trap showed a steep rise at around 50 K, which well corresponds to the enhancement of the matrix polymer motion observed by the dielectric measurement at the frequency of 0.1–4 kHz.

References

1   W. Galley and L. Stryer, *Proc. Natl. Acd. Sci. U. S. A.*, **60**, 108 (1968); J. Eisinger and R. G. Shulman, *Science*, **161**, 1311 (1968); Z. Wu and H. Morrison, *Photochem. Photobiol.*, **50**, 525 (1989).

2   J. B. Birks, *"Photophysics of Aromatic Molecules"*, Wiley, London, 1970.

3   N. J. Turro, *"Modern Molecular Photochemistry"*, Benjamin: Menlo Park, CA, 1978.

4   R. Richert, B. Ries, and H. Bässler, *Philos. Mag. B*, **49**, L25 (1984); R. Richert and H. Bässler, *J. Chem. Phys.*, **84**, 3567 (1986).

5   S. Ito, N. Numata, H. Katayama, and M. Yamamoto, *Macromolecules*, **22**, 2207 (1989).

6   H. Katayama, T. Tawa, G. W. Haggquist, S. Ito, and M. Yamamoto, *Macromolecules*, **26**, 1265 (1993).

7   S. Ito, H. Katayama, and M. Yamamoto, *Macromolecules*, **21**, 2456 (1988).

8   G. Schönherr, H. Bässler, and M. Silver, *Phil. Mag. B*, **44**, 47 (1981); R. Richert, A. Elshner, and H. Bässler, *Z. Phys. Chem. NF.*, **149**, 63 (1986).

9   H. Bässler, *Phys. Status Solidi B*, **107**, 9 (1981).

10   R. Richert and H. Bässler, *Chem. Phys. Lett.*, **95**, 13 (1983).

11   W. Klöpffer, *J. Chem. Phys.*, **50**, 2337 (1969); *Chem. Phys.*, **57**, 75 (1981); W. Klöpffer, and D. Fischer, *J. Polym. Sci. C*, **40**, 43 (1973).

12   A. Odajima, A. E. Woodward, and J. A. Sauer, *J. Polym. Sci.*, **55**, 181 (1961).

13   A. E. Woodward, *J. Polym. Sci. C*, **14**, 89 (1966).

14   K. Shimizu, O. Yano, and Y. Wada, *J. Polym. Sci. Polym. Phys. Ed.*, **13**, 1959 (1975).

Summary

The author discussed the triplet energy transfer and migration in polymer matrices. In Chapters 1–3, the triplet energy transfer in polymeric Langmuir–Blodgett films was investigated. In Chapter 4, the one-step energy transfer process was studied using bichromophoric compounds. In Chapters 5 and 6, the triplet energy migration was analyzed at low temperatures for the amorphous films of chromophoric copolymers. The studies described in Part I (Chapters 1–4) were performed from the standpoint of the effect of spatial distribution of chromophores. The studies described in Part II (Chapters 5 and 6), on the other hand, were focused on the effect of the energetic dispersity among the chromophores. The summary of each chapter is as follows.

Chapter 1 reported the triplet state interactions between carbazole chromophores in polymeric LB films. The interactions were related to the interchromophore distance and were analogous to those in amorphous polymer films. The carbazole moieties were in the hydrophobic area of the P(C-iB) monolayer and exhibited interlayer interaction at the interface of the hydrophobic layers. The interaction was depressed by using spacer layers or using P(C-OD) monolayers which have long side chains. This finding is useful for designing photofunctional LB films utilizing photophysical or photochemical processes *via* the excited triplet state.

In Chapter 2, triplet energy transfer between carbazole and bromonaphthalene moieties was measured in a two-dimensional plane made by LB films of poly(octadecyl methacrylate). When the content of carbazole monomer was 5 mol %, the dependence of the quenching efficiency of the carbazole triplet upon the bromonaphthalene density was represented by the active sphere model assuming a planar chromophore distribution. This indicates that the chromophores in LB films of poly(octadecyl methacrylate) situate in a planar distribution within the range of a few angstroms. Therefore the LB technique using such a preformed polymer having crystalline side chain, allows us to construct molecular systems involving a triplet energy transfer process. The triplet energy transfer is mechanistically equivalent to the electron transfer because it takes place through electron exchange interaction. This

suggests that the LB film made from this polymer is also able to regulate an electron transfer process. High crystallinity of the alkyl side chain plays an important role in the regulation of chromophore distribution.

In the following Chapter 3, the triplet exciton capture in a 2-dimensional plane was simulated by solving the differential equations relevant to energy migration and energy transfer. The calculated probability that the exciton was captured by the acceptor sites well agreed with the quenching efficiencies that were obtained experimentally for the LB films of chromophoric copolymers of octadecyl acrylate. This indicates that the triplet energy migration and transfer in a two-dimensional plane can be described by the mechanism described in the above simulation. The best-fit parameters were $L_{dd} = 0.094$ nm and $\nu_{dd} = 1.3 \times 10^{12}$ s^{-1} for the triplet energy migration between carbazole chromophores, and $L_{da} = 0.117$ nm and $\nu_{da} = 1.3 \times 10^{12}$ s^{-1} for the triplet energy transfer from carbazole to bromonaphthalene.

In Chapter 4, the intramolecular triplet–triplet (T–T) energy transfer of bichromophoric compounds connected with a flexible alkyl chain was directly analyzed by the decay measurements of phosphorescence and transient absorption. The distribution of donor–acceptor (D–A) distances was calculated by a conformational analysis, and the decay profile was calculated using Dexter's equation. The result of curve fitting was in fairly good agreement with the experimental value. For longer spacer samples, the pre-exponential factor, k_0, was acceptable in comparison with the previous results obtained for intermolecular T–T energy transfer. These results indicate that the *"through-space"* mechanism governs the intramolecular T–T energy transfer in D–A molecules with a flexible long spacer. However, when the spacer length became shorter, the k_0 value increased apparently by deviating from the ideal *"through-space"* mechanism described by Dexter's model. Temperature dependence of the intramolecular T–T energy transfer was also studied for Cz-10-Np. The rate of energy transfer rose exponentially with the increase of temperature.

In Chapter 5, the time resolved phosphorescence spectra were measured for the copolymer films containing phenanthrene moieties, P(PhMMA-*co*-MMA). At a high phenanthrene concentration, the phosphorescence spectra were shifted toward the lower energy side. This behavior was explained by the model that the triplet exciton hops among the sites having a Gaussian energy distribution (Gaussian DOS). In this model, the

population of the triplet excitons changes from the uniform distribution toward Boltzmann distribution with a elapse of time. The time evolution of the standard deviation of trap energy distribution and the mean value of triplet energies were estimated by a computer simulation. The temperature dependence of the dispersity of DOS was mainly attributed to the homogeneous broadening. At low temperatures, the site-energy distribution is one of the critical factors for determining the triplet energy migration.

In the last chapter, phosphorescence spectra and phosphorescence decay profiles of P(PhMMA-*co*-MMA) films were obtained at low temperatures. Phosphorescence decay profiles of P(PhMMA-*co*-MMA)H films with and without a triplet energy acceptor were fitted using a model in which the exciton hops among the sites having a Gaussian energy distribution. At the same temperature, both decay profiles were simulated by using same parameters; α, ν_0, t_0, and c_E. From the simulation, the concentrations of the super–trap in P(PhMMA-*co*-MMA)H film could be evaluated in the temperature range from 30 to 100 K. The concentration of super–trap showed a steep rise at around 50 K, which well corresponded to the enhancement of the matrix polymer motion observed by the dielectric measurement at the frequency of 0.1–4 kHz.

List of Publication

Chapter 1

"Triplet Energy Migration in Polymer Langmuir–Blodgett Films",

Kenji Hisada, Hideaki Katayama, Shinzaburo Ito, and Masahide Yamamoto, *J. Photopolym. Sci. Technol.*, **6**, 105 (1993).

"Triplet Excimer Formation in Langmuir–Blodgett Polymer Films of Poly[2-(9-carbazolyl)ethyl methacrylate-co-isobutyl methacrylate]",

Hideki Katayama, Kenji Hisada, Masayuki Yanagida, Satoru Ohmori, Shinzaburo Ito, and Masahide Yamamoto, *Thin Solid Films*, **224**, 253 (1993).

Chapter 2

"Triplet Energy Transfer from Carbazole to Bromonaphthalene in a Two-Dimensional Chromophore Plane Prepared by Poly(octadecyl methacrylate) Langmuir–Blodgett Films",

Kenji Hisada, Shinzaburo Ito, and Masahide Yamamoto, *Langmuir*, **11**, 996 (1995).

Chapter 3

"Two-Dimensional Triplet Energy Migration and Transfer in Polymer Langmuir–Blodgett Films",

Kenji Hisada, Shinzaburo Ito, and Masahide Yamamoto, *Langmuir*, **12**, 3682 (1996).

Chapter 4

"Intramolecular Triplet Energy Transfer. 4.   A Carbazole–Naphthalene System Having a Flexible Alkyl Spacer Doped in Poly(methyl methacrylate) Matrices",

Kenji Hisada, Akira Tsuchida, Shinzaburo Ito, and Masahide Yamamoto, submitted for

publication in *J. Phys. Chem. B.*

Chapter 5

"Triplet Energy Migration among Energetically Disordered Chromophores in Polymer Matrixes. 1. Monte Carlo Simulation for the Hopping of Triplet Excitons",

Kenji Hisada, Shinzaburo Ito, and Masahide Yamamoto, *J. Phys. Chem. B*, **101**, 6827 (1997).

Chapter 6

"Triplet Energy Migration among Energetically Disordered Chromophores in Polymer Matrixes. 2. Thermally Induced Super–Trap Formation",

Kenji Hisada, Shinzaburo Ito, and Masahide Yamamoto, submitted for publication in *J. Phys. Chem. B.*

Others

"Transient Ions and Triplet States in Polymers Containing Phenanthrene",

Gregory W. Haggquist, Kenji Hisada, Akira Tsuchida, and Masahide Yamamoto, *J. Phys. Chem.*, **98**, 10756, (1994).

"Synthesis and Properties of Dioxa[3.3](3,6)carbazolophane",

Keita Tani, Yasuo Tohda, Kenji Hisada, and Masahide Yamamoto. *Chem. Lett.*, **1996**, 145.

Acknowledgments

Acknowledgments

Finally, but not least, the author is sincerely grateful to his parents Kouji Hisada and Ryoko Hisada for their continuous support.

December, 1997

<div align="right">Kenji Hisada</div>